Adjacent Channel Interference in Overlapping Access Points of OFDM WLANs

by

Salman Aslam Khan

B. Sc., King Fahd University of Petroleum and Minerals, 2002

A THESIS SUBMITTED IN PARTIAL FULFILLMENT OF THE REQUIREMENTS FOR THE DEGREE OF

MASTER OF APPLIED SCIENCE

in

THE FACULTY OF GRADUATE STUDIES

(Electrical Engineering)

The University of British Columbia

February, 2006

Abstract

Interference analysis has always been a key issue for WLAN systems, because of the unregulated nature of the Industrial Scientific and Medical (ISM) bands that they operate in. However, an aspect of interference generally not considered is adjacent channel interference (ACI) from a neighboring WLAN operating on a standard defined non-overlapping channel. Because standard defined non-overlapping channels are not truly non-overlapping but are based on limits set on the transmit signal spectrum, situations may arise where this interference will significantly degrade performance. With escalating deployment of WLANs in overlapping areas and the limited number of valid operating channels available, ACI may become a major hindrance to the optimal functioning of WLANs.

In this work we present a detailed analysis of ACI that access points (APs) of OFDM WLANs deployed in overlaying coverage areas may experience when individual APs operate on IEEE 802.11a defined non-overlapping channels. We investigate scenarios where ACI is most likely to occur. We also investigate the parameters that affect the severity of this interference and how system performance is degraded in the presence of ACI (in terms of physical layer parameters). We use these results to suggest minimum separation distances between APs that would render the effects of ACI negligible. Furthermore, several ACI mitigation techniques are described and their effectiveness for various scenarios is investigated. Results from our analysis may be used to improve network deployment strategies for large scale multi-AP WLANs and to develop routines that allow better co-existence strategies for APs deployed in overlapping coverage areas.

Table of Contents

List of Tables

List of Figures

List of Abbreviations

A\D	Analog to Digital
AC	Adjacent Channel
ACI	Adjacent non-overlapping Channel Interference
AGC	Active Gain Control
AP	Access Point
BER	Bit Error Rate
BICM	Bit Interleaved Coded Modulation
BPSK	Binary Phase Shift Keying
BSSID	Basic Service Set Identification
CDMA	Code Division Multiple Access
CM	Coded Modulation
D\A	Digital to Analog
dBi	Antenna gain in dB with respect to an isotropic antenna
dBm	dB with respect to mW
dBr	dB with respect to the
DFT	Discrete Fourier Transform
DSSS	Direct Sequence Spread Spectrum
FFT	Fast Fourier Transform
FHSS	Frequency Hoping Spread Spectrum
FIR	Finite Impulse Response
GHz	Giga Hertz
GI	Guard Interval
IDFT	Inverse Discrete Fourier Transform
ISI	Inter Symbol Interference
LLR	Log Likelihood Ratio
LSE	Least Square Error
MAC	Medium Access Control Layer
MCM	Multi Carrier Modulation

MHz	Mega Hertz
NAC	Non-Adjacent Channel
NACI	Non-Adjacent non-overlapping Channel Interference
OFDM	Orthogonal Frequency Division Multiplexing
OOB	Out of Band Power Spectrum
PAM	Pulse Amplitude Modulation
PAPR	Peak to Average Power Ratio
PDP	Power Delay Profile
PER	Packet Error Rate
PHME	Physical layer Management Entity
PHY	Physical Layer
PLCP	Physical Layer Convergence Protocol
PMD	Physical Medium Dependent
PPDU	PLCP Protocol Data Unit
PSDU	Physical Sub-layer Data Unit
QAM	Quadrature Amplitude Modulation
QPSK	Quandary Phase Shift Keying
RC	Raised Cosine Window
RMS	Root Mean Square
SNIR	Signal to Noise plus Interference Ratio
SNR	Signal to Noise Ratio
TCM	Trellis Coding Modulation
UNII	Unlicensed National Information Infrastructure
WLAN	Wireless Local Area Network
β	Roll-off factor of raised cosine window

Acknowledgments

I would like to offer my sincere thanks to my supervisors Dr. Hussein Alnuweiri and Dr. Robert Schober for their valuable guidance and advice. I greatly appreciate the time they have spent contributing to this research and my personal growth. I would also like to thank all of my colleagues for their valuable advice and friendship. In particular, I would like to thank Chris Snow, Tamer Khattab and Rayan Saab for never hesitating to help me. Above all else, I would like to express my special thanks to my parents for the unconditional love and support that they have given me throughout my life.

Chapter 1

Introduction

Over the last decade, the telecommunications industry has experienced tremendous growth in the Wireless Local Area Network (WLAN) market. WLANs are being deployed in numerous places and the WLAN market has been listed among the most encouraging areas of high-tech growth in the years to come. The ever increasing demand for high rate data transmission through seamless connectivity has ensured a bright future for this field.

There are several reasons for WLAN's popularity and its incredible growth rate. Foremost of these is user mobility; users can stay connected to the network anywhere within the coverage area and move about while maintaining high data transfer rates. WLANs are also a very cost effective option for users as they have low infrastructure costs and need no wiring or licenses to transmit. WLAN networks are also very scaleable because of the simplicity of their network design and can be set up to serve a few users or expanded to form networks that span much larger coverage areas. Moreover, additional users can be added with relative ease by merely installing a network card in a device that requires access to the network. The ease of setting up and their user friendliness has undoubtedly contributed to this exceptional growth rate.

As their name suggests, WLANs are local area networks that provide access to the Internet at high data rates over wireless channels. Essentially, a WLAN is composed of a network management device, an Access Point (AP) and multiple users associated with this AP. All WLAN components operate on a single half-duplex channel. Only one component can use the channel at one time. An AP can either be a separate entity or a user that is designated to perform management functions. Most practical WLANs use the former layout. WLANs operate in the unregulated industrial scientific medical (ISM) bands of the radio spectrum. Hence, no licensing from regulatory bodies is required for operation. However, standardization committees have developed standards to facilitate future growth, minimize intersystem interference and ensure interoperability between products from

different vendors. Local radio regulatory bodies generally require the use of standard compliant WLANs.

In North America, the IEEE standardization committee defined the 802.11 standard [1] that specifies the medium access control (MAC) layer and the physical layer (PHY) of WLANs. However, due to the rapidly changing nature of the telecommunications industry several amendments were later added, in particular, amendments "b, g, and a" that define new PHY layers with higher bit rates. The very first PHY layers of WLANs were based on infra-red technology and required a direct line of sight between the AP and users. They provided maximum theoretical bit rates of 1 Mbps. To remove line of sight dependency, newer WLANs were designed to use radio waves. The first radio wave based WLANs used either direct sequence spread spectrum (DSSS) or frequency hopping spread spectrum (FHSS) technology and provided data rates of 1-2 Mbps. The base IEEE 802.11 standard [1] describes all the above PHY layers. Amendment "b" introduced modifications to DSSS WLANs that increased transmission rates up to 11 Mbps. All the above PHY layers operate in the 2.4 GHz ISM band.

IEEE 802.11a [1] was the first to use Orthogonal Frequency Division Multiplexing (OFDM). The many advantages OFDM offers for transmission in wireless environments [3] allowed these WLANs to drastically improve data rate to 54 Mbps. However, concerns of overcrowding the 2.4 GHz ISM band caused IEEE 802.11a based WLANs to be designed for operation in the 5 GHz ISM band. Yet, even though these OFDM based WLANs provided much higher data rates, they were not widely accepted. This was largely due to incompatibility issues with predecessor systems, smaller coverage areas because of higher signal attenuation due to path loss at higher frequencies and the lack of congruity between the 5 GHz ISM bands in different countries[4][5]. Realizing the many potentials of OFDM, in 2003, the IEEE published the IEEE 802.11g amendment which essentially used the same system as IEEE802.11a but operates in the 2.4 GHz ISM band. IEEE 802.11g compliant WLANs are capable of providing data rates of 54 Mbps and are compatible with previous systems. Because of the much higher rates they offer, it is likely that most WLANs in the future will be based on OFDM.

OFDM based WLANs, whether defined by amendment "a" or "g", operate on 20 MHz channels. The 2.4 GHz ISM band has only three such non-overlapping channels. On the other hand, the 5 GHz ISM

band offers 12 non-overlapping channels cf. Figure 2.6. Because of the unregulated nature of ISM bands, interference has always been a key issue for WLANs. Although much work has been done on various aspects of interference, studies have generally focused on interference between other systems that use the same ISM bands, such as Ultra Wideband (UWB) systems [6], Bluetooth devices [7] [8], government radars [9], microwaves [10] and other WLANs operating on the same channel [7], [11], [12]. An aspect generally not considered, but of increasing importance as the number of WLAN systems increases, is the interference from nearby WLANs operating on standard defined non-overlapping channels. This may happen because standard defined non-overlapping channels are not truly non-overlapping, but are based on limits set on the transmit signal spectrum (cf. Figure 2.7) and a maximum transmit power level per channel. The power spectra of WLANs are allowed to overlap into 'non-overlapping' channels because WLANs are not designed to work so close to each other that their coverage areas severely overlap. With sufficient distance between APs, pathloss should render this interference negligible. By permitting this overlap, lesser demands are placed on the design of the spectrum limiting techniques that the transmitter employs.

The objective of this work is to perform an in-depth analysis of this interference in indoor environments. We refer to this interference as adjacent channel interference (ACI) from a co-located WLAN. Of particular concern is the case similar to the near-far case often experienced in code division multiple access (CDMA) systems; a situation where two nearby APs that considerably overlap in coverage areas are operating. AP_1 of such a system is transmitting at full power to one of its users. At the same time, AP_2 is receiving from a distant user; one close to the boundary of its coverage area. The received signal from this far away user can be extremely weak because of signal attenuation. Spectral leakage from AP_1 even when it conforms to the spectral requirements of the standard will cause interference into the receiver of AP_2. We analyze various parameters that affect and are affected by this interference. We use the results of this analysis to suggest minimum separation between APs that would reduce this interference to negligible amounts. We also suggest and analyze the effectiveness of several mitigation techniques that can be used to minimize this interference if this minimum separation criterion cannot be met.

This thesis is organized as follows. In Chapter 2, OFDM systems and the advantages they offer for high bit rate transmission in wireless environments are discussed. We also describe requirements for

an OFDM based WLAN to be IEEE 802.11a compliant and the characteristics of an indoor channel environment. In Chapter 3 we describe receiver based performance enhancing alternatives for these systems and describe parameters generally used as WLAN performance measures. Chapter 4 describes the simulation models used in this analysis. In Chapter 5, we formally defined ACI and discuss scenarios where it is most likely to occur. We also investigate parameters that affect the levels of interference into nearby WLANs and describe how the performances of nearby WLANs are degraded. We then present results of extensive simulations of these scenarios and present minimum separation distances for negligible ACI. Finally, in Chapter 6 we conclude by suggesting mitigation techniques that can be used to limit this interference and investigate their effectiveness.

Chapter 2

OFDM Systems and the IEEE 802.11a Standard

2.1 OFDM Systems

Transmission over wireless channels causes time domain spreading of data symbols [13]. Through reflections, refractions, and diffractions from objects in the receiver's surrounding, multiple versions of the transmitted signal arrive at the receiver. Each multipath component arrives at a different time delay (relative to the first signal arrival) and with random amplitude and phase distortions due to different paths that each multipath component takes between the transmitter and the receiver [14]. The time between the arrival of the first and last multipath component is referred to as the delay spread of the channel. The receiver sees a distorted version of the transmitted signal due to the superpositioning of individual multipath components. When the transmit symbol duration is longer than the delay spread of the channel, at a particular time, all arriving multipath components are indistinguishable [13]. The receiver sees only the vector sum of all multipath components arriving within this interval. The frequency response of such a channel is flat across all frequencies and can be represented using a single tap in the channel impulse response [13] .

On the other hand, if the transmit symbol duration is less than the delay spread of the channel, multipath components of the next symbol start arriving well before all multipath components of the current symbol are received. In fact, arriving multipath components are not limited to consecutive symbols and may be of several transmitted symbols. Severe intersymbol interference (ISI) occurs and complex channel equalization techniques are needed to counter ISI at the receiver [15]. For receivers that have to deal with multiple symbol ISI, equalization is the dominating factor in receiver

complexity [3]. In such channel conditions, multipath components are distinguishable and different frequencies are attenuated by different factors. The channel is frequency selective and multiple channel taps are necessary to represent the channel response [13].

High bit rate transmissions over conventional single carrier systems generally encounter frequency selective fading channel conditions because of their short transmit symbol durations. In multicarrier modulation (MCM) systems, instead of transmitting data serially over the entire channel, the channel is divided into several lower rate sub-channels over which data is transmitted in parallel [3]. By transmitting data at lower bit rates over these sub-channels, the transmit symbol duration of each subcarrier can be extended beyond the channel delay spread. With a sufficient number of sub-channels, each sub-channel can be considered frequency flat. Parallel transmissions on all sub-channel ensures bit rate parity with a single carrier system operating on a similar channel. For reliable communication over these parallel sub-channels, individual sub-channels need to be independent and non-interfering. The simplest way this can be achieved is by dividing the channel into frequency non-overlapping channels. However, such a design is non-practical as it is spectrally inefficient [3]. Much greater spectral efficiency is possible if sub-channels are overlapped but made orthogonal to each other to prevent sub-channel interference. MCM systems with orthogonal overlapping frequency sub-channels are called orthogonal frequency division multiplexing (OFDM) systems [16]. Initial OFDM systems were highly impractical as they required banks of sub-channel oscillators and coherent demodulators. In [16], Weinstein and Ebert showed how an OFDM system can be practically implemented in the baseband using the discrete Fourier transform (DFT). The Fourier transformation represents the incoming data symbol as a sum of orthonormal sine waves. Therefore, at the output of the IFFT all incoming data symbols are modulated on a set of orthogonal overlapping subcarriers.

The minimal ISI that OFDM systems experience between successively transmitted symbols can be overcome by inserting a guard interval longer than the delay spread of the channel at the beginning of each symbol [3]. By doing so, all multipath components observed within a symbol duration will be of the same symbol. Theoretically, any signal including no signal at all can be used as the guard interval (GI). However, if OFDM symbols are cyclically prefixed using replicas from the end of the OFDM symbol, orthogonality between subcarriers can be ensured with simplistic receiver design. By removing ISI, the need for complex equalization at the receiver is avoided and a reduction in the

receiver complexity is achieved. The complexity of an OFDM receiver is largely dependent on its DFT block which is generally lower then that of an equalizer, especially when considering that the DFT can be efficiently implemented by using the Fast Fourier Transform (FFT) algorithm [3].

Because of the many advantages OFDM offers for high bit rate transmissions in frequency selective conditions, it is currently being used by several wireless data communication standards, including IEEE 802.11 amendments "a" [1] and "g", HiperlAN/2 [17], the IEEE 802.16 [18]. It is also used in ultra wideband systems [19] and is a strong candidate for fourth generation cellular networks. OFDM technology is also used in high definition terrestrial audio [20] and video broadcast [21] systems and most forms of digital subcarrier line technology [22].

2.1.1 Analytical Model

In deriving expressions for the signal transmitted by an OFDM transmitter, it is convenient to think of the OFDM transmitter as a bank of N subcarrier filters [23] (cf. Figure 2.1). Here N represents the number of sub-channels. The baseband impulse response of each subcarrier $g_n(t)$ in Figure 2.1 is given by

$$g_n(t) = e^{j2\pi(n-1)\left(\frac{t}{NT}\right)} \sum_{k_o=-\infty}^{\infty} \delta(t - k_o T) = \sum_{k_o=-\infty}^{\infty} e^{j2\pi(n-1)\left(\frac{k_o}{N}\right)} \delta(t - k_o T) \tag{2.1}$$

where $n \in [1 \ldots N]$ is the subcarrier index, k_o is the discrete sampling index, $\sum_{k_o=-\infty}^{\infty} \delta(t - k_o T)$ is an impulse train with impulses spaced by the subcarrier sampling time T, $e^{j2\pi(n-1)\left(\frac{t}{NT}\right)}$ represents modulation with frequency $(n\text{-}1)/NT$.

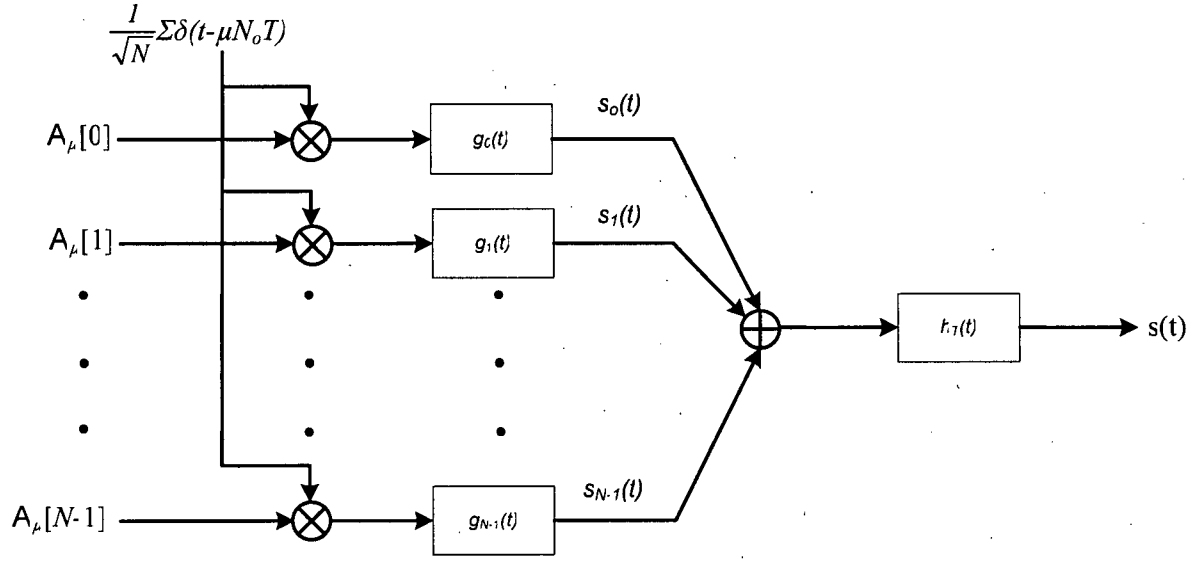

Figure 2.1: Filter bank representation of an OFDM transmitter [24]

Complex-valued modulated data symbols $A_\mu[n]$ taken from symbol set X are modulated onto subcarriers through multiplication with the filter response of the nth subcarrier. Each subcarrier is modulated with a single data symbol.

$$x_n(t) = \sum_{\mu=-\infty}^{\infty} \frac{1}{\sqrt{N}} A_\mu[n-1] g_n(t-\mu N_o T) \tag{2.2}$$

where μ is the index of the OFDM symbol, $N_o = (N+P)$, N is the number of subcarriers and P is the number of cyclic prefix symbols. The total duration of OFDM symbol μ, is then given by $N_o T$.

We assume that all subcarriers are modulated with data symbols from the same symbol set X. For a general OFDM system it is not necessary that all subcarriers be modulated with symbols from the same symbol set. In fact, system performance can greatly be enhanced if individual subcarriers are modulated with data constructed from a signal set that changes based on sub-channel channel conditions [25]. However, in IEEE 802.11a systems all data subcarriers are modulated with data from the same symbol set and we make the same assumption. The resulting continuous time OFDM symbol can be expressed as

$$x(t) = \left[\sum_{n=1}^{N} x_n(t)\right] * h_T(t) = \left[\frac{1}{\sqrt{N}} \sum_{n=1}^{N} \sum_{\mu=-\infty}^{\infty} A_\mu[n-1] g_n(t-\mu N_o T)\right] * h_T(t) \tag{2.3}$$

where * represents convolution, and $h_T(t)$ is the pulse shaping transmit filter. In general raised cosine window is used for symbol shaping in OFDM WLAN systems, cf. Section 3.4.2

Substituting (2.1) into (2.3),

$$x(t) = \left[\sum_{n=1}^{N} \frac{1}{\sqrt{N}} \sum_{\mu=-\infty}^{\infty} A_{\mu}[n-1] \sum_{k_o=-\infty}^{\infty} e^{j2\pi(n-1)\frac{k_o}{N}} \delta(t - k_o - \mu N_o T) \right] * h_T(t) \tag{2.4}$$

Rearranging (2.4), $s(t)$ can be written as

$$x(t) = \left[\sum_{\mu=-\infty}^{\infty} \sum_{k_o=-\infty}^{\infty} \delta(t - k_o - \mu N_o T) \left(\frac{1}{\sqrt{N}} \sum_{n=1}^{N} A_{\mu}[n-1] e^{j2\pi(n-1)\frac{k_o}{N}} \right) \right] * h_T(t) \tag{2.5}$$

In (2.5), $\frac{1}{\sqrt{N}} \sum_{n=0}^{N-1} A_{\mu}[n-1] e^{j2\pi n \frac{k_o}{N}}$ represents the discrete time signal after IFFT transformation and may be represented simply as $a_{\mu}[k_o]$, the discrete time transmit samples. Furthermore, since the IFFT is circularly periodic, and all values of k_o outside the interval [0, N-1] are identical to sample values obtained by modulo reduction by N, the cyclic prefix indices can be incorporated into (2.5)

$$x(t) = \left[\sum_{\mu=-\infty}^{\infty} \sum_{k_o=-\infty}^{\infty} \delta(t - k_o - \mu N_o T) \left(\frac{1}{\sqrt{N}} \sum_{n=1}^{N+P} A_{\mu}[n-1] e^{j2\pi(n-1)\frac{k_o}{N}} \right) \right] * h_T(t) \tag{2.6}$$

The transmitted OFDM signal can be expressed as

$$x(t) = \left[\sum_{\mu=-\infty}^{\infty} \sum_{k_o=-\infty}^{\infty} \delta(t - k_o - \mu N_o T) a_{\mu}[k_o] \right] * h_T(t) \tag{2.7}$$

2.2 The Indoor WLAN Channel

The random phase and amplitude distortion that a multipath component experiences also changes with time. The relative motion of the receiver, transmitter or objects in the surroundings will vary multipath components and also their amplitude and phase distortions. The time during which the multipath channel remains invariant is referred to as the coherence time of the channel. If the transmit

symbol duration is less than the coherence time of channel, the channel is said to be slowly fading or quasi-static. On the other hand if the duration of the transmit symbol duration is greater than the coherence time of the channel the channel is a fast fading channel.

As specified in [26] and [27] the indoor wireless channel can be characterized as highly frequency selective, and slowly varying with time. Because of the presence of several objects in the path between the transmitter and the receiver, several multipath components arrive at the receiver. Moreover, the power delay profile or the average receiver power of multipath components can be characterized as exponentially decaying. In addition to this, due to the small antennas and many objects in the surrounding there is generally no line of sight (LOS) component present. The distribution of the amplitude can therefore be taken as Rayleigh faded [15]. The phase distortion is generally taken as uniformly distributed as multipath components may arrive from any angle. Because of low mobility of users and objects in the surroundings, time variations of the channel are small and the indoor wireless channel is usually characterized as slow faded or quasi-static. For OFDM systems, the extended subcarrier transmit symbol duration is assumed to be shorter then the coherence time of the channel and the channel characteristics are constant over the duration of an OFDM symbol.

OFDM systems have the ability to turn frequency selective channel conditions into small frequency flat sub-channels. The receiver symbol on sub-channel n can then be expressed as:

$$r_n = \alpha_n e^{-j\Phi_n} x_n + w_n = C_n x_n + w_n \tag{2.8}$$

Where α_n is the Rayleigh distributed channel attenuation, Φ_n is a uniformly distributed phase distortion, and C_n is the complex channel frequency response on subcarrier n

In our simulation model of the indoor WLAN channel, quasi-static fading is modeled using the exponentially decaying power delay profile (PDP) of Channel A given in [28]. Channel A has been designed to model typical office environments for HiperLAN/2 systems through extensive measurements and analysis. Since Hiperlan/2 is the European equivalent of IEEE 802.11a systems and, as done in [29], we use it to model indoor channel conditions for our IEEE 802.11a based WLAN. Channel A is a simplified model of the Saleh-Valenzuela indoor model [27] as the number

of channel taps is fixed and the time separation between taps is equal. The root mean square (rms) delay spread is 50 ns. Table 2.1 below shows the PDP of Channel A. Each individual channel tap is an independent complex zero-mean Gaussian random process with variance defined by the PDP.

In packet based transmission systems the channel is assumed to be time invariant for the duration of the entire packet and not only the symbol.

Table 2.1: PDP of channel model A [28] obtained by interpolating to 50 ns intervals

Tap Number	Delay (ns)	Average Relative Power (dB)
0	0	0
1	50	-4.3
2	100	-5.98
3	150	-8.01
4	200	-12.5
5	250	-14.28
6	300	-18.59
7	350	-22.98

2.3 The IEEE 802.11a Standard [1]

The IEEE 802.11 standard [1] defines the medium access control (MAC) and physical (PHY) layers of wireless local area networks (WLANs). The MAC layer is primarily responsible for controlling access and permission to transmit on the shared channel. The PHY layer specifies the mechanisms used to transmit and receive over the channel. Based on its functionality, the PHY layer can be divided into three sublayers: (1) the physical layer convergence protocol (PLCP) sublayer, (2) the physical medium dependent (PMD) sublayer, and (3) the PHY layer management entity (PLME). The PLCP sublayer is responsible for data related communications between the MAC and PHY layers and is designed to minimize the MAC layer's dependence on the PMD sublayer. By doing so the same MAC layer can be used with different PMD PHY sublayers. The PMD sublayer defines the actual mechanisms used to transmit and receive data between users. Finally, the PLME manages all local PHY layer functions with the help of the MAC layer management entity. In the following section, specifications for the OFDM PHY layer as defined by the IEEE 802.11a standard are described. Moreover, only specifications relevant to the development of a baseband model and necessary for an analysis of interference between WLANs are defined. Complete PHY layer specifications can be found in [1] and [2].

2.3.1 Coding, Interleaving and Modulation

The IEEE 802.11a standard [1] allows for variable transmission bit rates. These transmission rates are the result of different coding and modulation combinations that can be used on the data bits that needs to be transmitted. We refer to these different combinations of coding and modulation as possible modes of transmission. The 802.11a standard defines eight valid modes that can be used. Table 2.2 below list these modes and other rate dependent parameters. Only one mode is used for all data bits in a packet, but it can change from one packet to the next. For all modes, normalized grey labeled signal constellations are considered. Normalizing factors for the modulation schemes are given in Table 2.2.

Table 2.2: Rate dependent parameters

Mode	Bit Rate (Mbps)	Modulation Type	Modulation Normalizing co-efficient	Coding Rate	Puncture Vector	Coded Bits per Subcarrier (N_{BPSC})	Coded Bits per OFDM Symbol (N_{CBPS})	Data Bits Per OFDM Symbol
1	6	BPSC	1	1/2	$\begin{bmatrix}1\\1\end{bmatrix}$	1	48	24
2	9	BPSK	1	3/4	$\begin{bmatrix}1 & 1 & 0\\1 & 0 & 1\end{bmatrix}$	1	48	36
3	12	QPSK	1/√2	1/2	$\begin{bmatrix}1\\1\end{bmatrix}$	2	96	48
4	16	QPSK	1/√2	3/4	$\begin{bmatrix}1 & 1 & 0\\1 & 0 & 1\end{bmatrix}$	2	96	72
5	24	16-QAM	1/√10	1/2	$\begin{bmatrix}1\\1\end{bmatrix}$	4	192	96
6	32	16-QAM	1/√10	3/4	$\begin{bmatrix}1 & 1 & 0\\1 & 0 & 1\end{bmatrix}$	4	192	144
7	48	64-QAM	1/√42	2/3	$\begin{bmatrix}1 & 1\\1 & 0\end{bmatrix}$	6	288	192
8	54	64-QAM	1/√42	3/4	$\begin{bmatrix}1 & 1 & 0\\1 & 0 & 1\end{bmatrix}$	6	288	216

2.3.1.1 Forward Error Correction

The forward error correction scheme specified in the standard is convolutional encoding. A fixed convolutional encoder is used and different coding rates are obtained through puncturing the output of the encoder. The specifications of the convolutional encoder are: constraint length $K = 7$, number of inputs $k = 1$, number of outputs $n = 2$, and rate $R = 1/2$ with generator polynomials, $g_1 = [1\ 0\ 1\ 1\ 0\ 1\ 1]$ and $g_2 = [1\ 1\ 1\ 1\ 0\ 0\ 1]$ or in octal form [133, 171]. Figure 2.2 below shows the convolutional encoder. Puncture vectors for coding rates of 2/3 and 3/4 are given in Table 2.2. The first row corresponds to the puncture vector of the first output branch of the encoder.

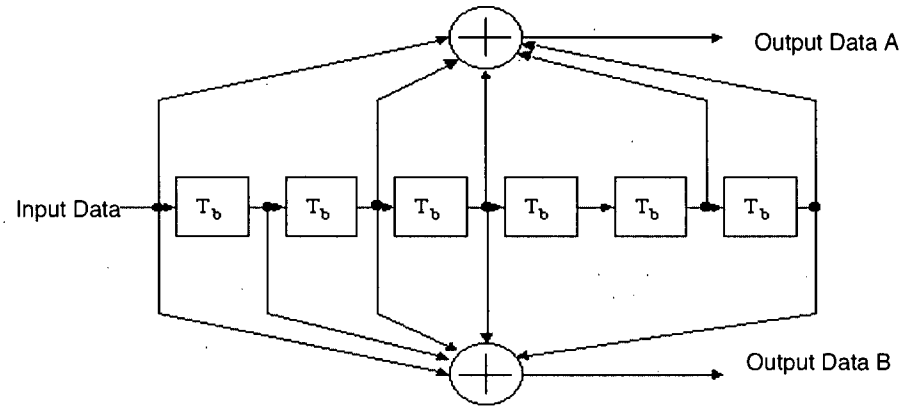

Figure 2.2: IEEE 802.11a convolutional encoder with generator polynomials (133, 171) [1]

2.3.1.2 Interleaving/Deinterleaving

The 802.11a standard prescribes bitwise interleaving of the encoded bits. A two step procedure for interleaving and deinterleaving is used. The first permutation is defined by

$$i = \left(\frac{N_{CBPS}}{16}\right) \bmod (k,\ 16) + \text{floor}\left(\frac{k}{16}\right) \quad \forall\, k \in [0:\ N_{CBPS} - 1] \tag{2.9}$$

where mod is the modulo operation, i is the index after the first permutation, k is the index of the code sequence before any permutations and N_{CBPS} is the number of coded bits per OFDM Symbol. Values for N_{CBPS} are given in Table 2.2.

The second permutation is defined by

$$j = s\text{floor}\left(\frac{i}{s}\right) + \text{mod}\left(s, \left(I + N_{CBPS} - \text{floor}\left(\frac{16i}{N_{CBPS}}\right)\right)\right) \quad \forall\ i \in [0: N_{CBPS} - 1] \tag{2.10}$$

where j is the index after the second permutation, s = max (N_{BPSC}/2, 1) and N_{BPSC} is the number of coded bits per subcarrier. The values for N_{BPSC} are also given in Table 2.2.

The deinterleaving permutations are given by

$$i = s\,\mathrm{floor}\left(\frac{j}{s}\right) + \mathrm{mod}\left(\left(j + \mathrm{floor}\left(\frac{16j}{N_{CBPS}}\right)\right), s\right) \quad \forall\ j = [0: N_{CBPS} - 1] \tag{2.11}$$

$$k = 16i - (N_{CBPS} - 1)\,\mathrm{floor}\left(\frac{16i}{N_{CBPS}}\right) \quad \forall\ i = [0: N_{CBPS} - 1] \tag{2.12}$$

In all permutations, indices are defined for a block size equal to the number of coded bits per OFDM symbol. Therefore, interleaving/deinterleaving is only across one OFDM symbol.

2.3.2 OFDM Frame Format

The transmitted OFDM packet, referred to as a PLCP protocol data unit (PPDU) is composed of OFDM data symbols prefixed with header symbols defined by the PLCP sublayer. Header symbols are used in the transmission and demodulation of the attached OFDM data symbols at the receiver. The number of header symbols is fixed for each PPDU frame but the number of attached data OFDM symbols is variable. The format of a PPDU frame is shown in Figure 2.3.

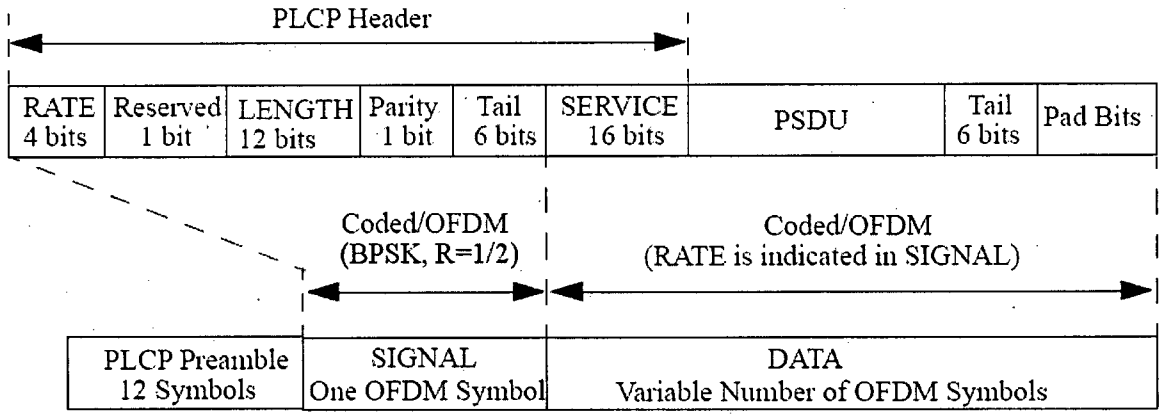

Figure 2.3: IEEE 802.11a PPDU frame format

2.3.2.1 PLCP Header

The PLCP header is composed of 12 preamble symbols, one OFDM SIGNAL symbol and service symbols that extend into the OFDM data field of the PPDU frame. Preamble symbols are composed of 10 short and 2 long training sequences. Training symbols are used for PPDU detection, active gain control (AGC), time/frequency synchronization, and channel estimation at the receiver. Each short

training sequence is 0.8 μs long while each long training sequence is 3.2 μs long. Collectively the training period of an OFDM frame is 16 μs, or equivalently, the length of four data carrying OFDM symbols. The GI of OFDM training symbols is twice as long as the GI of the OFDM data symbols. However, the GI is added to every two training OFDM symbols. The OFDM SIGNAL symbol carries control information is needed for demodulating the attached data OFDM symbols at the receiver. All data in the PLCP Header is transmitted using Mode 1, BPSK modulation with rate ½ encoding; as this mode provides the highest protection against channel induced errors.

Short Training OFDM Symbols

Short training sequences are generated by modulating the following sequence onto the subcarriers, p.short_training_seq = {0 0 1+1j 0 0 0 -1-1j 0 0 0 1+1j 0 0 0 -1-1j 0 0 0 -1-1j 0 0 0 +1+1j 0 0 0 0 0 0 0 -1-1j 0 0 0 -1-1j 0 0 0 1+1j 0 0 0 1+j 0 0 0 1+1j 0 0 0 1+1j 0 0 }. Subcarrier indices are described in the data OFDM symbols section. Only 12 subcarriers are used. To normalize the average power of the resulting OFDM symbol the sequence is multiplied by a factor of $\sqrt{\frac{52}{2(12)}} = \sqrt{\frac{13}{6}}$. The sequence above is used to generate training sequences for the duration of an FFT period, and will generate four short training sequences. Two such short training sequences are used to generate 8 short training symbols. The remaining two short training symbols are generated when the cyclic GI is prefixed to the two short training sequences.

Long Training OFDM Symbols

Two long training symbols are also transmitted with each OFDM frame. The sequence used to generate the long training sequence is, p.long_training_seq = [1 1 -1 -1 1 1 -1 1 -1 1 1 1 1 1 1 -1 -1 1 1 -1 1 -1 1 1 1 1 0 1 -1 -1 1 1 -1 1 -1 1 -1 -1 -1 -1 1 1 -1 -1 1 -1 1 -1 1 1 1 1 1]. As in the case of data OFDM symbols, 52 subcarriers are modulated while a zero is modulated onto the DC subcarrier. The remaining subcarriers are zero padded as done for Data OFDM subcarriers. Two long training sequences are transmitted in each PPDU frame. A cyclic GI is prefixed to the two long training sequences.

OFDM SIGNAL Symbol

The OFDM SIGNAL symbol, shown in Figure 2.4, has three fields: the rate, length, and the signal tail. The first four bits, 0-3, of the rate field specify the mode used to construct the data symbols. Bit 4 is reserved for future use. Table 2.3 lists the bits sequences that represent each mode. The length field is a 12 bit unsigned integer that indicates how many bytes of data are being transmitted in the frame. Bit 17 is an even parity bit for the first 0-16 bits of the OFDM symbol field. Zeros are transmitted on all six bits of the tail field.

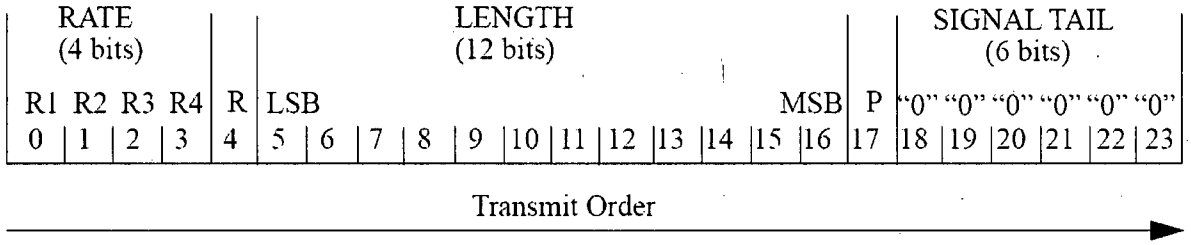

Figure 2.4: OFDM SIGNAL symbol frame format [1]

Table 2.3: Bit sequences for the rate field of the OFDM SIGNAL symbol

Mode	Bit Rate (MB/s)	Bit sequence (R1-R4)
1	6	1101
2	9	1111
3	12	0101
4	16	0111
5	24	1001
6	32	1011
7	48	0001
8	54	0011

2.3.2.2 Data Field

PLCP Header Service Field

The Service Field of the PLCP header extends into the data field of the PPDU frame. It is composed of 16 bits. Bits 0-6 are used to synchronize the scrambler at the receiver. The remaining bits are reserved for future use. All reserve bits are set to zero.

PSDU

The PSDU field contains the data stream passed down from the MAC layer to be transmitted in the current packet. The PSDU data stream needs to be zero padded to ensure it is a multiple of N_{DPSC}. At least six zeros need to be padded onto the PSDU data stream to accommodate the six zero tail bits of the data field. This data stream is modulated onto data OFDM symbols prior to fitting into the PPDU frame. After encoding, puncturing, interleaving, and symbol mapping, the modulated complex data symbols stream is reshaped into 48 data streams for parallel transmission. In a data OFDM symbol only 48 out of a total of 64 subcarriers are used to transmit data. Data symbols, d_n are modulated onto subcarriers at positions [-26:-22 -20:8 -6:-1 1:6 8:20 22:26]. The positions, n, are referenced with respect to the central subcarrier, DC. Four pilots symbols P_n are inserted at positions [-21 -7 7 21]. A zero is transmitted on the DC subcarrier to prevent D/A and A/D conversion complexities. The remaining 11 subcarriers are zero padded to lower out of band spectrum and to allow for the implementation of practical filters. The format of a data OFDM symbol is shown in Figure 2.5.

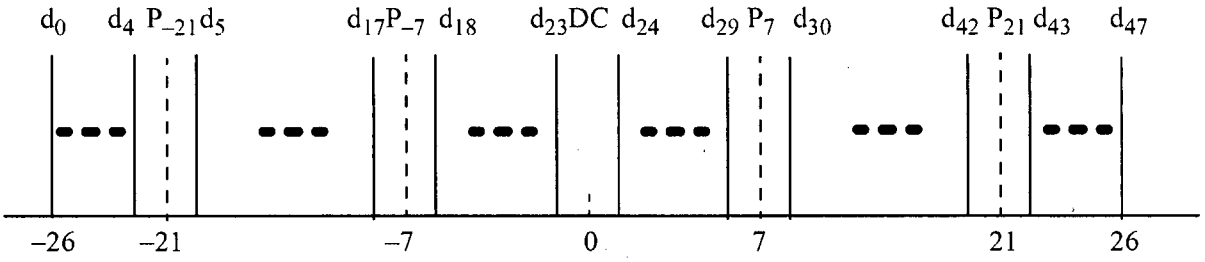

Figure 2.5: IEEE 802.11a OFDM data symbol format [1]

The resulting 64 modulated subcarriers are passed through the IFFT block to form a time domain OFDM data symbol. An IFFT of period 3.2 μs is specified in the standard with subcarriers spaced at 0.3125 MHz. A cyclic guard interval (GI) of ¼ the length of an OFDM symbol is prefixed to the time domain OFDM data symbol to form the transmitted OFDM data symbol. The duration of the transmitted OFDM data symbol including the guard interval is 4μs. This along with other time related parameters of the PPDU frame are listed in Table 2.4 below. These transmitted OFDM data symbols are then fitted into the PSDU subfield of the Data field of the PPDU frame.

Table 2.4: IEEE 802.11a time dependent parameters [1]

Parameter	Value
N_{SD}: Number of data subcarriers	48
N_{SP}: Number of pilot subcarriers	4
N_{ST}: Number of subcarriers, total	52 ($N_{SD} + N_{SP}$)
Δ_F: Subcarrier frequency spacing	0.3125 MHz (=20 MHz/64)
T_{FFT}: IFFT/FFT period	3.2 μs ($1/\Delta_F$)
$T_{PREAMBLE}$: PLCP preamble duration	16 μs ($T_{SHORT} + T_{LONG}$)
T_{SIGNAL}: Duration of the SIGNAL BPSK-OFDM symbol	4.0 μs ($T_{GI} + T_{FFT}$)
T_{GI}: GI duration	0.8 μs ($T_{FFT}/4$)
T_{GI2}: Training symbol GI duration	1.6 μs ($T_{FFT}/2$)
T_{SYM}: Symbol interval	4 μs ($T_{GI} + T_{FFT}$)
T_{SHORT}: Short training sequence duration	8 μs ($10 \times T_{FFT}/4$)
T_{LONG}: Long training sequence duration	8 μs ($T_{GI2} + 2 \times T_{FFT}$)

Tail Bits

Six zero bits are inserted to return the convolutional encoder to the zero state.

Zero Pad

The complete data field is zero padded to make it a multiple of N_{CBSC}. The number of zeros padded, N_{PAD} is calculated using:

$$N_{SYM} = \text{Ceiling}\left((16 + 8LENGTH + 6)/N_{DBPS}\right) \quad (2.13)$$

$$N_{DATA} = N_{SYM} \; N_{DBPS} \quad (2.14)$$

$$N_{PAD} = N_{DATA} \; (16 + 8 \times LENGTH + 6) \quad (2.15)$$

where $LENGTH$ is the original length of the PSDU data stream, N_{SYM} is the number of OFDM Data symbols in the PPDU frame and N_{DATA} is the total number of bits in the data field.

2.3.3 IEEE 802.11a Spectral Requirements

The bandwidth of the transmit OFDM signal is 16.6 MHz. All components of a WLAN transmit and receive on one 20 MHz channel.

2.3.3.1 Valid Operating Channels

The actual channelization of the 5 GHz ISM band into channels for WLANs is subject to radio spectrum regulatory bodies in the geographic specific domain. Although no licensing is required to transmit in these bands, mandatory regulations are defined by the standard to limit inter-system interference and permit the coexistence of neighboring WLANs. In the US, the Federal Communications Commission (FCC) is the governing body. The FCC defines 12 non-overlapping 20 MHz channels in the 5 GHz ISM band. In the US the 5 GHz ISM band is formally referred to as the 5 GHz Unlicensed National Information Infrastructure (U-NII) band, see Figure 2.6. The central frequencies, f_c, of these channels are given in Table 2.5. Channels in the middle and upper U-NII bands are generally used for outdoor systems while channels in the lower U-NII band are reserved for indoor WLANs.

Table 2.5: Valid operating channels in the 5GHz U-NII band [1]

Regulatory domain	Band (GHz)	Operating channel numbers	Channel center frequencies (MHz)
United States	U-NII lower band (5.15–5.25)	36 40 44 48	5180 5200 5220 5240
United States	U-NII middle band (5.25–5.35)	52 56 60 64	5260 5280 5300 5320
United States	U-NII upper band (5.725–5.825)	149 153 157 161	5745 5765 5785 5805

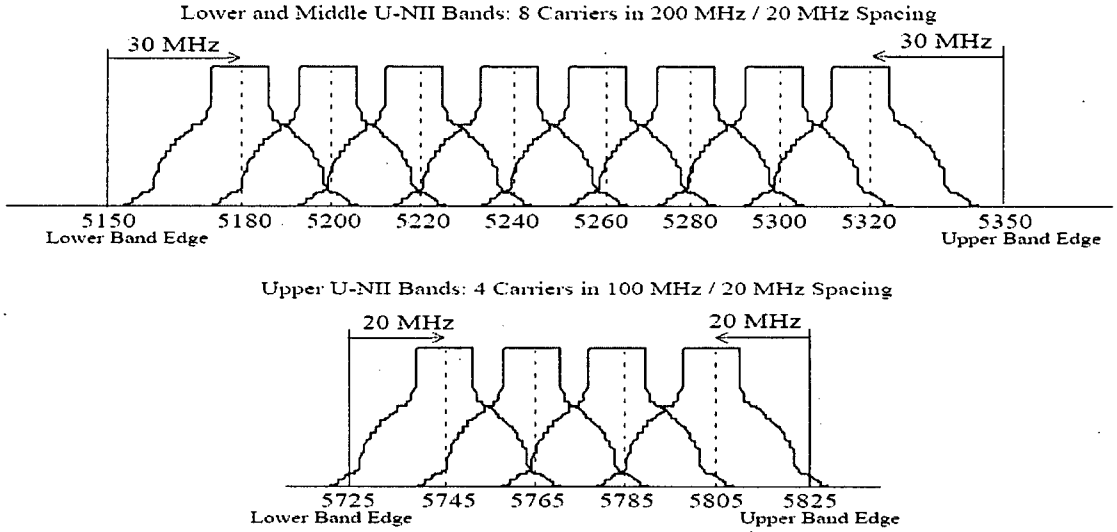

Figure 2.6: Frequency channels in the 5 GHz UNII band in the US [1]

2.3.3.2 Spectrum MASK and Maximum Transmit Power

The standard defined limits on the transmit signals spectrum are in the form of a spectral mask, cf. Figure 2.7, over the power spectral density of the transmitted signal and a maximum transmit signal power limit for a channel. Spectrum mask limits are defined over a range of ± 30 MHz of the channel's central frequency, f_c. The power spectral density must be 0 dBr (dB relative to the maximum spectral density of the signal) for frequencies within ± 9 MHz of f_c, -20 dBr at ± 11 MHz of f_c, -28dBr at ± 20 MHz of f_c and -40 dBr at ±30 MHz and higher frequencies from f_c. The maximum transmit power differs for different U-NII bands and are given in Table 2.6.

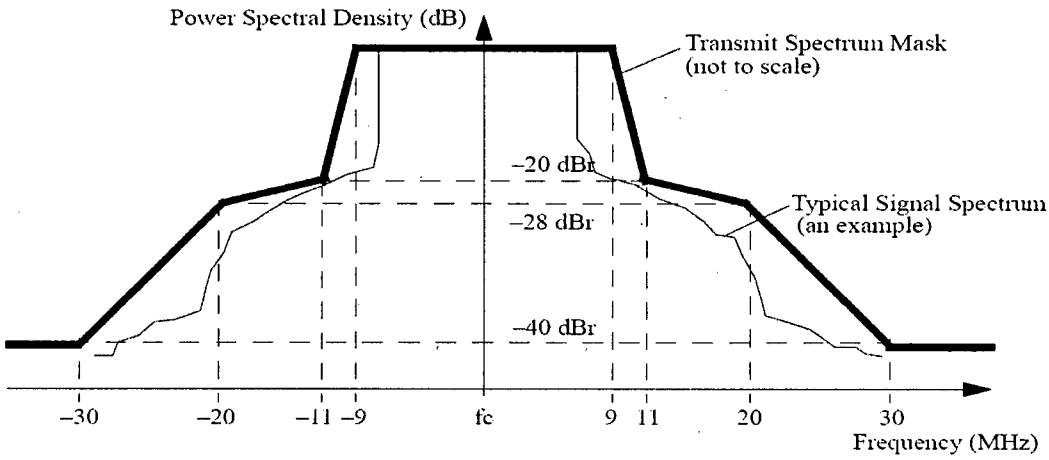

Figure 2.7: Typical OFDM transmit signal spectrum and IEEE 802.11a spectrum mask [1]

2.3.3.3 Transmitter Spectral Flatness

The average power of each subcarriers within the subcarrier positions [-16,-1] and [1, 16] should not deviate more than ±2 dB of the total average power of all subcarriers within these limits. For subcarriers within positions [-27,-17] and [17-27] the average power of individual subcarriers should not deviate more then +2/-4 dB from the average power of subcarriers between [-16,-1] and [1, 16].

Table 2.6: Transmit Power Levels for the North America in the 5 GHz ISM band [1]

Frequency Band(GHz)	Maximum Output Power with up to 6 dBi Antenna Gain (mW)
5.15-5.25	40
5.25-5.35	200
5.725-5.825	800

2.3.4 Receiver Specifications

The actual implementation of the receiver is left to the developer. However, specifications are prescribed in terms of minimum sensitivities and tolerance limits. In the IEEE 802.11a standard [1], the 10 % packet error rate (PER) for a PSDU packet size of 1000 bytes is defined as the minimum operational requirement for a particular mode. If performance falls below this level, the system must switch to a lower mode that's PER conforms to this criterion. The minimum sensitivity of an OFDM receiver is defined in Table 2.7. A receiver must be able to detect signals with the indicated power levels for each mode. For decoding purposes a Viterbi decoder is recommended. Several other PHY layer specifications are also defined in [1], however, we are interested in requirements for baseband simulation only.

Table 2.7: Minimum receiver sensitivity for data rates of IEEE 802.11a [1]

Data Rate (Mbps)	Receiver Minimum Sensitivity (dBm)
6	-82
9	-81
12	-79
18	-77
24	-74
36	-70
48	-66
54	-65

Chapter 3

General Theory

3.1 Bit Interleaved Coded Modulation

In the design of band-limited wireless communications systems, coding and modulation is used to improve performance; coding adds controlled redundancy to the transmitted signal, providing much needed error protection while using higher non-binary modulation schemes increases the maximum allowable transmission rate. However, coding increases bandwidth requirements if the information transmission rate is kept the same and the use of higher order modulation schemes lowers error resilience at a given Signal-to-Noise Ratio (SNR). Furthermore, an increase in coding or modulation increases receiver complexity. The interdependence of these parameters necessitates the joint optimization of coding and modulation schemes for band-limited wireless channels. Although any coding scheme can be used in conjunction with any modulation scheme, for the rest of this discussion we focus on convolutional coding and Binary/Quaternary phase shift keying (BPSK/QPSK) and 16/64-Quadrature Amplitude Modulation (16/64 QAM), as these are used in the IEEE 802.11a standard [1].

3.1.1 Background

In [30], Ungerboeck introduced Trellis Coding Modulation (TCM) as an efficient means of transmitting coded data over band-limited AWGN channels. TCM schemes use higher order non-binary modulation schemes with binary codes designed for maximizing the minimum Euclidean distance between consecutive symbols. Through symbol set expansion and set-partitioning labels, pairs of codewords are mapped to symbol points with maximum possible Euclidean distance between them, thereby, ensuring that the transmitted sequence has maximum Euclidean distance between consecutive symbols. In AWGN channels, where code performance is dominated by the minimum

Euclidean distance [30], TCM systems achieve significantly higher performance compared to uncoded higher order modulation systems. However, TCM schemes deployed in multipath environments are unable to replicate the same success. Transmission over multipath channels correlates consecutive symbols. For optimum decoding the Viterbi decoder expects independently distorted input symbols [15]. This channel induced correlation results in bursts of error at the decoder's output.

Symbol based interleaving was proposed to break the correlation between consecutive symbols and restore independence at the Viterbi decoder's input. In [31], Divsalar analyzed the performance of coded systems in fading channels with symbol based interleaving/deinterleaving. He showed that unlike in AWGN channels, error events that dominate performance in fading channels depend more on the minimum Hamming distance, the Code Diversity, of the code than on the minimum Euclidean distance. These results were particularly true for high SNR Rayleigh fading channels, conditions typical of WLAN environments [32].

Symbol interleaved TCM systems suffer from two main problems. First, TCM codes optimized for both Hamming and Euclidean distances are extremely difficult to design and with increasing code length, receiver's complexity increases considerably. Second, the coding gain achievable by symbol interleaved TCM systems is limited to the number of distinct symbols between two codewords [33]. This implies that the diversity of the system can only be increased by designing the code to avoid parallel transitions or by increasing the constraint length of the code. In [33], Zehavi proposed Bit Interleaved Coded Modulation (BICM) as an alternative mechanism to increase the diversity order of coded modulation schemes in fading channels. By inserting a bit-wise interleaver between the coding and modulation blocks, he showed that the diversity order of the code can be increased to the minimum number of bits rather than the number of distinct channel symbols. Furthermore, by separating the coding from the modulation he was able to use codes optimized for Hamming distances. By doing so, he was able to achieve the full diversity order of the underlying code and at the same time, use readily available well established codes.

Zehavi's analysis was limited to the case of an 8-PSK system in Rayleigh fading environments. In [34], Caire extended BICM analysis to other modulation and coding schemes. In particular, tools and

techniques for analyzing the BER performance for any combination of coding and modulation were defined. We use these to study the BER and packet error rate (PER) performance of BICM as used in IEEE 802.11a systems.

3.1.2 Branch Metrics for the Viterbi Decoder of a BICM OFDM System

The following discussion is based on Caire's paper [34]. In deriving the bit metrics for the Viterbi decoder, the equations in [34] are modified for an OFDM system. A BICM system can be formed by serially concatenating a binary encoder of code C, a bitwise interleaver π, and an N-dimensional memoryless modulator of cardinality , $X = M = 2^m$ which has a one-to-one mapping function, μ, between all possible code words and symbol points on the constellation. Figure 3.1, shows the basic blocks of a BICM system.

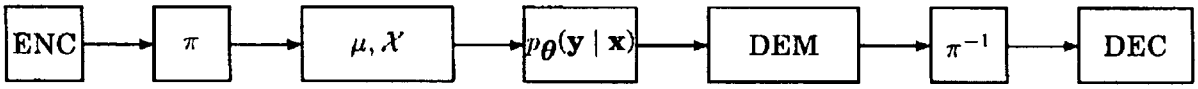

Figure 3.1: Block diagram of a BICM system [34]. π denotes a bit-wise interleaver

Incoming binary information bits are passed through the encoder to form the coded sequence, $\boldsymbol{c}$. This encoded sequence is interleaved $\pi(\boldsymbol{c})$ and broken down into sequences of m bits. The modulators mapping function maps these m bit sequences to points on the symbol constellation, $\mu : \{ 0, 1 \}^m \rightarrow X$. The resulting sequence of symbols, x is transmitted over the channel. There is a one-to-one correspondence between the transmitted bits and the interleaved bits, π: $k \rightarrow (k', i)$. Where k is the time ordering of the modulated bits, k' is the time ordering of the modulated symbol $\boldsymbol{x}_{k'}$ and i is the position of bit c_k in the label of $x_{k'}$. Here, the label of $x_{k'}$ refers to the bit sequence of the symbol transmitted at time $t_{k'}$. Caire [34] and Goff [35] show that Grey labeling provides the best results for non-iterative optimal decoding. For OFDM systems, coding and modulation is preformed in the frequency domain. It would be more appropriate to use subcarrier indices rather than time indices. The one-to-one mapping between the transmitted bits and the interleaved bits can then be expressed as π: $k \rightarrow (n, i)$, where, n is the subcarrier index.

We define $l^i(x)$ as the *ith* bit in the label of the modulated symbol x, X_b^i as the subset of X which have bit $b \in \{0, 1\}$ at their *ith* position and y as the channel output resulting from the transmission of x.

The conditional probability of y given $l^i(x) = b \in \{0, 1\}$ and the channel state information, θ can is

$$p_\theta(y \mid l^i(x) = b) = \sum_{x \in X} p_\theta(y \mid x) P(x \mid l^i(x)) \tag{3.1}$$

However, given $l^i(x)$, the conditional probability of x is

$$p_\theta(x \mid l^i(x) = b) = \begin{cases} 0 & \text{if } l^i(x) = \overline{b} \\ \dfrac{1}{2^{(m-1)}} & \text{if } l^i(x) = b \end{cases} \tag{3.2}$$

where $\overline{b}$ denotes the complement of bit b. Since only half the symbols in X have b in the *ith* position and any symbol in the subset that has b in their *ith* position is equally likely as we assume incoming bits are equally likely, $P(b = 0) = P(b = 1) = ½$.

In addition to this, the conditional probability of y, given $l^i(x)$ is the same as if x was given

$$p_\theta(y \mid l^i(x) = b) = p_\theta(y \mid x) \tag{3.3}$$

Substituting (3.2) and (3.3) in (3.1)

$$p_\theta(y \mid l^i(x) = b) = \frac{1}{2^{(m-1)}} \sum_{x \in X_b^i} p_\theta(y \mid x) \tag{3.4}$$

At the OFDM receiver, for the *nth* subcarrier, the maximum likelihood demodulator computes the branch metrics

$$\lambda^i(y_n, b) = \log \sum_{x \in X_b^i} p_{\theta_n}(y_n \mid x) \quad i \in \{1, \ldots, m\}, \quad b \in \{0,1\} \tag{3.5}$$

where perfect channel state information is assumed.

The maximum likelihood decoder then makes decisions based on

$$\hat{c} = \max_{c \in C} \sum_k \lambda^i(y_n, c_k) \tag{3.6}$$

Where $\hat{c}$ is the estimated transmitted code sequence.

However, for practical systems the branch metrics in (3.5) may be too computationally intense to implement. Zehavi and Caire suggest sub-optimum metrics which can be used. These sub-optimum metrics are derived from the log sum approximation, $\log \sum_j z_j \cong \max_j \log(z_j)$.

The branch metrics in (3.5) can then be replaced by these sub-optimal branch metrics

$$\tilde{\lambda}^i(y_n, b) = \max_{x_k \in X_b^i} \log(p_{\theta_n}(y_n \mid x) \tag{3.7}$$

3.1.2.1 LLR Metrics from the Received Signal

In an OFDM system, the fade experienced by individual subcarriers is assumed to be frequency non-selective and constant over the duration of a symbol. Mathematically, this can be represented as a random multiplicative process of constant amplitude. In WLAN environments normally there is no line of sight component and this multiplicative fading is taken as Rayleigh distributed. Therefore, the received signal on each subcarrier of an OFDM system, previously derived as (2.8), at time t_k, can be re-written as

$$r_n = C_n x_n + w_n \tag{3.8}$$

where w_n is complex AWGN with a variance of 1, and C_n is the complex channel frequency response seen by the transmitted symbol x_n on subcarrier n.

Assuming ideal interleaving and coherent detection, i.e., the receiver has perfect knowledge of the channel, the conditional probability $p(r_n \mid x)$ can be expressed as [15]

$$p_{\theta_n}(r_n \mid x) = \frac{1}{\pi\sigma^2} \exp\left(\frac{-|r_n - C_n x|^2}{\sigma^2}\right) \tag{3.9}$$

where σ^2 is the variance of the complex AWGN process.

Since we are only interested in maximizing this conditional probability and not evaluating it exactly, by taking the natural logarithm and removing extra terms, maximizing the above equation is equivalent to maximizing [15]

$$p_{\theta n}(r_n \mid x) \equiv -|r_n - C_n x|^2 = -D_{\theta n}(r_n \mid x) \tag{3.10}$$

where $D_{\theta n}(r_n \mid x)$ is defined as a distance metric and is the Euclidean distance between the received symbol, r_n and symbol x in X.

Therefore, maximizing the conditional probability is equivalent to minimizing the distance metrics, $D_{\theta n}(r_n \mid x)$. The suboptimal branch metrics given by (3.7) can then be expressed as,

$$\tilde{\lambda}^i(r_n, b) = \min_{x \in X_b^i} \log\left(D_{\theta_n}(r_n \mid x)\right) = \min_{x \in X_b^i} \log\left(\left|r_n - C_n x\right|^2\right) \tag{3.11}$$

The Viterbi decoder makes a decision in favor of 1 or 0, depending on whether $\tilde{\lambda}^i(r_n, b=1)$ or $\tilde{\lambda}^i(r_n, b=0)$ is greater. Alternatively, and as implemented in our model, the log likelihood ratio (LLR) can be used. By using LLR ratios only one value needs to be stored in the trellis.

$$LLR\ (r_n, i) = \tilde{\lambda}^i(r_n, b=0) - \tilde{\lambda}^i(r_n, b=1) \tag{3.12}$$

The Viterbi decoder decides the *ith* bit is a 0 if LLR $(r_n, i) > 0$ and 1 if LLR $(r_n, i) < 0$

3.1.2.2 LLR Metrics from the Received Signal after Equalization

For higher order constellations, such as 16/64-QAM, the computation of these LLR metrics can still be to computationally intense to implement practically, especially in WLAN receivers, where cost needs to be kept to a minimum. In [36], Tosato derives simplified LLR metrics using the inherent symmetry of Grey labeled higher order square constellations. Channel induced distortions modify the received symbols constellation and the inherent symmetry of the Grey labeled constellation cannot be used. However, if the received symbols are equalized prior to entering the decoder simplifications to these LLR metrics can be made.

The received symbol on the *nth* subcarrier, after single step equalization can be expressed as

$$y_n = x_n + \frac{w_n}{C_n} \tag{3.13}$$

Once again, assuming ideal interleaving and coherent detection, the conditional probability $p(y_n, x)$ can be expressed as [15]:

$$p_{\theta_n}(y_n \mid x) = \frac{1}{\pi\left(\frac{\sigma}{|C_n|}\right)^2} \exp\left(\frac{-|y_n - x|^2}{\left(\frac{\sigma}{|C_n|}\right)^2}\right) \tag{3.14}$$

Maximizing the above equation is equivalent to maximizing the expression,

$$p_{\theta n}(y_n \mid x) \equiv -\frac{|C_n|^2}{2\sigma^2}|y_n - x|^2 \tag{3.15}$$

Normalizing equation (3.15) by $2\sigma^2$ yields

$$p_{\theta n}(y_n \mid x) \equiv -|C_n|^2|y_n - x|^2 = -|C_n|^2 D_{\theta n}(y_n \mid x) \tag{3.16}$$

The LLR in equation (3.12) for the equalized symbols can then be expressed as

$$LLR(y_n, i) = |C_n|^2 \left\{ \min_{x \in X_0^i} \log(|y_n - x|^2) - \min_{x \in X_1^i} \log(|y_n - x|^2) \right\} \tag{3.17}$$

If Grey labeling is used, subsets X_b^i and $X_{\bar{b}}^i$ of the equalized symbols can be separated by either vertical or horizontal boundaries for all values of $i = \{1, \ldots, m\}$. For example, boundaries for 16-QAM are shown in Figure 3.2 below

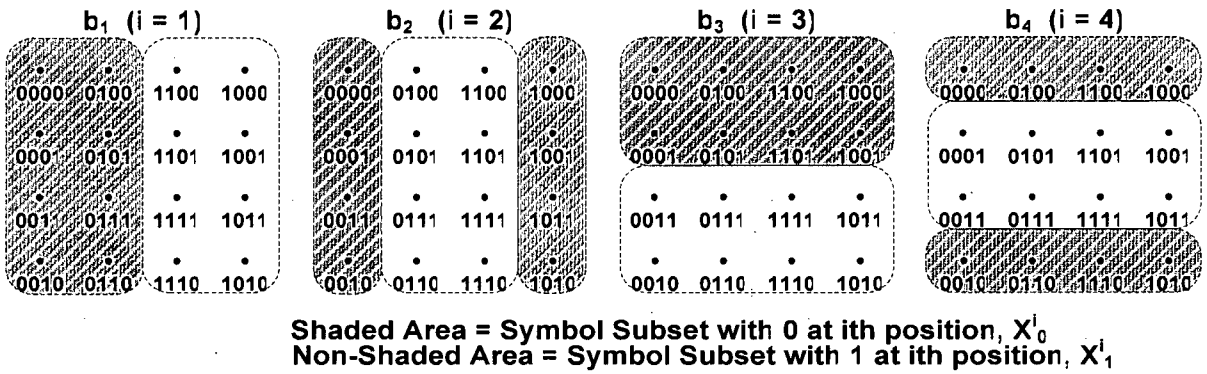

Figure 3.2: Symbol subset boundaries for a Grey labeled 16-QAM constellation

Tosato showed that the two symbol points, one in each subset X_b^i and $X_{\bar{b}}^i$, that were closest in terms of Euclidean Distance from the received symbol lie in the same row if the boundaries are vertical and in the same column if the boundaries are horizontal. Therefore, if the two subsets X_b^i and $X_{\bar{b}}^i$, are separated by vertical boundaries, only the real parts contribute to the LLR. Since the imaginary parts of these two symbols are exactly the same, they can be ignored in the calculation of the LLR metrics. The opposite is true for symbol subsets separated by horizontal boundaries.

Therefore, LLR equation can be rewritten as

$$\begin{aligned} LLR(y_n,i) &= |C_n|^2 \left\{ \min_{x\in\Re\{X_0^i\}} \log\left(|y_n - x|^2\right) - \min_{x\in\Re\{X_1^i\}} \log\left(|y_n - x|^2\right) \right\} \quad \forall i \in \left\{1,\ldots,\frac{m}{2}\right\} \\ LLR(y_n,i) &= |C_n|^2 \left\{ \min_{x\in\Im\{X_0^i\}} \log\left(|y_n - x|^2\right) - \min_{x\in\Im\{X_1^i\}} \log\left(|y_n - x|^2\right) \right\} \quad \forall i \in \left\{\frac{m}{2}+1,\ldots,m\right\} \end{aligned} \tag{3.18}$$

where $\Re(X_1^i)$ is the real part of the complex symbols of subset X_b^i and $\Im(X_1^i)$ is the imaginary part of the complex symbols of subset X_b^i.

If we let,

$$D_I(y_n,i) = \left\{ \min_{x\in\Re\{X_0^i\}} \log\left(|y_n - x|^2\right) - \min_{x\in\Re\{X_1^i\}} \log\left(|y_n - x|^2\right) \right\} \tag{3.19}$$

$$D_Q(y_n,i) = \frac{1}{4}\left\{ \min_{x\in\Im\{X_0^i\}} \log\left(|y_n - x|^2\right) - \min_{x\in\Im\{X_1^i\}} \log\left(|y_n - x|^2\right) \right\} \tag{3.20}$$

Substituting (3.19) and (3.20) back into the LLR ratios yields

$$LLR(y_n,i) = |C_n|^2 D_I(y_n,i) \;\; \forall i \in \left\{1,\ldots,\frac{m}{2}\right\}$$
$$LLR(y_n,i) = |C_n|^2 D_Q(y_n,i) \;\; \forall i \in \left\{\frac{m}{2}+1,\ldots,m\right\} \tag{3.21}$$

Values of $D_I(y_n,i)$ and $D_Q(y_n,i)$ for both 16 and 64-QAM are presented in Table 3.1 and Table 3.2, along with further simplified equivalent terms derived in [36]. In the appendix of [36], Tosato shows that the Viterbi decoder will decode the same bit sequence whether the sub-optimum or simplified LLR metrics are used. For BPSK/QPSK modulation the actual sub-optimum metrics are used.

Table 3.1: Values for $D_I(y_n,i)$ and $D_Q(y_n,i)$ for 16-QAM Modulation[1] [36]

Modulation Type: 16-QAM	Sub-optimal	Simplified
$D_I(y_n,1)$	$\begin{cases} -y_I[n] & \lvert y_I[n]\rvert \le 2 \\ 2(-y_I[n]-1) & y_I[n] > 2 \\ 2(-y_I[n]+1) & y_I[n] < -2 \end{cases}$	$y_I[n]$
$D_I(y_n,2)$	$-\lvert y_I[n]\rvert + 2$	$-\lvert y_I[n]\rvert + 2$
$D_Q(y_n,3)$	$\begin{cases} -y_Q[n] & \lvert y_Q[n]\rvert \le 2 \\ 2(-y_Q[n]-1) & y_Q[n] > 2 \\ 2(-y_Q[n]+1) & y_Q[n] < -2 \end{cases}$	$y_Q[n]$
$D_Q(y_n,4)$	$-\lvert y_Q[n]\rvert + 2$	$-\lvert y_Q[n]\rvert + 2$

[1] In Table 3.1 and, Table 3.2, $Y_I[n]$ is the in-phase component of the received symbol on subcarrier n and $Y_Q[n]$ is the quadrature component.

Table 3.2: Values for $D_I(y_n,i)$ and $D_Q(y_n,i)$ for 64-QAM modulation [36]

Modulation Type : 64-QAM	Sub-optimal	Simplified
$D_I(y_n,1)$	$\begin{cases} y_I[n] & \lvert y_I[n]\rvert \le 2 \\ 2(y_I[n]-1) & 2 < y_I[n] \le 4 \\ 3(y_I[n]-2) & 4 < y_I[n] \le 6 \\ 4(y_I[n]-3) & y_I[n] > 6 \\ 2(y_I[n]+1) & -4 < y_I[n] \le -2 \\ 3(y_I[n]+2) & -6 < y_I[n] \le -4 \\ 4(y_I[n]+3) & y_I[n] < -6 \end{cases}$	$y_I[n]$
$D_I(y_n,2)$	$\begin{cases} 2(-\lvert y_I[n]\rvert+3) & \lvert y_I[n]\rvert \le 2 \\ 4-\lvert y_I[n]\rvert & 2 < \lvert y_I[n]\rvert \le 6 \\ 2(-\lvert y_I[n]\rvert+5) & \lvert y_I[n]\rvert > 2 \end{cases}$	$-\lvert y_I[n]-4\rvert+2$
$D_I(y_n,3)$	$\begin{cases} \lvert y_I[n]\rvert - 2 & \lvert y_I[n]\rvert \le 4 \\ -\lvert y_I[n]\rvert + 6 & \lvert y_I[n]\rvert > 4 \end{cases}$	$-\lvert y_I[n]-4\rvert+2$
$D_Q(y_n,4)$	$\begin{cases} y_Q[n] & \lvert y_Q[n]\rvert \le 2 \\ 2(y_Q[n]-1) & 2 < y_Q[n] \le 4 \\ 3(y_Q[n]-2) & 4 < y_Q[n] \le 6 \\ 4(y_Q[n]-3) & y_Q[n] > 6 \\ 2(y_Q[n]+1) & -4 < y_Q[n] \le -2 \\ 3(y_Q[n]+2) & -6 < y_Q[n] \le -4 \\ 4(y_Q[n]+3) & y_Q[n] < -6 \end{cases}$	$y_Q[n]$
$D_Q(y_n,5)$	$\begin{cases} 2(-\lvert y_Q[n]\rvert+3) & \lvert y_Q[n]\rvert \le 2 \\ 4-\lvert y_Q[n]\rvert & 2 < \lvert y_Q[n]\rvert \le 6 \\ 2(-\lvert y_Q[n]\rvert+5) & \lvert y_Q[n]\rvert > 2 \end{cases}$	$-\lvert y_Q[n]\rvert+4$
$D_Q(y_n,6)$	$\begin{cases} \lvert y_Q[n]\rvert - 2 & \lvert y_Q[n]\rvert \le 4 \\ -\lvert y_Q[n]\rvert + 6 & \lvert y_Q[n]\rvert > 4 \end{cases}$	$-\lvert y_Q[n]-4\rvert+2$

3.1.3 Probability of Error in IEEE 802.11a WLANs

As stated in [33] and [34], at high SNRs and under ideal interleaving with perfect channel estimation, the coding gain, the increase in efficiency that a coded signal provides over an uncoded signal, of BICM systems in Rayleigh fading conditions is equal to the code diversity of the code; it's free Hamming distance. Free Hamming distances of all coding rates used in IEEE 802.11a systems are shown in Table 3.3. Based on the discussion provided by Caire in [34], a tangent line drawn on a semi log plot of BER versus the SNR should approach a slope equal to the negative free Hamming distance of the coding employed.

Table 3.3: Free distance values for coding rates used in IEEE 802.11a standard

Code Rate	d_{FREE}
1/2	10
2/3	6
3/4	5

However, in [32] and [37] it is shown that IEEE 802.11a systems operating in indoor environments do not achieve full code diversity. In typical indoor WLAN channels due to low user mobility, the time variations of the channel are small within a packet. In fact, multipath fading in indoor WLAN channels is quasi-static; the transmit symbol duration is shorter then the coherence time of the channel. For packet switched systems, a quasi-static channel remains invariant over the duration of a packet but may change from one packet to the next. Because the channel remains constant for the duration of a packet there is high correlation between the channel responses of OFDM symbols within the packet and this compromises the performance of the viterbi decoder. In addition, interleaving/deinterleaving in IEEE 802.11a systems is done across one OFDM symbol. The depth of the interleaver is finite and the assumption of ideal interleaving usually associated with probability of error analysis of BICM systems [34] does not hold. Therefore, even in non quasi-static fading environments, an IEEE 802.11a system cannot achieve full diversity. In [32], Song et al also show that increasing code diversity will not improve the performance of the IEEE 802.11a systems due to the limited frequency selectivity of the channel.

Exact performance analysis of BICM under quasi-static fading channels is complex and outside the scope of this thesis. However, simulation results for BERs for all modes defined in the standard under the assumption of perfect channel estimation are shown in Figure 3.3 and Figure 3.4. In Figure 3.3, the BER performance of all the modes operating in an independent identically faded (IID) channel are shown, while in Figure 3.4, the BER performance of all the modes in a quasi-static fading channel, Channel A in [13] (cf. Section 2.2), are shown. In the IID fading channel each subcarrier is faded with an independent identically distributed complex gaussian processes. From the BER plots in Figure 3.3, it can be seen that individual modes do not achieve performance gain equal to the code diversity even when in non-quasi static conditions, as proved by Song et al in [32]. Moreover, as the mode increases performance gains approach code diversity. As the mode value increases the number of bits per OFDM symbol also increases, cf. Table 2.2. Since bit interleaving is done across one OFDM symbol the depth of the interleaver increases with the mode. Therefore performances of higher modes are closer to the predicted results then for lower modes. From the BER plots of Figure 3.4, performance in typical WLAN channel conditions, system performance is much worse compared to an IID faded channel. Therefore, BER performance of IEEE 802.11a systems in typical indoor environments is also degraded by the limited time variations of the channel. The performance curves also show that modes with higher coding rates outperform other lower coded modes at high SNRs. This as explain before is due to the higher code diversity of these modes.

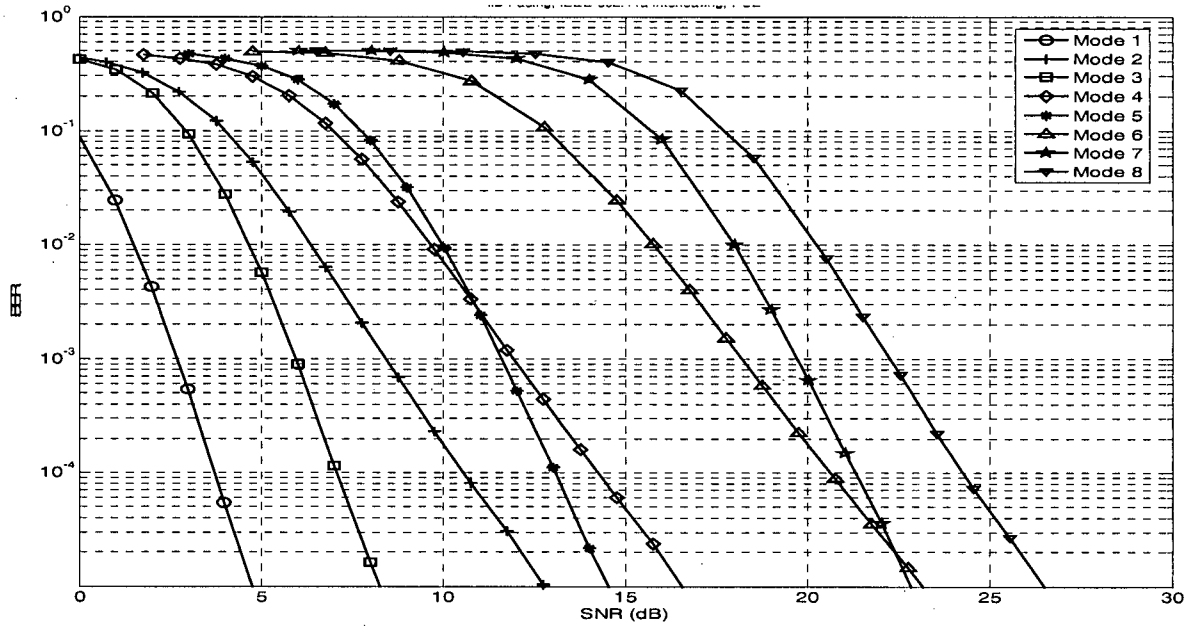

Figure 3.3: BER performance of all modes in IID fading channel, perfect channel estimation assumed

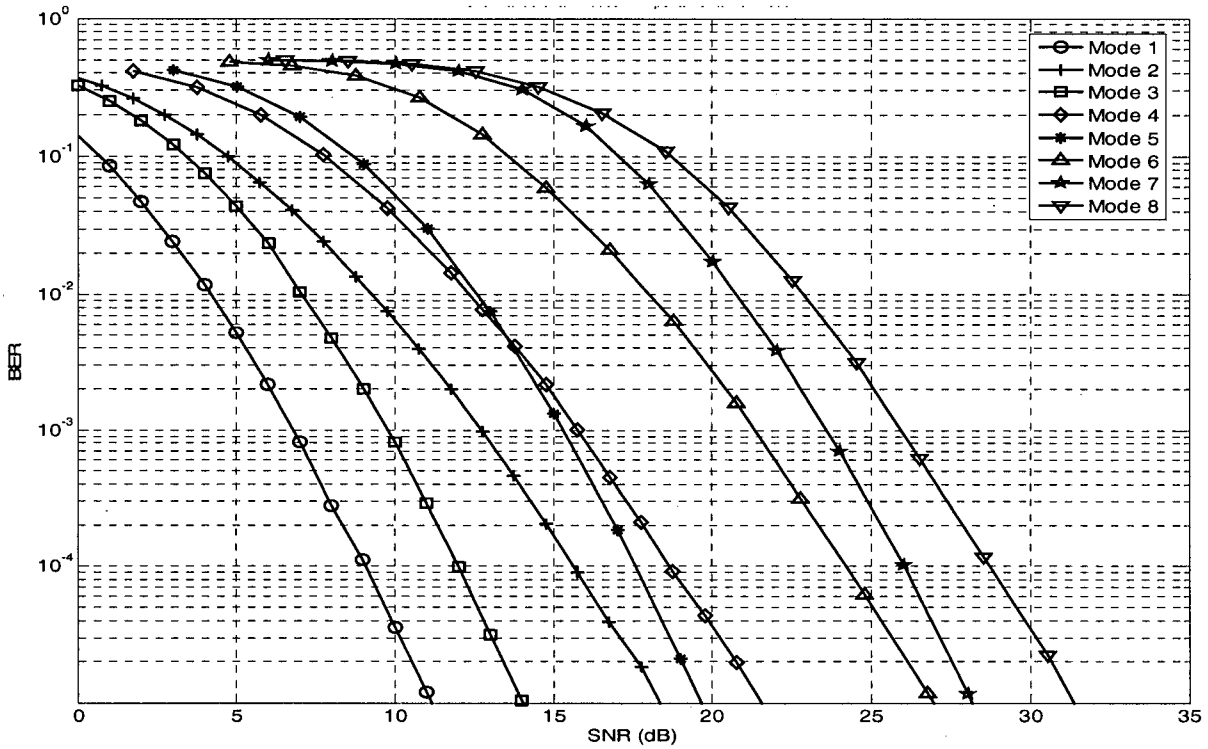

Figure 3.4: BER performance of all modes in quasi-static fading channel, Channel A in [28], perfect channel estimation assumed

3.2 Channel Estimation in OFDM Systems

The assumption of perfect knowledge of the channel at the receiver in the previous section is not a practical one and is only useful for analysis purposes. In this section we present a practical channel estimation algorithm that can be used at the IEEE 802.11a receiver. The IEEE 802.11a OFDM frame has 12 training OFDM symbols and 4 pilot tones on each OFDM data symbol that can be used for estimation. Several algorithms for channel estimation that use any combination of these training and pilot symbols are possible; a good overview of these can be found in [38]. For simplicity and to avoid using interpolation, only the two long training symbols composed of pilot tones on all subcarriers are used. Estimation using known pilots on every subcarrier is known as block type pilot based estimation.

At the receiver, channel estimation can be preformed in either the time domain, where the channel impulse response is calculated and converted into the channel frequency response or directly in the

frequency domain. Better performance is achieved through time domain estimation as a lesser number of variables need to be estimated [38]; in OFDM systems, the length of the cyclic prefix is always assumed to be longer then the delay spread of the channel and is a fraction of the length of an OFDM symbol. In our model we use the least square error (LSE) algorithm, described in [38], to estimate the channel impulse response. An extra FFT block is needed at the receiver to calculate the channel frequency response from the estimated impulse response.

Using (2.8) at time t_k, the received pilot tone on subcarrier n after OFDM demodulation is

$$y_n = C_n p_n + w_n \qquad \forall\, n = [1, 2, ..., N] \tag{3.22}$$

where C_n is the channel frequency response on subcarrier n, p_n is the pilot tone transmitted on subcarrier n, and w_n is complex AWGN with a variance of σ^2. Compared to (2.8), the time index is dropped for notational brevity.

The channel impulse response at time t_k, can be expressed as

$$c = [c_0 .... c_{L-1}] \tag{3.23}$$

where L is the length of the channel impulse response.

If we define an L x N Fourier matrix, $\boldsymbol{F}_{l,n}$ whose coefficients are given by

$$F_{l,n} = \exp\left(j\frac{2\pi}{N}(l-1)(n-1) \right) \tag{3.24}$$

Then the channel impulse response and frequency response can be related through $C_n = f_n c$. where $\boldsymbol{f}_n$ is the nth column of the $\boldsymbol{F}_{l,n}$ matrix.

Using matrices notation and using (3.22), the received pilot symbols at time t_k, are

$$\boldsymbol{y} = D(\boldsymbol{P})\boldsymbol{C} + \boldsymbol{w} = D(\boldsymbol{P})\boldsymbol{F}_{l,n}\boldsymbol{c} + \boldsymbol{w} \tag{3.25}$$

Where $\boldsymbol{y} = [y_1 \ \ldots \ y_N]$, $\boldsymbol{p} = [p_1 \ldots p_N]$, $\boldsymbol{C} = [C_1 \ldots C_N]$, $\boldsymbol{w} = [w_1 \ldots w_N]$, and $D(\boldsymbol{P})$ is a diagonal matrix with p_n on its diagonals and N is the total number of subcarriers.

The receiver estimates the LSE channel estimates [38]

$$\hat{c} = \left((F_{l,n} D^H(P) D(P) F_{l,n}^H)^{-1} (D(P) F_{l,n}^H)^H \right) y \tag{3.26}$$

Since two OFDM training symbols are used, the calculated channel impulse responses are averaged prior to transforming into the frequency domain.

$$\hat{C}_n = f_n^H \hat{c} \tag{3.27}$$

In general, error rate performances of packet based systems are expressed in terms of packet error rates (PER) in preference to BERs [32]. This is because such systems generally employ packet re-transmission schemes; if a packet has not been correctly received the receiver will ask for a repeat transmission. Moreover, the minimum performance criteria specified in the standard is given in terms of PER, section 2.3.4. In [29], Doufexi provides PER plots of all modes of an IEEE 802.11a system for different multipath channels including channel A of [28] and also for different PSDU packet sizes. We show the BER (Figure 3.5) and PER curves (Figure 3.6) of all modes of an IEEE 802.11a system operating in a block fading multipath channel. In a block fading multipath environment the transmitted packet is faded by the same attenuation factor.

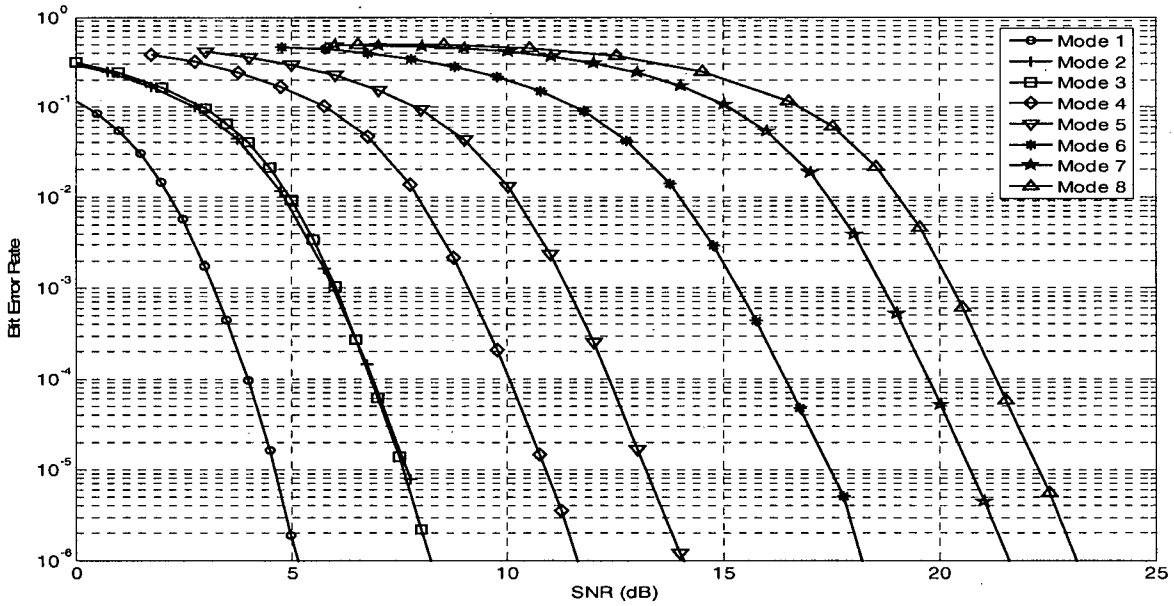

Figure 3.5: BER performance of all modes in a block fading channel, Time domain least square channel estimation used

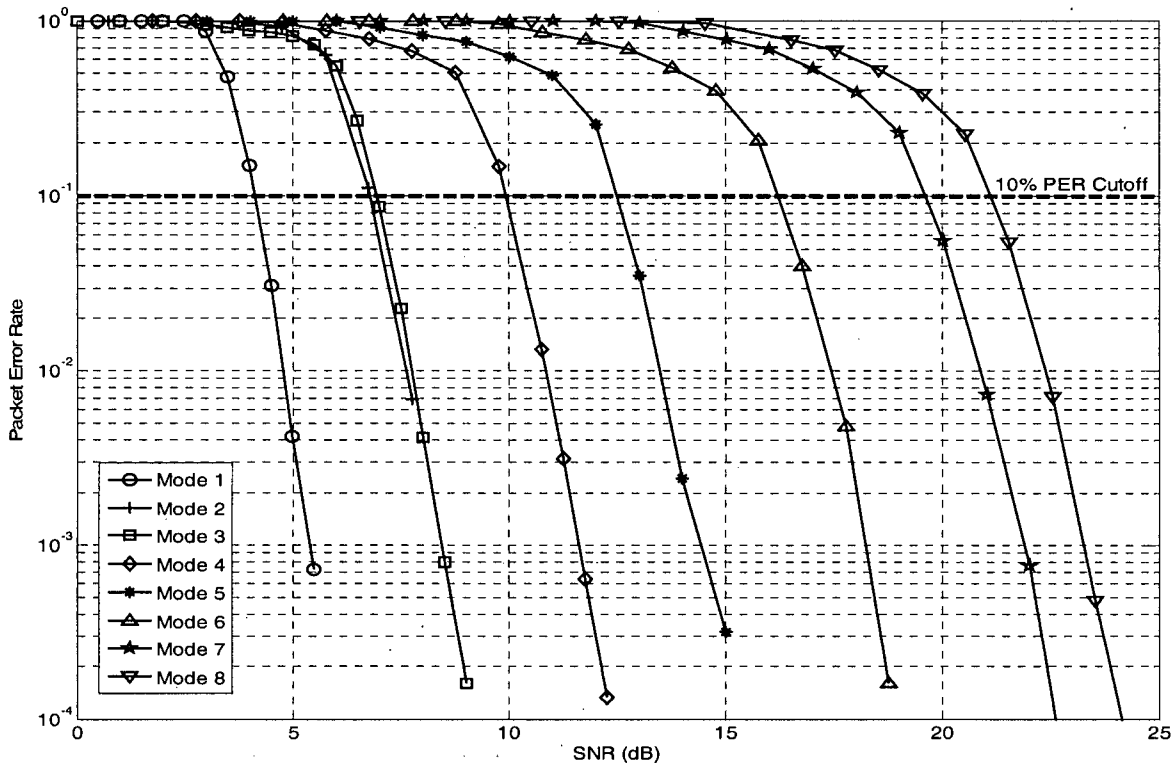

Figure 3.6: PER performance of all modes in a block fading channel, time domain least square channel estimation used

3.3 Link Adaptive Modulation and Coding

The ability of IEEE 802.11a systems to select different modulation and coding rates permits the use of higher more spectrally efficient modulation schemes and lower coding if channel conditions are good and to switch to lower less sensitive to channel errors modes if channel conditions are bad. By dynamically switching between modes more packets can be transmitted with fewer errors compared to a fixed mode system.

The link adaptation algorithm is responsible for sending information back to the transmitter to dynamically change certain transmission related parameters based on knowledge of the channel the receiver has estimated from previous transmissions. The IEEE 802.11a standard does not specify which link adaptive algorithm to use and the choice is left to the implementer. We present a simplistic link adaptation scheme that uses average receiver SNIR across all subcarriers to select one of the eight possible modes that can be used to transmit data. This mode value is sent back to the transmitter.

The objective of the link adaptation scheme is to limit PER to less than 10%, while trying to provide the user with the highest data rate possible. The system switches to a higher mode whenever the current SNIR value is greater than the 10% PER of the mode directly above. When the SNIR falls below the 10 % PER SNIR threshold of the current mode the system switches to the mode directly under it. The mode switchover thresholds, Normal thresholds, are assigned to exactly the 10% PER cutoff points to maximize throughput. These SNR thresholds are defined for a PSDU packet size of 1000 Bytes for a WLAN operating in the block fading channel and are given in Table 3.4. Here, the thresholds are taken from Figure 3.6.We use the block fading channel in the interference analysis section to reduce simulation time as several simulations need to be run. The mode switch over threshold values for the other multipath channels can be found through the same procedure.

Table 3.4: Mode switchover thresholds arrays for link adaptive system

Mode	Bit Rate (Mbps)	Normal Thresholds
1	6	-∞
2	9	7
3	12	7
4	18	10
5	24	13
6	36	16.5
7	48	20
8	54	21.5

The 10% PER cutoff SNIR for Mode 2 and Mode 3 are similar and the link adaptive system is designed to switch directly from Mode 1 to Mode 3 as Mode 3 offers higher data rates compared to Mode 2. BER rates from the IID fading channel. Figure 3.3, and the quasi-static fading channel, Figure 3.4, also show that mode 3 outperforms mode 2 at any SNR.

3.4 The IEEE 802.11a Transmit Signal Spectrum

3.4.1 Analytical Representation of the Baseband OFDM Spectrum

The transmitted OFDM signal previously derived as (2.7) can also be represented in the time domain as a sum of N pulse amplitude modulated (PAM) symbols [24]

$$x(t) = \left[\frac{1}{\sqrt{N}} \sum_{n=1}^{N} x_n(t) \right] * h_T(t) \tag{3.28}$$

where

$$x_n(t) = \sum_{k_o=-\infty}^{\infty} a_n[k_o] g_n(t - k_o T_o) \tag{3.29}$$

and

$$g_n(t) = \sum_{k=0}^{N+P-1} \delta(t - kT) e^{j\frac{2\pi}{N}(n-1)k} \tag{3.30}$$

here k denotes the subcarrier index which in the previous section was denoted by n.

To find the power spectrum of $g_n(t)$ it is convenient to express equation (4.1) as

$$g_n(t) = e^{j\frac{2\pi(n-1)t}{NT}} \left(\sum_{k=-\infty}^{\infty} \delta(t - kT) \right) \cdot \text{rect}\left(\frac{t - (T_o - T)/2}{T_o} \right) \tag{3.31}$$

The spectrum of which can easily expressed as

$$G_n(f) = \delta\left(f - \frac{n-1}{NT} \right) * \left(\frac{1}{T} \sum_{k=-\infty}^{\infty} \delta\left(f - \frac{k}{T} \right) \right) * T_o \, \text{sinc}(\pi f T_o) e^{-j2\pi f (T_o - T)/2} \tag{3.32}$$

$$= \frac{T_o}{T} \sum_{k=-\infty}^{\infty} \text{sinc}\left(\pi T_o \left(f - \frac{k}{T} - \frac{n-1}{NT} \right) \right) e^{-j2\pi \left(f - \frac{k}{T} - \frac{n-1}{NT} \right)(T_o - T)/2}$$

$$= \frac{T_o}{T} \sum_{k=-\infty}^{\infty} \text{sinc}(\pi T_o (f - \Delta f (Nk + n - 1))) e^{-j\pi \frac{N+P-1}{N} \left(\frac{f}{\Delta f} - (Nk+n-1) \right)} \tag{3.33}$$

Where $\Delta f = 1/NT$ is the subcarrier spacing and the substitution, $T_o = (N+P)T$ has been made.

For large values of N, the magnitude of $G_n(f)$ may be approximated as

$$|G_n(f)|^2 \approx \left(\frac{T_o}{T} \right) \sum_{k=-\infty}^{\infty} \text{sinc}^2 (\pi T_o (f - \Delta f (Nk + n - 1))) \tag{3.34}$$

If we assume independent data symbols with zero mean and a variance of σ^2, then the power spectrum of each time domain PAM symbol given in (3.29) can be expressed as,

$$\Phi_{s_n s_n}(f) = \frac{\sigma_n^2}{T_o} |G_n(f)|^2 \tag{3.35}$$

and the power spectrum of the transmit signal as

$$\Phi_{ss}(f) = \frac{|H_T(f)|^2}{NT_o} \sum_{n=1}^{N} \sigma_n{}^2 |G_n(f)|^2 \tag{3.36}$$

where $|H_T(f)|^2$ is the spectrum of the transmit filter.

For the large N approximation

$$\Phi_{ss}(f) = \frac{(N+P)}{NT} |H_T(f)|^2 \sum_{n=1}^{N} \sigma_n{}^2 \sum_{k=-\infty}^{\infty} \text{sinc}^2(\pi T_o(f - \Delta f(Nk + n - 1))) \tag{3.37}$$

An OFDM symbol is formed by taking the inverse discrete Fourier Transform (IDFT) of a set of N complex modulated symbols $\{X_n, n = 0,1,...,N-1\}$. Each data symbol is loaded onto a subcarrier by multiplying with a pulse of duration equal to the OFDM symbol transmission time. The power spectrum of each subcarrier follows a $\text{sinc}^2(x)$ type decay because of the rectangular input pulses, section 3.4.1. All subcarriers are orthogonal to each other and the data modulated onto different subcarriers is independent. Therefore, the spectrum of an OFDM symbol is the sum of the spectra of all its subcarriers. Although the main lobes of these independent subcarriers do not interfere with the main lobe of other subcarriers, they do interfere with each others side lobes and this contributes to the slow decay of the OFDM spectrum, especially when a finite number of subcarriers are used [39]. Transmitting zeros on outer subcarriers is generally used to reduce this out-of-band (OOB) spectrum. In the IEEE 802.11a standard [1], when a 64-point FFT is taken, 5 zero subcarriers are padding at the front and 6 are padded at the end of the OFDM signal, In addition to this, a zero DC subcarrier is also used. Figure 3.7 shows the spectrum of a single OFDM symbol and the effects of zero padding the end subcarriers.

From Figure 3.7, zero padding the end subcarriers considerably lowers the OOB spectrum of an OFDM symbol. However when individual OFDM symbols are concatenated to form an OFDM Frame, sharp phase transitions at the symbol boundaries regenerate OOB spectral components. These results from the variable amplitude and phase levels used to modulate the data. On each subcarrier transitions from one data symbol to the next only occur once during an OFDM symbol. The upsampled spectrum of an OFDM symbol after concatenation is shown in Figure 3.8. The dashed line represents the spectrum mask defined in Figure 2.7. Clearly, without any OOB spectrum reduction the

transmit signal spectrum does not fall within these limits. Therefore windowing or filtering must be employed to lower OOB spectrum to within standard prescribed limits, cf. Section 2.3.3.

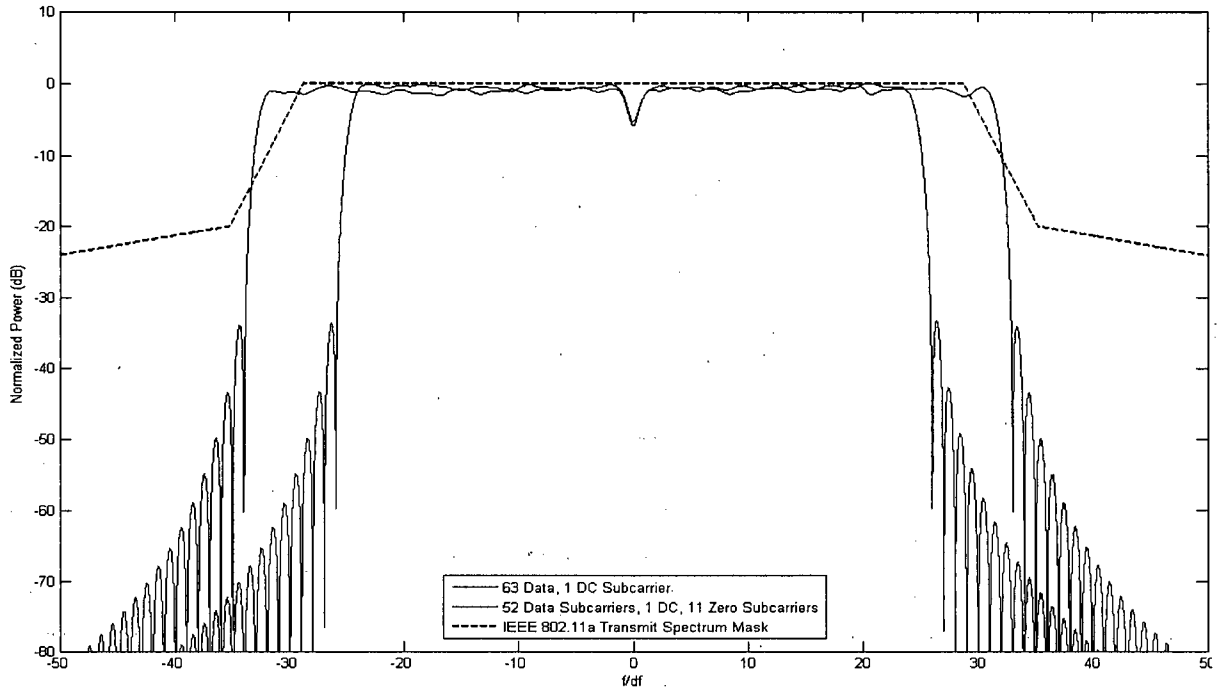

Figure 3.7: OFDM symbol spectrum with 64 subcarriers, (a) all 64 data subcarriers (b) 52 data subcarriers and 12 zero subcarriers as defined in [1]. Where df is the subcarrier frequency spacing. For IEEE 802.11a systems df is 0.3125 MHz

The spectrum in Figure 3.8 is that of an upsampled version of the transmit signal. Using the baseband sampling rate, only in-band frequency components, within $\left[-\frac{fs}{2}, \frac{fs}{2}-1\right]$ can be observed. However for our interference analysis, we are also interested in spectrum outside the 20 MHz channel. For this reason and to observe the effectiveness of the OOB spectrum reduction technique used we an upsampled version of the transmit signal. Upsampling is generally preformed on the time domain signal during digital to analog conversion prior to transmission. Alternatively, it can also be done by inserting zeros in the middle of each frequency domain OFDM symbol. Zero padding in the frequency domain results in a trigonometric interpolation of the time domain signal [48]. In our model, an oversized 512-point IFFT is used instead of the normal 64-point IFFT. An upsampling factor of 8 is used because we are interested in spectral components as far away as 50 MHz from the central frequency of the channel.

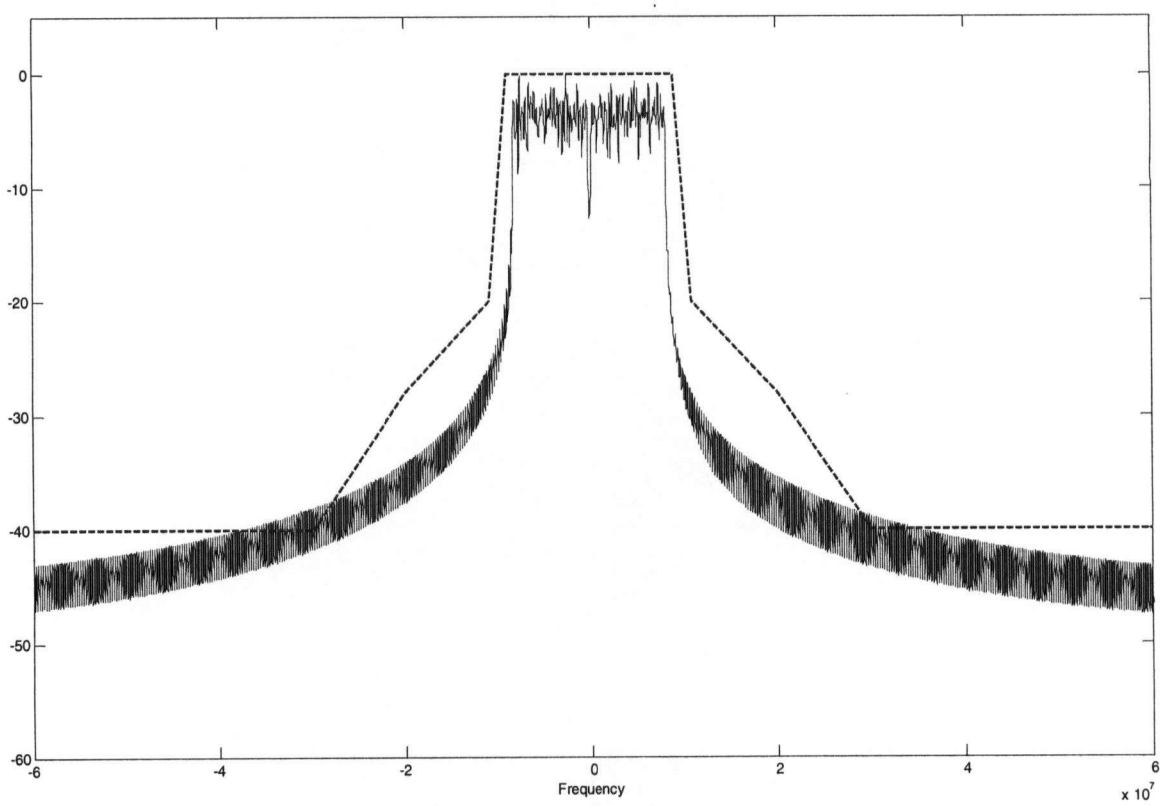

Figure 3.8: Spectrum of the upsampled IEEE 802.11a transmit symbol with no spectrum shaping

Another major contributor to high OOB spectral components is transmitter induced non-linearities [47] [48]. In an OFDM symbol, when frequency domain data symbols are converted to their time domain equivalents, each time domain symbol formed is a summation of contributions from every frequency domain data symbol. This results in the non-constant envelope of the time domain OFDM symbol. Occasionally, this superpositioning gives raise to a time domain data symbol equivalent with much higher amplitude than the average. Most practical non-linear transmit power amplifiers are not designed to handle such a wide range. When these large amplitude time domain symbols pass through the amplifier, it forces the amplifier to operate above its saturation point thereby introducing non-linearities in the transmitted signal which result in OOB spectral components. In general, Peak to Average Power Ratio (PAPR) reduction techniques are needed to use practical amplifiers with OFDM systems.

The simplest ways to combat high PAPR is by amplitude clipping the symbols after IFFT modulation [47]. High amplitude time domain symbols rarely occur, and clipping the amplitude above a certain threshold can prevent power amplifiers from operating above their saturation points. However, clipping is also a non-linear operation and results in OOB spectrum regeneration as well as in-band distortion which degrades BER performance. The shoulder regrowth in the typical signal spectrum of Figure 2.7 can be attributed to amplitude clipping [47]. For simplicity, we restrict ourselves to OOB spectrum components generated only through sharp transitions at OFDM symbol boundaries. Filtering after clipping can be used to reduce OOB spectrum but care must be taken as filtering results in some peak regrowth. It does not improve the BER degradation caused by clipping either. A good overview of the tradeoffs between filtering, clipping and BER performance can be found in [47],

3.4.2 Transmit Spectrum Reduction Techniques

The IEEE 802.11a standard does not specify which OOB power suppression technique to use. The only requirements are that the transmit signal spectrum must lie within the spectrum mask of Figure 2.7 and the transmit power must be less than the values defined in Table 2.6. In selecting an OOB spectrum reduction techniques trade-offs between system complexities, control over the OOB spectrum, performance and multipath tolerance need to be considered. We describe two types of OOB spectrum reduction techniques: raised cosine (RC) windowing and high order filtering.

3.4.2.1 Raised Cosine Windowing

RC windowing is an OOB spectrum reduction technique commonly used in 802.11a systems because of the simplicity of its implementation. It is also cited in the standard [1] as a candidate OOB spectrum reduction technique. As mentioned earlier, sharp phase transitions at OFDM symbol boundaries result in high OOB spectral components. By multiplying each OFDM symbol in the OFDM frame with an RC window, boundary symbols are smoothly decreased to zero. To avoid corrupting the actual data symbol, βNT cyclic postfix symbols, replicated from the start of the OFDM symbol, are appended to the end of each OFDM symbol in addition to the cyclic prefixed symbols at the beginning of each OFDM symbol. Here, β is the raised cosine roll-off factor. The window does not affect the actual data symbols and only the prefix and postfix symbols. Both overlapping and non-overlapping windows can be used. However, overlapping windows are preferred as fewer symbols per OFDM symbol need to be modified. In overlapping windows, the defined window is βT times

longer then the length of an OFDM symbol, and consecutive windows are overlapped by a factor of $\beta T/2$. The structure of an overlapping RC Window is shown in Figure 3.9.

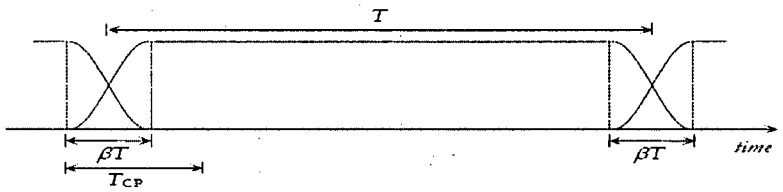

Figure 3.9: Time Domain Windowed OFDM Symbol [39]

The expression for the RC window are given in [3] as

$$h_T(t) = \begin{cases} \frac{1}{2} + \frac{1}{2}\cos\left(\pi\left(\frac{t+1}{\beta NT}\right)\right) & t < \beta T \\ 1 & \beta T \le t \le T \\ \frac{1}{2} + \frac{1}{2}\cos\left(\pi\left(\frac{t-T}{\beta NT}\right)\right) & t > T \end{cases} \tag{3.38}$$

The RC window mentioned in the standard has a β value of 0.0125. The amount of OOB suppression an RC window can achieve is directly related to β; with higher β more OOB suppression can be achieved. However, with higher β more postfix symbols need to be added and more cyclic prefixed symbols of the next OFDM symbol are destroyed as more post fix symbols need to be added and overlapped. Since the cyclic prefix symbols are needed to prevent ISI, when transmitting in a multipath environment, using a high β decreases the multipath tolerance of the system. The OFDM transmit signal spectrum after RC windowing with various β values is shown in Figure 3.10.

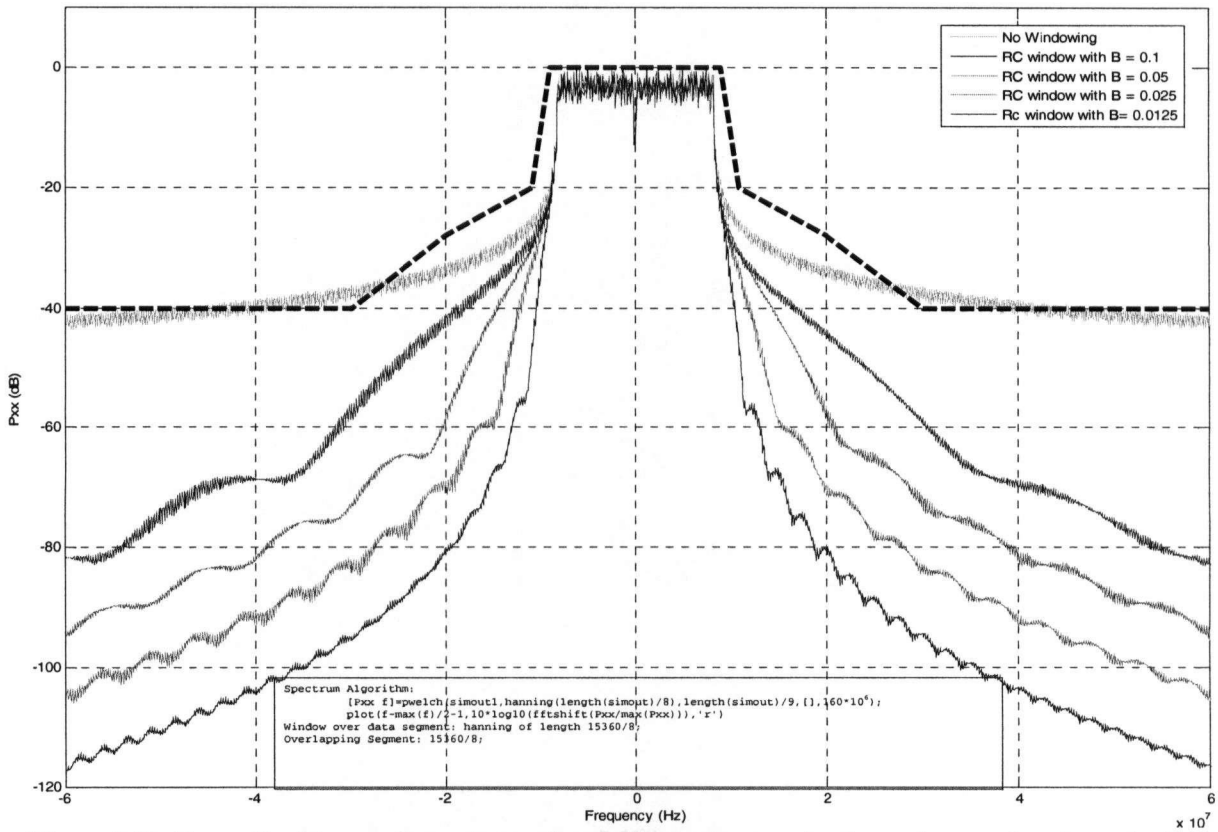

Figure 3.10: Normalized transmit spectrum after OOB spectrum reduction using overlapping raised cosine windowing with different roll off factors.

3.4.2.2 Higher Order Digital Filtering

Conventional filtering techniques can also be used to contain the OOB spectrum of OFDM symbols. With filtering the IFFTed symbols are convolved with the filter's impulse response. Much greater control over OOB spectrum can be achieved but filtering also increases system complexity. In addition, when using filtering high order filters are needed to prevent the filters passband rippling effects from causing in-band distortion as this decreases BER performance and also tolerance to the delay spread of the channel [3]. The filter used in our simulation is a least square error (LSE) finite impulse response filter (FIR) of order 128. Parameters for the filter are given in Table 3.5 below. The impulse and frequency response of the filter are shown in the Figure 3.11. The OFDM transmit signal spectrum after filtering with the transmit filter is shown in Figure 5.2.

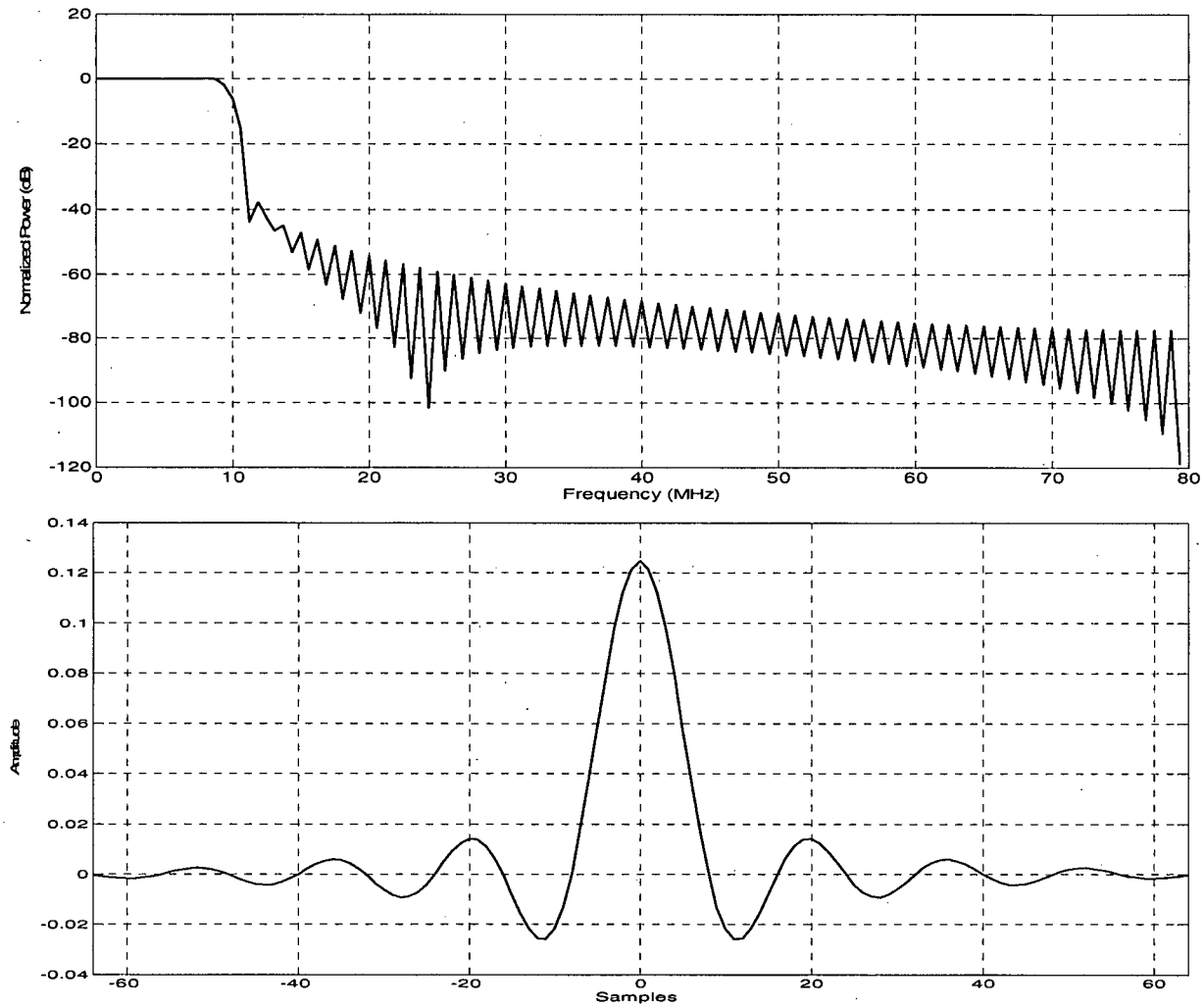

Figure 3.11: (a) Transfer function and (b) Impulse response of transmit filter

Table 3.5: Parameters of the transmit filter

Parameter Description	Parameter Name	Parameter Values
Normalized Filter Cutoff Points(MHz)	Attn	[0 9 11 80] /80
Attenuation associated with Cutoff Points	cutoffs	[1 1 0 0]
Filter Sample Time(MHz)	Fs	160
Filter Order	N	128
Impulse response of Filter	B	B= Firls(N, Attn, cutoffs)
Filter defined in Matlab		Freqz(B,1,128,160)

Chapter 4

System Model Description

The model used in our analysis is based on the Clark's Matlab Simulink baseband model of the IEEE 802.11a OFDM WLAN, taken from Matlab's Central File Exchange website [50]. The model is now included as a demo model in Matlab 7/Simulink Release 14. However, several modifications have been made to make it more standard compliant, improve its performance and to adapt it for an analysis of our interference study. Modifications made to the model include:

1. PPDU frame duration and subcarrier spacing changed to those defined in the standard
2. Modified PPDU frame format to include 2 short and 2 long training symbols. Original model does not include short training sequences.
3. Modified interleaving/deinterleaving to match standard defined algorithms
4. Proper subcarrier positioning prior to IFFT at transmitter
5. Proper GI interval description for training sequences
6. Included effects of spectrum shaping.
7. Included upsampling/down sampling to generate out of band spectral components
8. Modified channel model to use quasi-static multipath fading and IID fading
9. Changed channel estimation to time domain LSE from frequency domain zero forcing.
10. Changed Viterbi decoding from hard to soft with bit metrics based on BICM theory.
11. Modified link adaptive mode selection algorithm
12. Defined two different algorithms to calculate SNIR.
13. Redefined PER according to the standard definition that is based on PSDU frame length
14. Added channel shift capability. Allows multiple WLANs to be simulated simultaneously

4.1 Single Access Point Model

4.1.1 Transmitter

The transmitter diagram is shown in Figure 4.1. The incoming PSDU data steam is modeled as random data generated by a zero mean uniform Gaussian random process in the variable rate data generator block. The modulator bank is responsible for preparing the incoming binary data for transmission over the channel. This includes coding, interleaving and modulating. All routines are implemented according to the dictates of the standard. The transmission of an acknowledge (ACK) packet back to the transmitter in response to a correctly received PPDU frame at the receiver is not modeled as it involves the MAC layer. Instead we implement a simplified version of these events. A variable called the mode is sent back from the receiver to the transmitter informing it what mode to use in the transmission of the next PPDU frame. At the receiver, mode selection is controlled by the signal to noise plus interference ratio (SNIR) averaged across all subcarriers and all OFDM symbols in the previous PPDU frame. The mode switches to a higher value each time this averaged SNIR crosses the 10% PER cutoff threshold of the mode directly above it and to a lower mode each time the averaged SNIR ratio falls below the 10% PER cutoff threshold of the current mode. By doing so, maximum throughput is achieved while the 10% PER criteria for each mode is met.

The transmitter generates 960 data symbols for each PPDU frame no matter what mode is used. Therefore, the number of binary data bits generated varies depending on what mode value is received. The number of data symbols transmitted is modeled as stationary to fix the size of the transmitted PPDU frame. Variable PPDU frame sizes are not modeled. In addition to this, the OFDM SIGNAL symbol is not modeled either. All information necessary to demodulate the PPDU frame is provided by the mode.

The complex modulated data is fed into the OFDM Modulator, which places the data on the designated data subcarriers and also adds the zero and pilot subcarriers necessary to form OFDM data symbols. IFFT is preformed on the subcarriers to form the time domain data OFDM symbol. Training symbols are added to form the header of the PPDU frame. A 512 point IFFT is preformed on the data by zero padding each OFDM symbol instead of the normal 64 points. This frequency domain zero

padding is done to generate the out-of-band spectrum without adding an extra upsampling block at the transmitter. The time domain output is an upsampled version of the 64 point IFFT OFDM symbol. These symbols are then cyclically prefixed and spectrally shaped by filtering or windowing before being amplified and serially transmitted over the channel. The transmit spectrum shaping block can either uses either the transmit filter or RC windowing with variable β.

4.1.2 Channel Model

Two different types of multipath channels are modeled: IID fading and quasi-static fading. In each case, the individual symbols in the PPDU frame are convolved with the impulse response of the multipath channel. Complex zero-mean AWGN is then added to the symbols before the PPDU frame is sent to the receiver.

4.1.3 Receiver

The receiver diagram is shown in Figure 4.2. No PPDU detection routines are implemented and a continuous stream of data is received from the transmitter via the channel. Perfect frequency and time synchronization is also assumed. The received data is reformed into the PPDU frame format after OOB spectrum suppression and normalization. The guard intervals from all OFDM symbols are then removed. These OFDM symbols are converted back to the frequency domain by taking a 512 point FFT. Frequency domain OFDM symbols are downsampled by removing all upsampling zeros. After this training symbols and data symbols are separated. The training symbols are sent into the channel estimation block, where time domain LSE channel estimation is preformed using locally generated training symbols. Only long training symbols are used in channel estimation. Estimates of the channel frequency response on each subcarrier are sent into the Demodulator bank. Pilot symbols and zero subcarriers are removed from the data OFDM symbols before they are sent into the demodulator bank. Inside the demodulator bank, soft demodulation of the data symbols is done using the channel frequency response obtained from the training symbols and BICM theory to generate soft input bit metrics for the viterbi decoder. Non-iterative, soft input viterbi decoding is used to limit decoder complexity. Prior to entering the viterbi decoder, deinterleaving and de-puncturing of the soft input metrics is preformed to reverse the corresponding processes preformed at the transmitter.

The decoded bits are sent to the BER\PER calculator where they are compared to the original bit stream. The averaged SNIR of the received PPDU frame is sent into the link adaptive mode control block where it is compared to 10% PER thresholds of different modes. Based on this comparison, the receiver selects a mode value to be used on the next PPDU frame, which it then sends back to the transmitter.

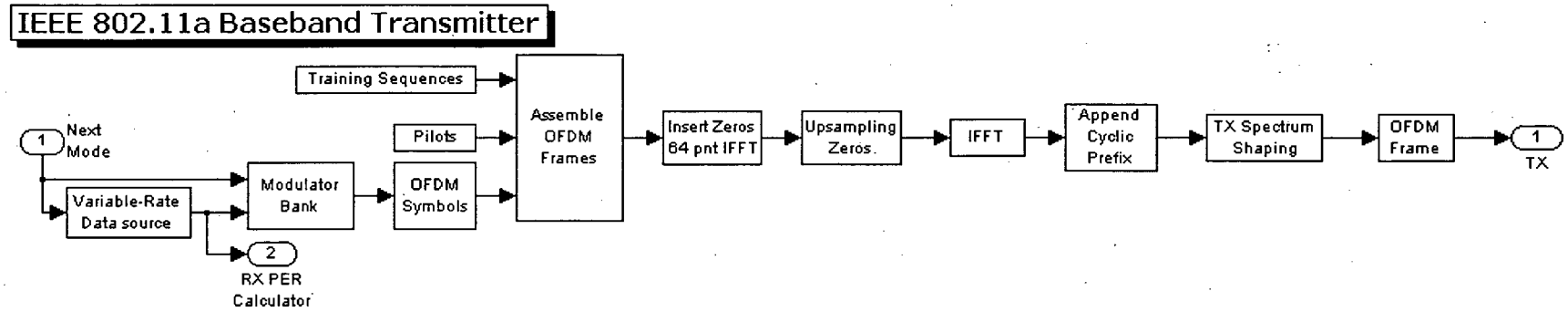

Figure 4.1: IEEE 802.11a baseband transmitter model

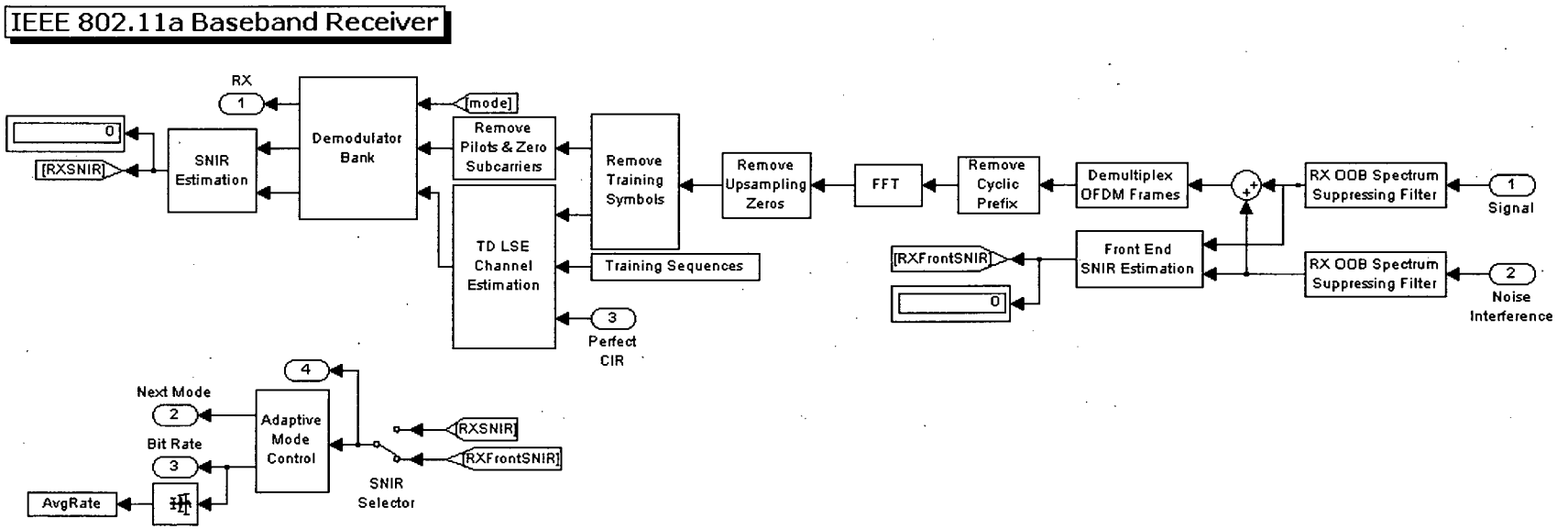

Figure 4.2: IEEE 802.11a baseband receiver model

4.2 Multi Access Point Model

The multi-AP model is used in the interference analysis of co-located WLANs. The model is displayed in Figure 4.4. The current implementation models two co-located WLANs. However it can easily be modified to include more WLANs. The basic transmitter and receiver models are the same as those used in the single AP model described in the previous section except for two extra blocks that have been added to the transmitter and one extra block at the receiver. A frequency shift block is added to the end of the transmitter prior to transmission. The block is used to model an AP operating on an adjacent or a non adjacent channel. Only the frequency separations between the channels of WLAN systems are modeled and there is no shifting to the actual passband channels. In the current model the first WLAN is centered at 0 MHz, the adjacent channel interferer at 20 MHz and the Non-adjacent Channel interferer at 40 MHz. A power amplifier block is also added to normalize the power of the received signal. The power amplifier is added after the signal and the noise plus interference signals have been added together just before it enters the rest of the receiver. The first WLAN system is modeled in full, i.e., both the transmitter and receiver are modeled. Only the transmitter of the second WLAN is modeled as we are only interested in the performance of the first system in the presence of interference for nearby APs.

The channel model is modified to include pathloss. A description of the pathloss models used is given in Section 5.4.2. The channel model of the first WLAN system includes the effects of pathloss and multipath fading. Transmissions from the second WLAN system are modeled as the interference signal. AWGN noise is added to the interference signals and transmitted separately into the receiver of the first WLAN system. This is done so that the receiver front end SNIR can be calculated. After the power of the signal and the noise plus interference signal are calculated, the two signals are added together and sent into the rest of the receiver. A receiver Noise Figure (*NF*) of 6 dB and an antenna gain of 0 dBi are assumed. The noise power at the input of the receiver, *N*, is calculated using

$$\begin{aligned} N = KTB &= 10 \cdot \log_{10}(K) + 10 \cdot \log_{10}(290) \\ &\quad + 10 \cdot \log_{10}(NF) + 10 \cdot \log_{10}(B), \end{aligned} \tag{4.1}$$

where K is Boltzman constant = 1.38×10^{-23}J/K, T is the receiver noise temperature assumed to be 290°K and B is the bandwidth of the signal. Numerically; N = -124.9772 dB. Values of the noise floor and the antenna gain are given as typical values for practical IEEE 802.11a systems in [6].

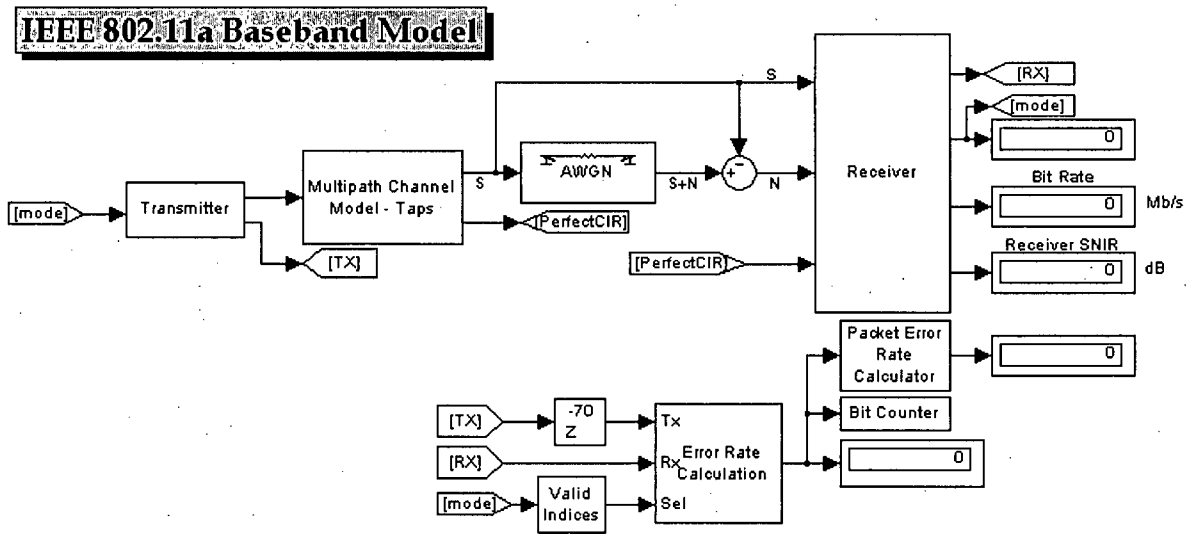

Figure 4.3: IEEE 802.11a single access point model

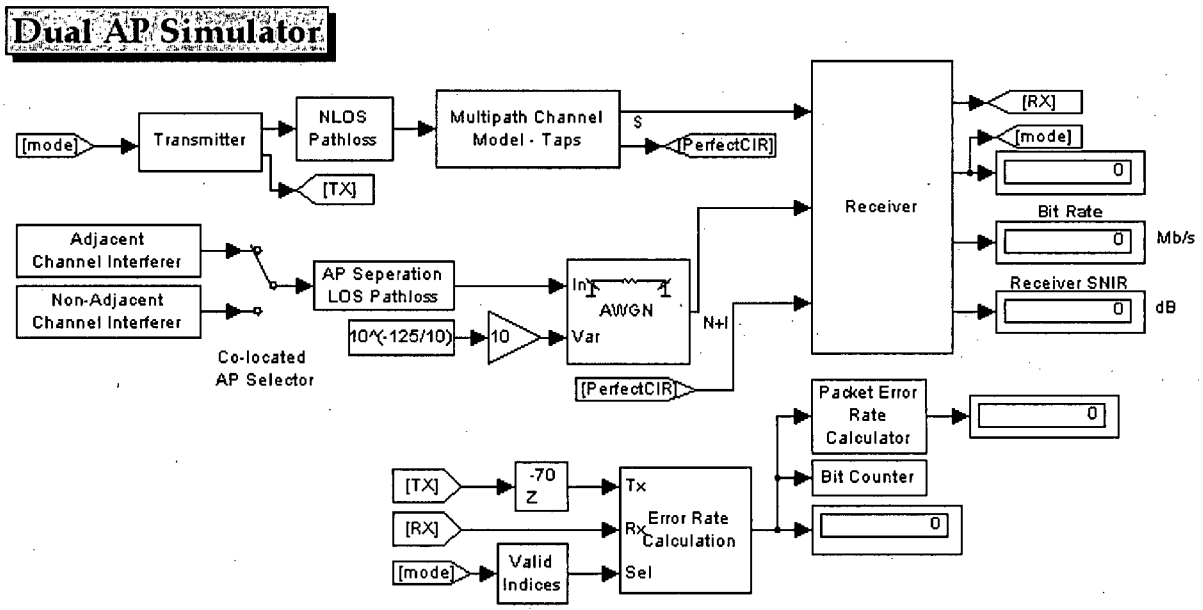

Figure 4.4: Multi access point baseband model

Chapter 5

Adjacent Channel Interference in Co-located WLANs

5.1 Background

Recent years have seen widespread deployment of WLANs in applications ranging from single AP private networks to multiple AP public networks employed in areas such as public internet access hotspots and campus/corporate-wide networks. Such trends have led to an increase in the use of multiple APs in overlying coverage areas (co-located APs) and a corresponding rise in inter-cell interference. A cell refers to the coverage area of a single AP. Obviously, interference from co-located APs operating on the same channel will have the most detrimental effect on system performance. However, inter-cell interference from such an AP is easily detected[2] and routines can be implemented to switch over to other channels if necessary. In multi-AP networks, network planning is used to avoid co-located APs from operating on the same channel. Furthermore, before a WLAN AP selects a channel for use, a survey of signal energy levels on all valid channels is done to find the lowest activity channel [1]. Therefore, interference from a co-located AP operating on the same channel is well accounted for and is not a problem if each co-located AP can operate on a separate channel.

---

[2] A functional AP periodically transmits beacons on its channel advertising it's availably to users. Each beacon has a basic service set identification (BSSID) unique to its cell. A beacon received by an AP with a different BSSID would tell the AP that a second AP is operating on the same channel in its vicinity.

A less obvious source of interference is from co-located APs operating on standard defined non-overlapping channels. We refer to this as adjacent channel interference (ACI). ACI from nearby APs may be felt because standard defined non-overlapping channels are not truly non-overlapping but are based on limits set on the transmit signal's power spectrum. Depending on a range of factors that include the spatial separation between APs, the frequency separation between their operating channels and the out-of-band (OOB) spectrum of the interfering AP, the effects of ACI can be significant. In terms of physical layer (PHY) parameters ACI may cause a reduction in the coverage area and the receiver SNIR. The latter will cause a corresponding drop in the achievable data rates within the constricted coverage area. Furthermore, interference levels greater than the expected receive signal strength may be interpreted as a busy channel by users, leading users to delay their transmissions, and thereby increasing system latency [41].

The existence of this source of inter-cell interference has been cited a few times in the literature [41] - [11]. However, most previous studies have focused on a MAC layer prospective. In [41], Dunat studies the impact of inter-cell interference of APs of IEEE 802.11a Networks in terms of the MAC layer parameters: the number of retransmissions and the effective MAC Layer throughput, the goodput. In particular, Figures 2, 3 and 4 in [41] show that for APs separated by less then 5 m, the goodput performance is severely affected by this source of interference.

In this work, we complement the analysis of Dunat by providing results in terms of PHY layer parameters; more specifically coverage area, receiver SNIR and achievable data rates. First, through simulations several scenarios of overlapping WLANs are examined to show the existence of this interference and the impact it can have on network performance. We then deduce minimum separation distances that allow two conventional WLAN systems to co-exist while maintaining acceptable individual performance. We also propose the use of an OOB spectrum shaping transmit filter that lessen degradation compared to conventional WLAN systems. In addition to this, we develop routines which may be used to limit this interference if the derived minimum separation distances cannot be met. Results from our study may be used to develop guidelines that allow better co-existence strategies for overlapping WLANs. Moreover, the results of our analysis may also be useful in developing APs that have the ability to use multiple channels simultaneously.

In our analysis we restrict ourselves to interference between APs only. Obviously, interference may occur between users and APs and/or between users themselves. However, interference from a user will be less disruptive on overall performance as users do not transmit continuously or as frequently as APs. Interference between APs will have a much more crippling effect on overall system performance, especially when APs are in infrastructure mode where all transmission occurs via the AP. This is in general the case for practical WLANs.

5.2 Overlapping Coverage Areas

The limited power and coverage area of a single AP necessitates the use of multiple APs in covering large areas. Deployment strategies for these large-scale multi-AP systems consist of two main parts: AP deployment to cover the desired area and RF channel allotment to the component APs. In AP deployment, coverage overlap is employed either to cover large areas with a desired signal quality or to increase system capacity in high user density areas [11] [12]. In coverage-oriented systems, optimization techniques try to maximize AP separation and minimize coverage overlap while maintaining the desired signal strength. In capacity-oriented systems, multiple APs are made available to users within the same coverage area and the main emphasis is on supporting as many users as possible [11]. As the number of users per AP increases the average goodput offered by the AP per user decreases. In such situations deploying another in the same coverage area can be used to increase the average goodput per user. Most practical large-scale multi-AP WLANs combine both layouts depending on the needs of the area that needs to be covered.

Once cells have been defined, RF channels are assigned to constituent APs to minimize co-channel interference between neighboring cells. Interference from co-located APs on non-overlapping channels is generally not taken into consideration. In coverage-oriented systems, APs are usually sufficiently spatially separated to neglect this interference; signal strength loss due to propagation drops the amount of interference a co-located AP operating on a non-overlapping channel will cause to negligible levels. However, recent trends to provide large coverage areas with high data rates are bringing AP closer together, thereby increasing the risk of ACI and the importance of accounting for this source of interference. In capacity-oriented systems, the smaller separation distance between APs further emphasizes these needs.

The presence of this interference may also be felt in areas with high WLAN deployment where no network planning is used. For example, dense residential areas, such as apartments, where individuals have personal WLANs set up. Because there is no governing rules regulating AP deployment, situations may arise where APs are placed close enough to feel this interference. In addition to this, the past few years have seen several new WLAN products that have the ability to use multiple channels enter the market. Such systems can potentially double or triple the bit rates that users associated with the AP can use. Depending on the number of channels the system is using. If component APs are designed to use individual channel separately, the proximity of the APs can cause individual AP to interfere with each other.

5.3 Adjacent Channel Interference Limits

According to the standard, a WLAN operating on a valid channel is defined as non-interfering with adjacent WLANs if its power spectrum lies within limits defined around its central frequency, f_c, as shown in Figure 2.7. Limits are defined over a range of ±30 MHz of f_c while valid channels are spaced 20 MHz apart, Figure 2.6. Furthermore, the maximum power limit set for any frequency outside the allocated band is -40 dB relative to the in-band transmit power. For channels in the lower UNII 5 GHz ISM band, channels designated for indoor WLAN use, the maximum allowable transmit power is -13.97 dBW. Indoor WLAN systems need to operate with received signal strengths as low as -112 dBW, Table 2.7. Thus, interference from an AP operating on a non-overlapping channel can severely impact of other WLANs operating in its vicinity.

From Figure 2.7 and [1], AP_1 centered at fc1, and transmitting at full power can cause interference of up to -20dBr (relative to the maximum transmit power on channel 1) on the outer sub-carriers of AP_2, that is centered at f_{c2}, on the side closest to channel 1. This interference gradually drops to about -28 dBr at the center frequency of channel 2 and drops further to -40dBr at the outer sub-carriers on the side away from channel 1, as shown in Figure 5.1. If AP_2 is receiving transmission from a far away user depending on the separation between the two APs and the strength of the signal AP_2 is receiving, this interference may severely affect performance.

AP_2 will interpret this interference as noise. Therefore, the simultaneous operation of the two channels will increase the noise power of both systems. Higher signal power values will be needed to make the system switch to higher modulation schemes and bit rates will suffer. Moreover, the interference across the subcarriers of AP_2 is not flat; those closer to AP_1 will experience more distortion. If AP_1 is on a non-adjacent non-overlapping channel, AP_1 can cause a maximum of -40dBr across all subcarriers of AP_2

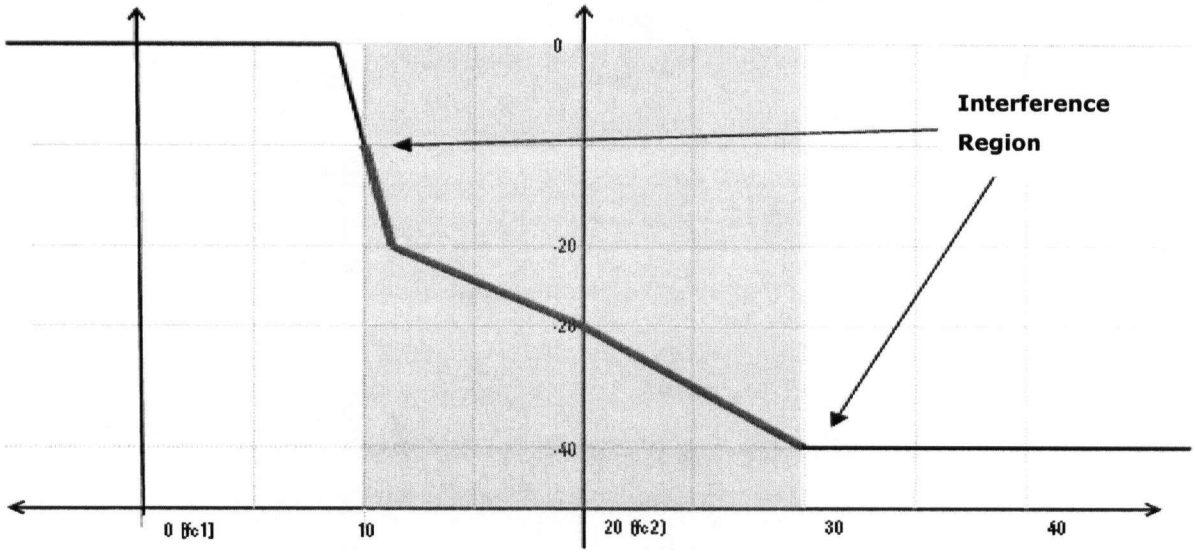

Figure 5.1: OOB spectral leakage limits from an adjacent non-overlapping channels in IEEE 802.11a

The interference limits described above are for the most severe case. Such levels will only occur if the two APs are located at exactly the same location and operating on adjacent channels; there is no separation between the antennas of the two APs. In addition, AP_1 needs to be transmitting at full power while AP_2 needs to be receiving a week signal from a far away user. ACI may also be felt for other combinations of transmit and receiver between the two APs, but this particular situation will experience the biggest impact of ACI. However, such a separation distance between APs is non-practical as explained in section 5.4.2

5.4 Parameters Affecting Non-Overlapping Channel Inter-cell Interference

5.4.1 Out-of-Band Power Spectrum of Interfering AP

As previously explained in Section 3.4, an OFDM signal has high out of band spectral components, and OOB spectrum reduction is necessary to lower OOB components to levels defined by the spectral mask of IEEE 802.11a. Because of the limited frequency separation between IEEE 802.11a channels any OOB spectral component lies in the in-band of other WLANs. Therefore, the OOB spectrum reduction technique used by the interfering AP will have a direct impact on the amount of interference it can cause on co-located APs. Although a number of techniques can be used for OOB spectrum reduction we consider the two techniques described in Section 3.4.2: RC windowing with $\beta = 0.0125$ and high order filtering. The former is taken as the conventional OOB spectrum reduction technique used in most WLANs, for reasons also explained previously. The transmit signal spectrum after the two OOB spectrum have been applied is shown in Figure 5.2 below.

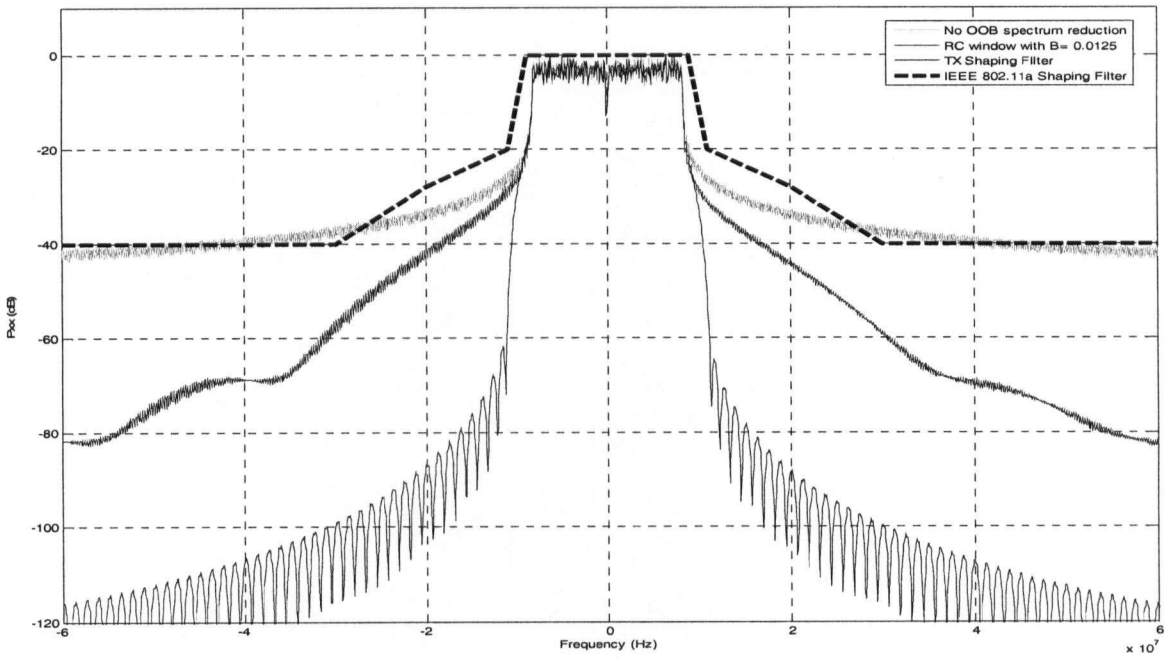

Figure 5.2: Normalized transmit signal spectrum before and after RC windowing with $\beta = 0.0125$ and transmit filtering for OOB spectrum reduction

5.4.2 Spatial Distance between APs

The amount of interference a co-located AP can cause is inversely related to the separation distance between the two APs, more specifically, on the separation distance between their antennas. The decay of signal power with distance, large scale variations of wireless channels, is modeled using pathloss models. These models can be based on empirical measurements where the model obtained is specific to the geographic area where the measurements were conducted or alternatively, on statistical models that are based on statistically modeling of dominant channel characteristics. Models obtained from the latter are less accurate but are not limited to a specific geographical area. Most models used are a combination of the two; parameters of the analytically derived statistical model are determined through empirical measurements. Several statistical models for the indoor wireless channel exist. However, there is not one generally accepted model. A good overview of the types of indoor pathloss models and the differences between an indoor wireless channel for a fixed broadband system and the conventional mobile channel can be found in [26][49]. The pathloss model used in the simulations is of the log distance type with a fixed pathloss exponent and is taken from [6].

$$PL(d) = PL_0 + 10\gamma \log_{10}(d) + S \tag{5.1}$$

where d is the distance between the antennas, γ is the Pathloss coefficient, S is the shadow fading random process, PL_0 is the pathloss at reference distance of 1m. PL_0 and γ are empirically determined for various channel conditions in [6]. For NLOS Rayleigh faded channels, conditions typical of environments WLANs operate in, PL_0 is given as 51 dB and γ as 3.5 respectively, while for LOS conditions they are 47 dB and 1.7 respectively.

An important point to mention is that most pathloss models have a reference point, PL_0, the power loss at a reference distance associated with them. This reference distance specifies the distance beyond which the electrical field radiated by the antenna can be considered far-field. In the far-field region, the fields generated by the antenna are planar and orthogonal to each other and to the direction of propagation. All Energy from the antenna can be considered radiating in the direction of propagation. In this region, the effects of the antenna can be excluded from the pathloss model. By doing so pathloss models are made independent of the antenna and describe the loss in power due to distance and the environment in which they operate only.

For smaller distances, within the reactive near field of the antenna, reactive energy is stored in the electric and magnetic fields which is not radiated. If a devise capable of coupling energy from these fields is placed in this region it can develop a received signal. This, mutual coupling between the two antennas and possibly other electronic components may result in impedance miss-match between transmitter and receiver components which would lead to a less then optimum transfer of power between the two [46]. Furthermore, at such small distances, electrical and magnetic fields can no longer be considered uniform and both horizontal and vertical displacement between the antennas needs to be considered. With vertical displacement the antenna pattern can not be considered omni-directional as dipole antennas are omni-directional in the x plane at such short distances.

In general, systems are designed to work at distances greater then this reference distance and published antenna specifications are for far field regions only. However, separation distances of a few centimeters also need to be considered as the dimensions of practical AP are in orders of centimeters. For the current investigation we limit ourselves to a minimum separation of 1m between APs, thereby guaranteeing that we operate in the far fields of the antennas and far enough to ignore the effects of mutual coupling. An investigation on the effects of non-uniform antenna patterns and coupling between electronic components on performance is left as a topic for future work [46].

The S in equation (5.1) represents the variation of the instantaneous pathloss around the mean value calculated by the rest of the equation. In indoor wireless channels, large variations in the pathloss are possible due to the presence of several scatters and the generally NLOS conditions between the AP and the receiver [26]. In [6], S is modeled as a zero mean Gaussian random processes with a variance of 7.6 dB for NLOS and 5.6dB for LOS. Shadow fading in a link adaptive receiver is generally mitigated by including a cushioning factor on the desired cutoff rates for the different modes (combination of the coding and modulation scheme used). The adaptive system becomes more tolerant to errors but the system throughput suffers. In our system we use this cushioning factor to handle the non-constant interference caused by the interfering WLAN. To prevent system throughput from decreasing too severely we assume stationary conditions for the user and objects in its surrounding. APs are always assumed to be fixed in position. Hence, (5.1) for our analysis can be re written as

$$PL(d) = PL_0 + 10\gamma \log_{10}(d) \tag{5.2}$$

5.4.3 Operating Channels

The IEEE 802.11a standard [1], defines 12 non-overlapping 20 MHz channels in the 5 GHz UNII band, which a WLAN can operate on, see Figure 2.6. However, only four channels in the lower 5 GHz UNII are defined explicitly for indoor WLAN use. We restrict ourselves to these channels only. For our interference analysis, an interfering AP can be operating on an adjacent channel (AC), or on a non-adjacent channel (NAC). An adjacent channel is defined as a non-overlapping channel with a frequency separation of 20 MHz between the central frequencies of both Channels. A non-adjacent channel is one in which the central frequencies are separated by more then 20 MHz. All channels other than the adjacent channel cause the same level interference (cf. Figure 2.7). Interference from a co-located AP on an adjacent channel is much more disruptive as the power spectrum limits defined by the mask in Figure 5.1 are lower and non-constant over the 20 MHz bandwidth. These limits were defined in Section 5.3. A non-adjacent channel interfering AP will cause a maximum interference of -40dBr relative to its maximum transmit power. Furthermore, interference from a non-adjacent channel will generally be spectrally flat across the channel.

5.4.4 Transmit Signal Power

Obviously, the transmit power of the interfering signal will have a direct bearing on the amount of interference it will cause. The maximum allowable transmit power for the four lower UNII 5 GHz band channels is defined in [1] as 40 mW in a 20 MHz bandwidth. We assume that all APs transmit at maximum power to provide maximum coverage areas to its users. Although variable transmit power can be used as a means of reducing inter-cell interference it is not within the scope of this project and is left for a possible topic for future work.

5.5 Parameters Affected by Adjacent Channel Interference

5.5.1 Coverage Area

We define the coverage area of the WLAN system under investigation to be concentric circles centered at the AP with cut-off boundaries for the different operational modes defined by the 10% Packet Error Rate (PER) for a Physical Sub-layer Data Unit (PSDU) of length 1000 bytes. In the 802.11a standard [1], this is defined as the minimal operational requirement for any particular mode. If performance falls below this level, the system switches to a lower mode that is more resilient to channel induced errors. Obviously, the actual coverage area will be affected by the geographical area and other sources of interference in its vicinity. However, since we are only interested in studying the mutual interference between APs we ignore the impact of these factors and assume that loss in average signal strength is only due to pathloss and interference from the nearby AP. Based on the above assumptions the coverage area around a single AP, that is using an omni-directional antenna, with an antenna gain of 0 dBi, and is show in Figure 5.3 below. Here, dBi is antenna gain in dB with reference to an isotropic antenna. The cutoff SNIR values for the different modes are given in Table 3.4 for a block fading channel. As explained previously, the block fading channel is used to reduce simulation run time.

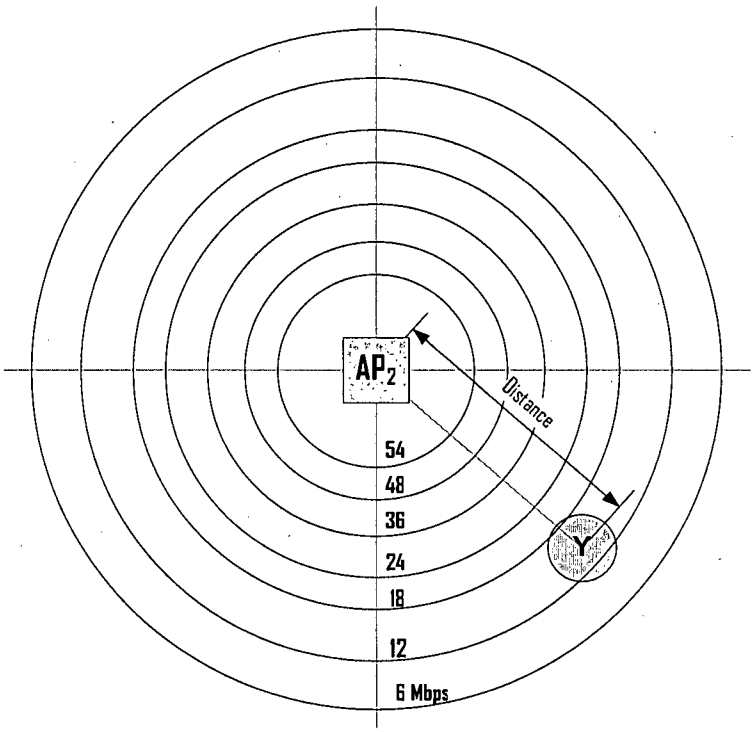

Figure 5.3: Coverage Area of a single AP with no nearby sources of interference.

5.5.2 Signal-to-Noise-plus-Interference Ratio

Two definitions of receiver signal-to-noise-plus-interference-ratio (SNIR) are used in our analysis. The first is defined at the front end of the receiver, and is termed as receiver front end SNIR. The transmitted signal and the noise-plus-interference signals are sent separately into the receiver. Power levels on both signals are calculated to find the receiver front end SNIR prior to mixing the two signals and conveying it to the rest of the receiver. Receiver front end SNIR is used to calculate the individual SNIR across subcarriers. The second SNIR ratio is defined after the received bits have passed through the demodulation process. The demodulated bits are re-modulated to data symbols which are multiplied with appropriate channel transfer function to generate a vector of error terms. The power of this error vector is used to calculate the receiver. In our simulations, we study the impact of using both definitions for the link adaptive system.

5.5.3 Link Adaptation Scheme

Details on the link adaptive scheme can be found in Section 3.3. The mode switchover thresholds defined as normal thresholds in Table 3.4 are assigned to exactly the 10 % PER cutoff points to maximize throughputs.

5.6 Simulation Setup

The Dual Channel Model described in Section 4.2 is used to investigate a scenario where a user Y at distance d from AP_2 is transmitting on channel 2. Concurrently, AP_1 which is at distance $D_{separation}$ from AP_2 is transmitting to user X on channel 1, see Figure 5.4. We ignore the cases where either one or both APs are idle as interference would not be a problem in terms of PHY layer parameters for these cases. Two links need to be modeled: first, the link between AP_2 and user Y and second the interfering link between the two APs. Multipath is only modeled on the link between an AP_2 and user Y. For the current investigation, we assume that the two APs are insight of one another. Because of their proximity and the LOS channel between the two APs there is always one dominant path present. Hence, fading will have a minimal effect and is not modeled on this link. Signal strength loss on this link is due to pathloss and receiver induced distortions only. Recall that the pathloss model has also been made deterministic by ignoring the effects of shadow fading, cf. Section 5.4.2.

The separation distance between the two APs is fixed in the beginning of each simulation and the performance of the receiver at AP_2 in terms of SNIR and the average bit rate is calculated as user **Y** moves away from AP_2. The original and the noise-plus-interference signals are sent separately into AP_2's receiver only to calculate the front end SNIR after which they are combined together and sent into the rest of the receiver, Figure 4.2. User Y's receiver is not monitored as we assume there is a sufficient separation between it and AP_1.

Three different cases are considered: (1) the no interference case, which is used as a reference to compare performances with, (2) a co-located AP operating on a non-overlapping adjacent channel (ACI) and (3) a co-located AP operating on a non-overlapping non-adjacent channel (NACI). Each case is divided into two parts. In part (a), the mode of user X is fixed and the 10% PER is found as a function of the distance between AP_2 and user X for $D_{separation}$ of 1 m. Distances are rounded off to

the nearest 0.5 m point that meets the 10% PER criteria. No information is sent back to the receiver. In part (b), the link adaptive system is simulated and the average bit rate and average SNIR of the system as a function of distance is calculated for various values of $D_{separation.}$ Each simulation is run twice using one of the outlined OOB spectrum reduction techniques. A minimum of $20*10^6$ bits are transmitted for each run to obtain average values. For all cases, the block fading channel described in Section 3.2 is used. At the receiver, time domain LSE channel estimation is used. The BER and PER as a function of SNR are shown in Figure 3.5 and Figure 3.6 respectively.

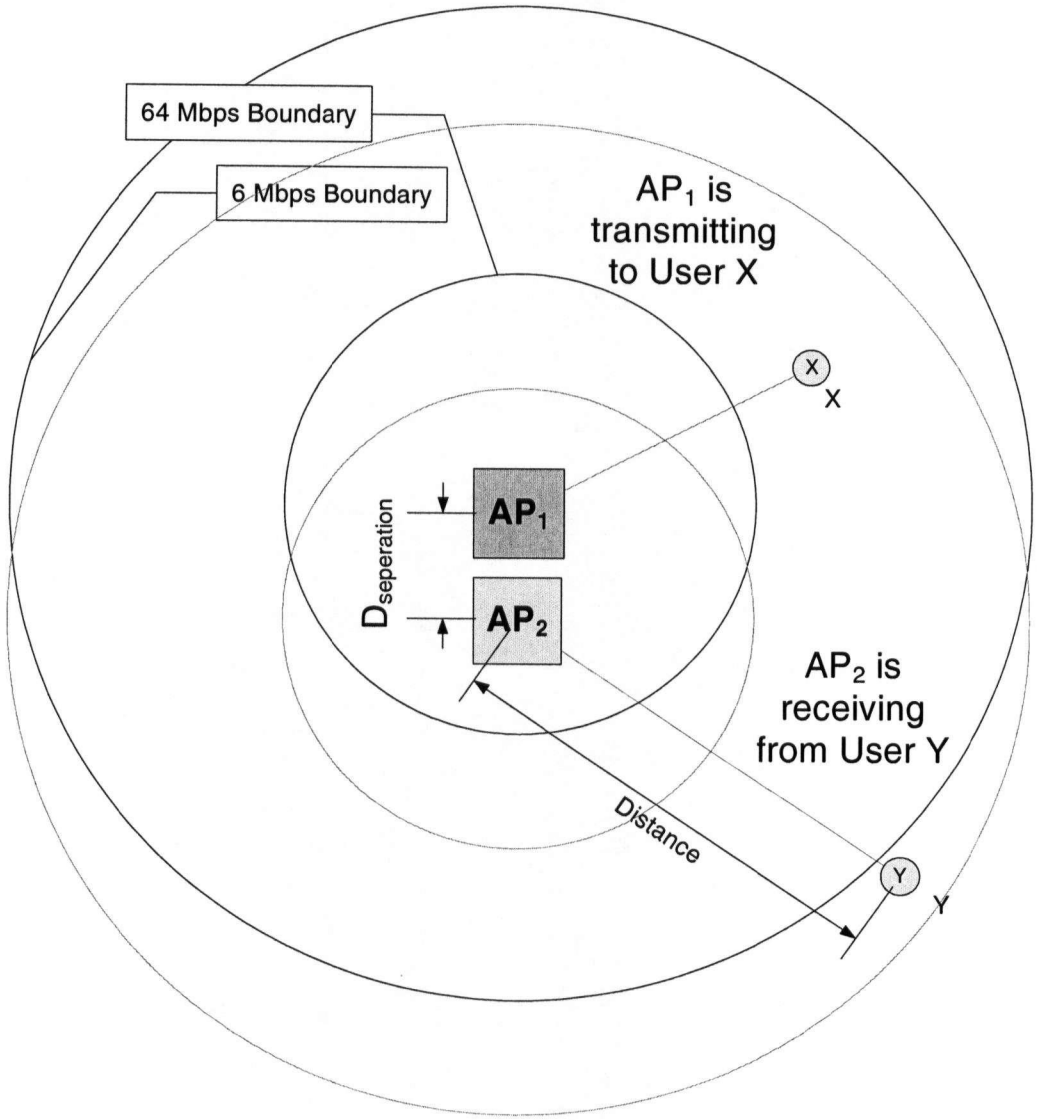

Figure 5.4: Simulation scenario - AP_1 transmitting to user X, AP_2 receiving from user Y

5.7 Simulation Results

5.7.1 No Interference

For the no interference case, Figure 5.5 presents the PER as a function of distance for all fixed mode systems. Here we consider only the performance of the receiver of AP_2 as it receives from user Y; no interference from AP_1 is present. The 10% cutoff distances are used to plot the region over which a mode can provide reliable coverage in Figure 5.6 as the dashed stair case line. Here, it is assumed that beyond its 10% PER cutoff distance, a mode can no longer provide reliable communication. At a particular distance, only the mode that provides the highest bit rate and conforms to the 10% PER criterion is plotted. All lower modes are capable of providing reliable communication at any point.

Up to a distance of 6 m, the AP is capable of providing reliable communication at the highest possible data rate. Beyond a distance of 20.5 m, the system is unable to provide reliable communication in any mode under the assumed channel conditions. Furthermore, the results also show that the performance of Mode 2 and Mode 3 are similar, cf. Section 3.3. Figure 5.6 shows the performance of the link adaptive system for the no interference case. Two link adaptive system performance curves are shown. In the first, the link adaptive system uses the *normal* switch-over thresholds described in Section 3.3. In the second, the link adaptive system employs the *upped* switch over thresholds. This is one of the interference mitigation techniques we describe in Section 6.1 to counter ACI and NACI.

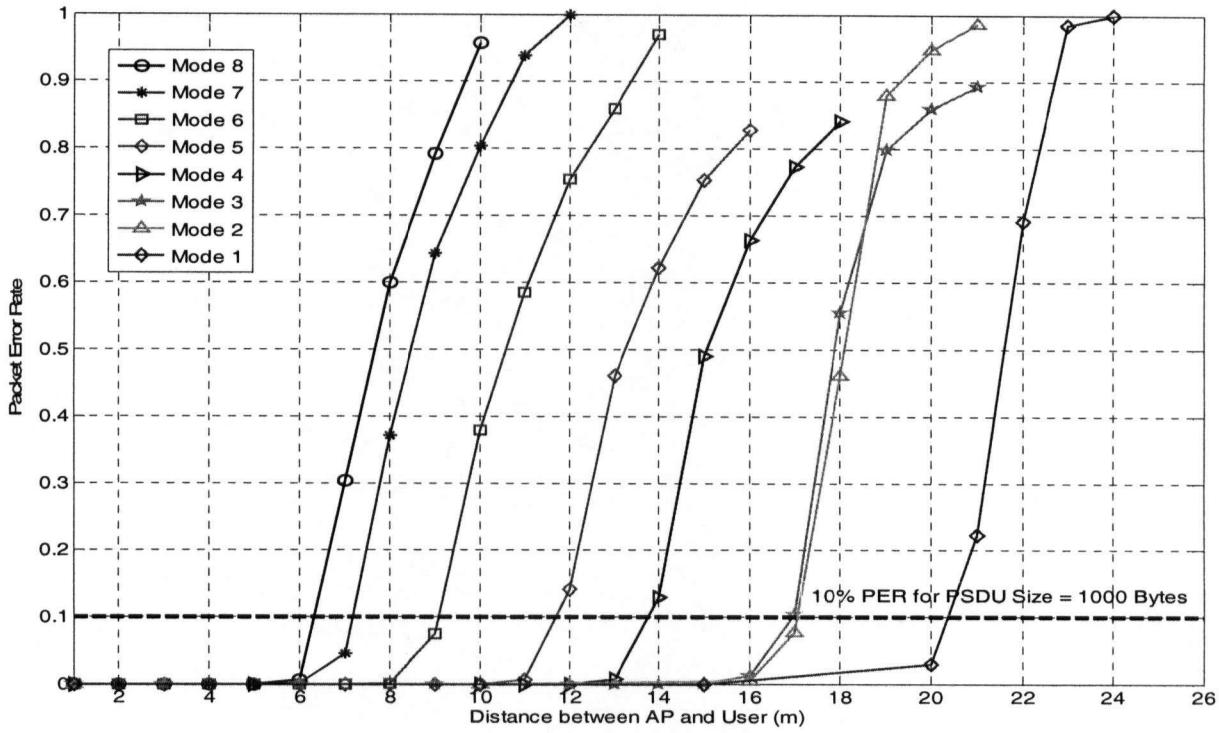

Figure 5.5: 10% PER cutoff distances for fixed modes without interference, PER vs. distance

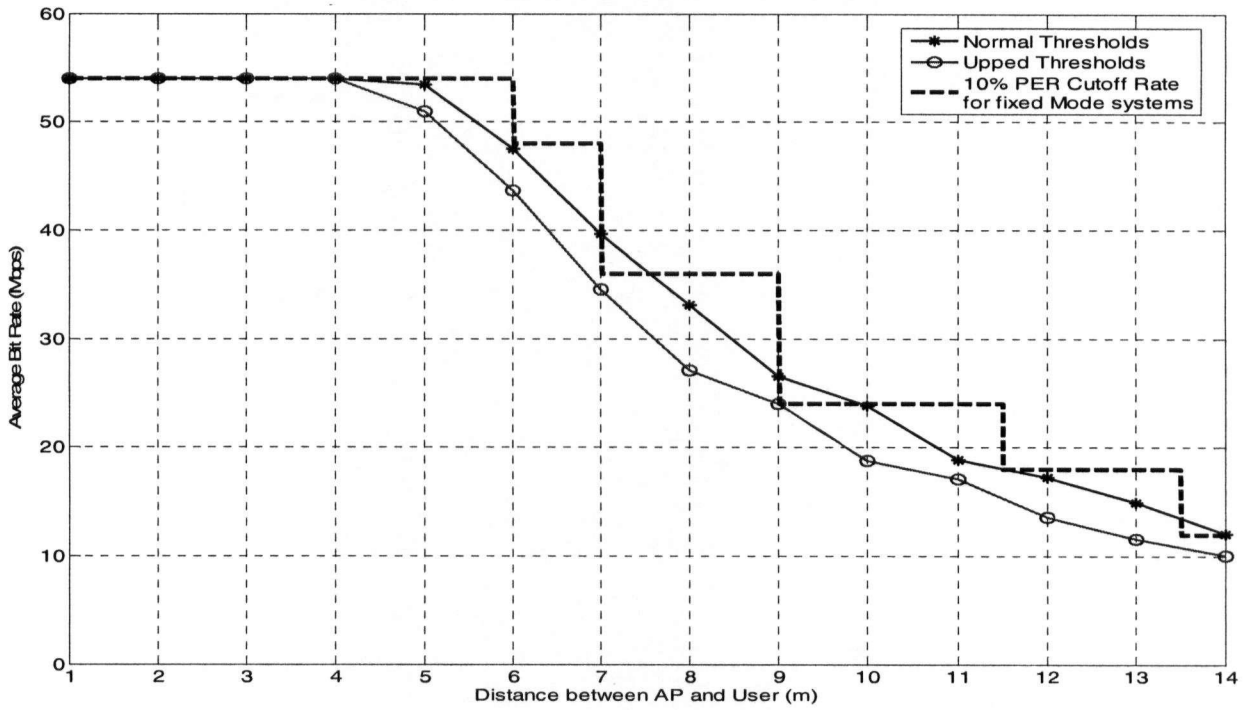

Figure 5.6: Bit Rate vs. Distance for Link Adaptive System with no interference

5.7.2 Adjacent Channel Interference

For the case of ACI from a co-located AP, results of part (a), $D_{separation}$ fixed at 1m, are shown in Figure 5.8, Figure 5.9, and Figure 5.10. In Figure 5.8 and Figure 5.9, bit rate vs. distance for an interfering AP using RC windowing with β = 0.0125 and for the transmit filter for OOB spectrum suppression are shown respectively. As in the previous section, performance of fixed mode simulations are plotted as dashed lines and that of link adaptive systems as continuous lines. The PER vs. distance of the link adaptive systems for both spectrum reduction techniques are shown in Figure 5.10.

Comparing the fixed mode system bit rate vs. distance graphs in Figure 5.8 and the no interference case in Figure 5.6, there is significant degradation in coverage areas and achievable bit rates within the coverage area in the presence of ACI from a co-located AP that is using RC windowing with β = 0.0125 for OOB spectrum reduction. In fact, compared to the results of all other scenarios modeled, this case causes the most severe degradation. Reliable communication at the highest possible data rate is only possible within a distance of 2m from the AP, a drop of 4 m compared to the no interference case. No reliable communication is possible beyond a distance of 6m, a drop of 14.5 m compared to the no interference case. The drop in the cutoff distances for all modes compared to the no interference case are given in Table 5.1. Moreover, a comparison of link adaptive and fixed mode system bit rate vs. distance curves shows that the link adaptive system under-performs the fixed mode simulations. Unlike for the no interference case, the link adaptive system under performs the fixed mode simulations when the link adaptive system is using *normal* mode switch-over thresholds. This may be due to the unsuitability of these thresholds when such interference is present. The PER vs. distance of this case, shown in Figure 5.10, increases unbound beyond a distance of 6 m from the AP, once again showing that this case results in severe degradation.

Performance is slightly better if the interfering AP is using the transmit filter for OOB spectrum reduction, but only when fixed mode systems are considered, cf. Figure 5.9. For the highest data rate, reliable communication is possible up to 3 m away from the AP, a drop of 3 m compared to the no interference case. Reliable communication using any mode can be maintained up to 11.5 m away from the AP. This corresponds to a drop of 8.5 m compared to the no interference case. However, the

results of the link adaptive system differ from this significantly. Even though the fixed mode simulations provide much higher cutoff distances, the PER within the coverage area is above 10 % for certain distances. In Figure 5.10 only points that meet the 10% PER criterion are plotted. For distances between 3m and 9m, the PER is not contained within the 10% PER limit. This trend can also been seen in the PER curves of the system in Figure 5.10.

This implies that the SNIR cutoff thresholds defined for the no interference case do not function properly when ACI is present. A possible reason for this may be due to the non-gaussian nature of the interfering signal leaking into the in-band channel of AP_2 and user Y. Because of this non-flat interference signal, outer subcarriers on the side closest to the channel of the interfering AP experience much higher levels of distortion than the average subcarrier SNIR, cf. Figure 5.7. Although the receiver itself works with variable subcarrier SNIRs, the information sent back to the transmitter is based on a value that is averaged over all subcarriers' SNIR. Therefore, a PER of greater then 10% may be observed even when the average SNIR value sent back to the transmitter is less then the 10% PER cutoff value. From Figure 5.7, if the interfering AP is using RC windowing for OOB spectrum reduction there is a greater disparity between the SNIR of end subcarriers and the average SNIR across all subcarriers.

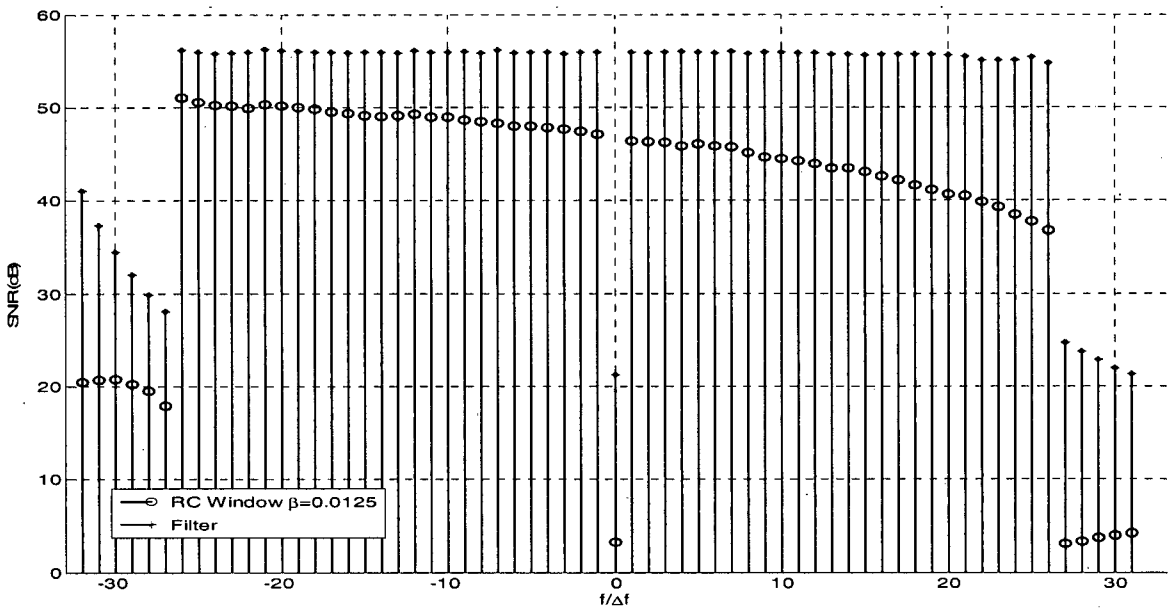

Figure 5.7: Individual subcarrier SNIR in the presence of ACI from an AP at $D_{separation}$ = 1m.

In Figure 5.10, the hump in the PER curves for the case of ACI from a co-located AP at a $D_{separation}$ of 1m that is using a transmit filter for OOB spectrum reduction is related to the amount of switching between modes. At distances close enough to the AP, signal strength is much stronger then the interfering signal. The link operates at the highest mode providing the user with maximum bit rate. At slightly further distances, interfering signal strength becomes comparable to signal strength, i.e. the user's SNIR ratio is within the defined mode switchover thresholds. The link switches modes frequently to adapt to the time varying channel conditions and to keep the PER under 10%. However, the *normal* switch over thresholds are not designed to deal with this non-gaussian interfering signal, and the PER increases to more then 10%. At further distances, the link stops switching between modes and operates in its lowest mode and the PER falls slightly. This may also explain why there is reliable communication at distances 9-11m in Figure 5.10. Finally, at distances greater then the cutoff distance of the lowest mode, the PER starts increasing and goes to one. At this point all transmitted packets are in error.

This trend is also visible in the PER curves of NACI from an AP using either the transmit filter or the RC window for OOB spectrum reduction. The PER curve of ACI from an AP using RC windowing with β = 0.0125 do not show this trend. This may be due to the fact that interference for this case is too severe.

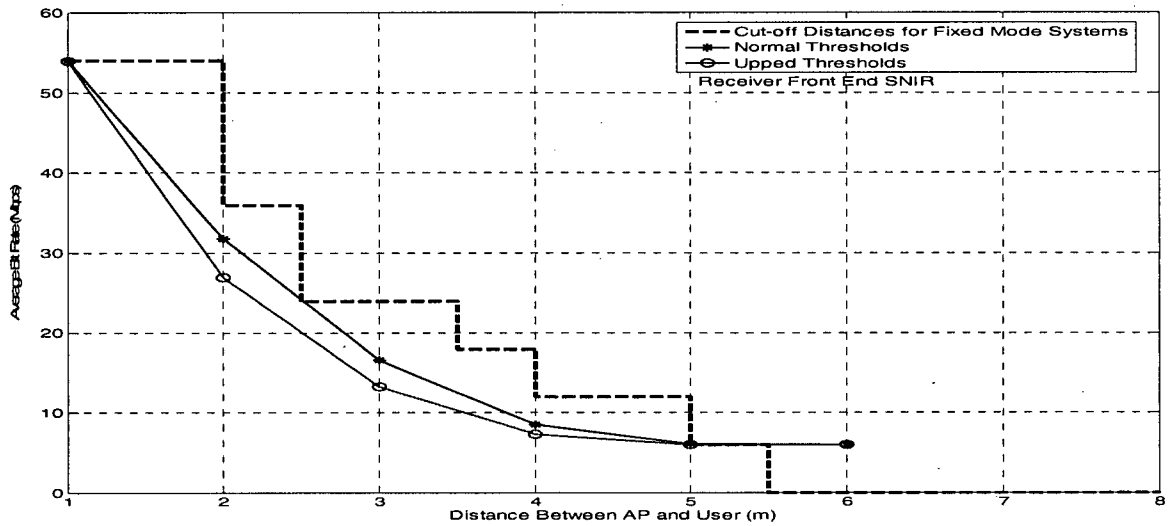

Figure 5.8: Bit rate vs. distance in the presence of ACI from an AP at $D_{separation}$ = 1m, Interfering AP using RC windowing with β = 0.0125 for OOB spectrumn reduction.

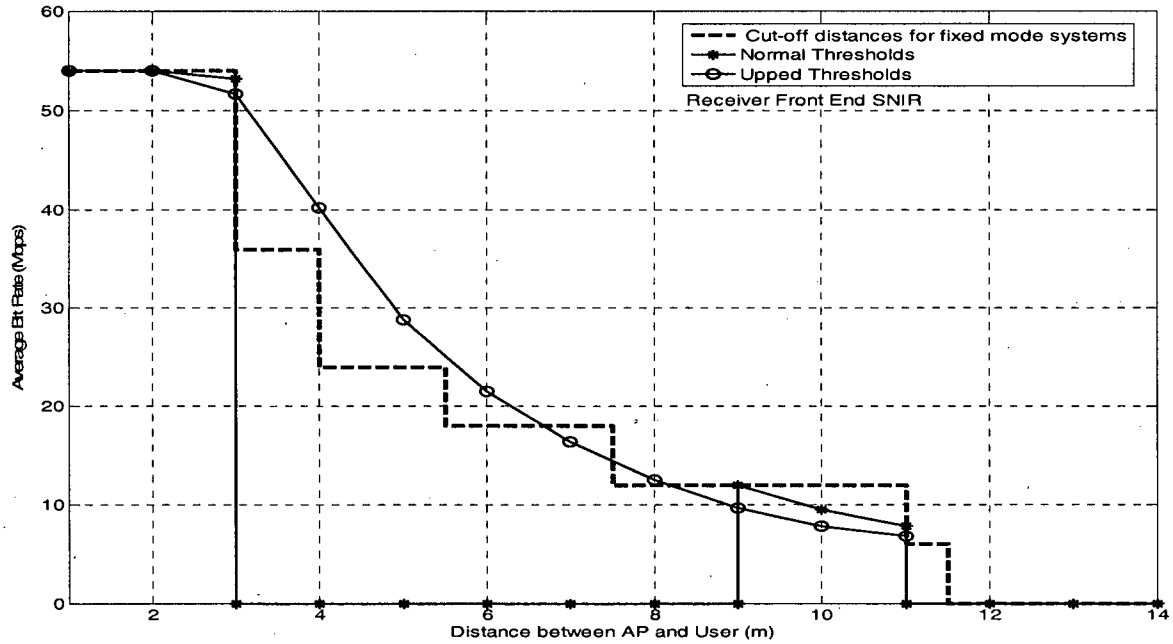

Figure 5.9: Bit Rate vs. distance in the presence of ACI from an AP at $D_{separation}$ = 1m, Interfering AP using the Transmit filter for OOB spectrum reduction[3]

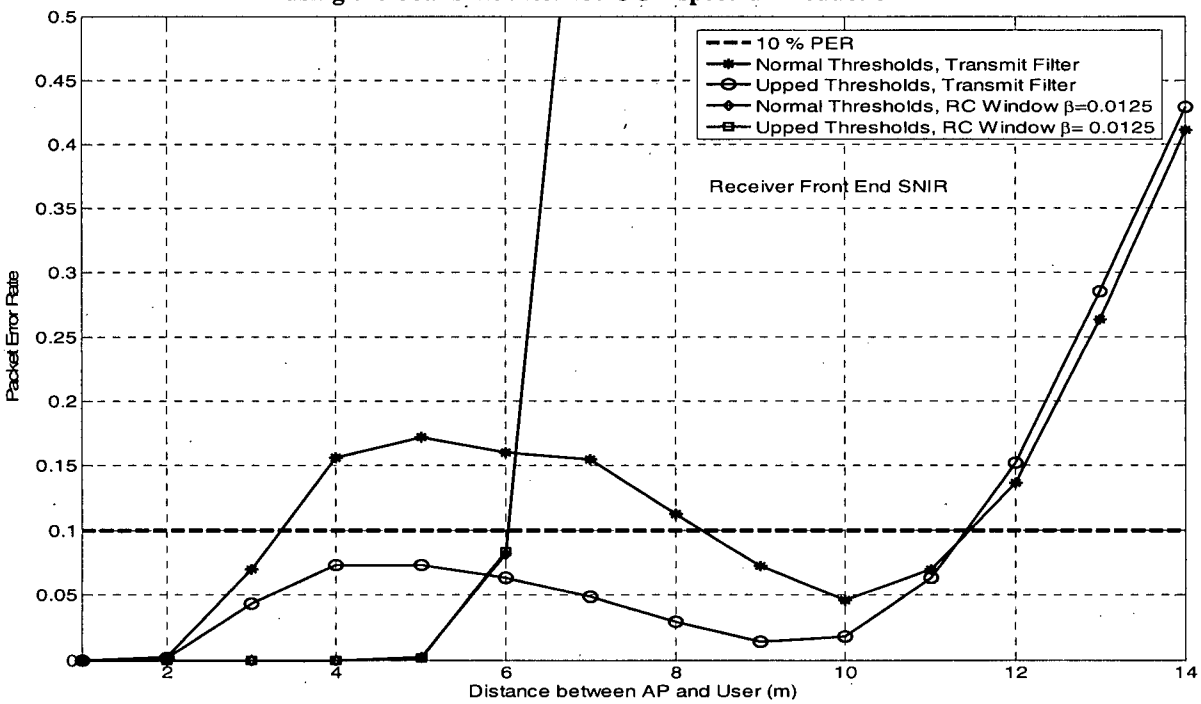

Figure 5.10: PER vs. distance in the presence of ACI from an AP at $D_{separation}$ = 1m

[3] In all bit rate vs. distance figures, only points with a PER of less then 10% are plotted.

Results for part (b), variable $D_{separation}$ distances for the case of ACI from a co-located AP are shown in Figure 5.11 and Figure 5.12. In Figure 5.11 link adaptive system bit rates vs. distance results for varying $D_{separation}$ are shown for both OOB spectrum reduction techniques. Only points that conform to the 10% PER criterion are plotted. The corresponding curves for receiver front end SNIR as a function of distance are shown in Figure 5.12.

As shown in the previous section, for the case of the interfering AP using the transmit filter, severe performance degradation occurs at a $D_{separation}$ of 1m. Reliable communication is not possible within the coverage area. Furthermore, from Figure 5.12, there is a drop of about 8 dB compared to the SNIR of the no interference case. For $D_{separation}$ distances of 3m, there is significantly less distortion; there is approximately a 3 dB loss compared to the no interference SNIR. Furthermore, reliable communication is maintained within the coverage area. A $D_{separation}$ of 5m is sufficient to make effects of ACI negligible.

For the case of the interfering AP using RC windowing, although reliable communication is possible for all distances within the coverage area, the coverage area is much more constricted for all $D_{separation}$ distances compared to an interfering AP that is using the transmit filter for OOB spectrum reduction. Compared to the no interference case, there is a drop of 20 dB in receiver front end SNIR for this case. However, for increasing $D_{separation}$ distances performance does not improve as dramatically as it did in the case of the interfering AP using the transmit filter for OOB spectrum reduction. In fact, performance in terms of both receiver front end SNIR and achievable bit rate is significantly degraded even for a $D_{separation}$ as far away as 10m. This is due to the non-uniformity of individual subcarrier SNIRs (cf. Figure 5.7). As a result, as soon as receiver SNIR comes within range of the mode switchover thresholds performance drops considerably. This can be seen as the sharper drop in bit rate curves for RC windowing in Figure 5.11. For larger $D_{separation}$ distances the decline in bit rates is more gradual.

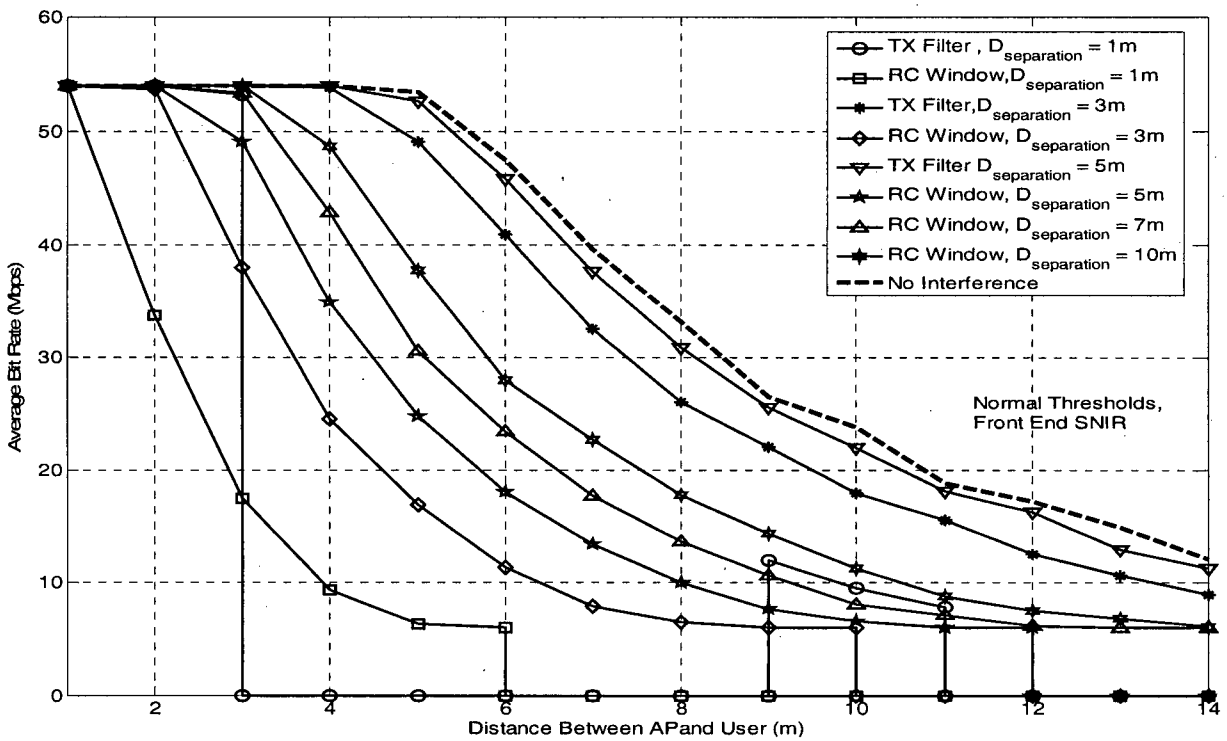

Figure 5.11: Bit rate vs. distance for various $D_{separation}$ for ACI from a co-located AP, link Adaptive System using Normal thresholds and Front End SNIR

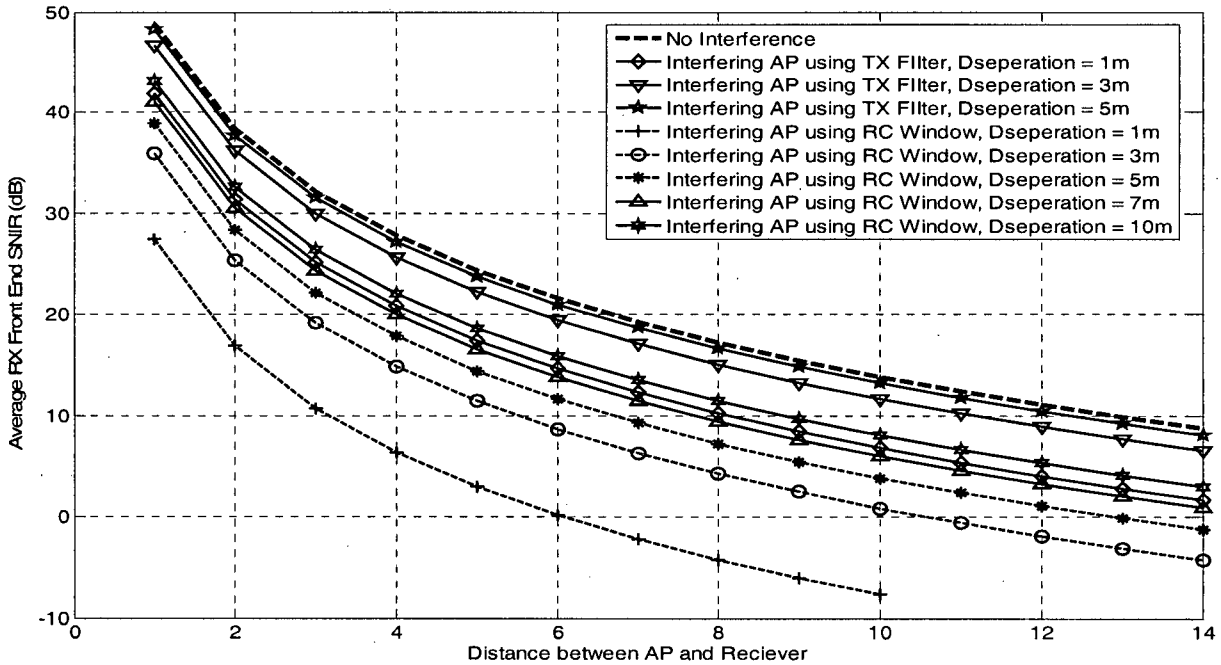

Figure 5.12: RX front end SNIR vs. distance for various $D_{separation}$ for ACI from a co-located AP

5.7.3 Non-Adjacent Channel Interference

For the case of NACI from a co-located AP, results of part (a) ($D_{separation}$ fixed at 1m), bit rate vs. distance plots are shown in Figure 5.13 (RC windowing) and Figure 5.14 (Transmit filtering) while PER vs. distance plots are shown in Figure 5.15. As done previously, performance of fixed mode simulations are plotted as dashed lines and that of link adaptive systems as continuous lines.

On comparing the fixed mode system bit rate vs. distance in Figure 5.13 with the no interference case (cf. Figure 5.6), it is seen that the highest mode provides reliable communication up to a distance of 3.5m, a drop of 2.5 m. Reliable communication using any mode is possible up to a distance of 14.5 m, a drop of 5.5m compared to the no interference case. Furthermore, compared to the corresponding ACI cases, better performance is seen as reliable communication can be maintained over larger distances. Interfering signal strength is much weaker as there is greater frequency separation between the channels of the two APs. The drop in the cutoff distances for all modes compared to the no interference case are given in Table 5.1. As in the case of ACI, fixed mode system performance is slightly better if the interfering AP uses transmit filtering for OOB spectrum reduction. For this case, reliable communication at the highest bit rate is possible up to 4 m away from the AP, a drop of 2 m compared to the no interference case.

When performance of the link adaptive system with *normal* thresholds is analyzed for both OOB spectrum reduction techniques, the results follow a similar trend to the one that is observed in the case of ACI with transmit filtering; within the coverage area there are points where PER is not under 10%, cf. Figure 5.15. Although the IEEE spectrum mask limits of the interference signal are spectrally flat for a non-adjacent channel, OOB spectrum reduction techniques introduce decaying power spectrum strength with frequency away from the valid channel. This results in a spectrally non-flat interfering signal in the channel of a co-located AP. For these co-located APs, as soon as their SNIR comes within range of the mode switch-over thresholds, PER will rise to values above 10% as previously explained, Therefore, even NACI may result in non-flat interfering signals and cause performance degradation in co-located APs although not as severe as that for an ACI from a co-located AP. Link adaptive systems using *upped* thresholds are also shown in Figure 5.13 and Figure 5.14, these are related to a mitigation technique to counter ACI and NACI that we describe in Section 6.1

The PER curves in Figure 5.15 also follow a hump shape. However, compared to the PER curve of the ACI case (cf. Figure 5.10), the hump starts at a later distance and are broader. The weaker interference signal in this case comes within range of the mode switch over thresholds at further distances.

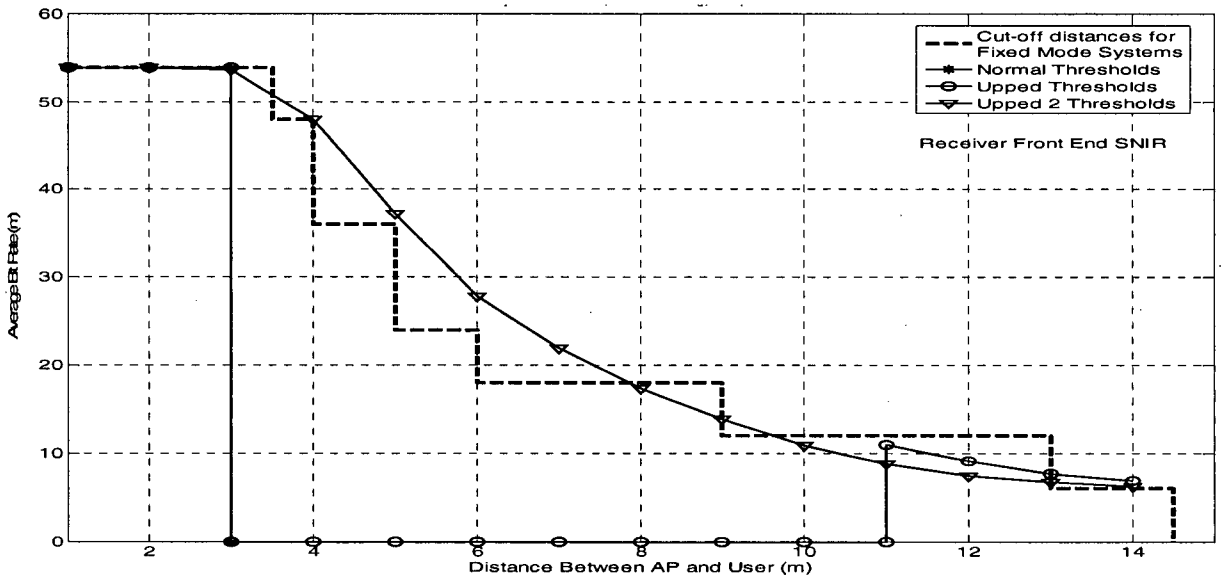

Figure 5.13: Bit Rate vs. distance in the presence of NACI from an AP at Dseparation = 1m, Interfering AP using RC windowing with β = 0.0125 for OOB spectrum reduction.

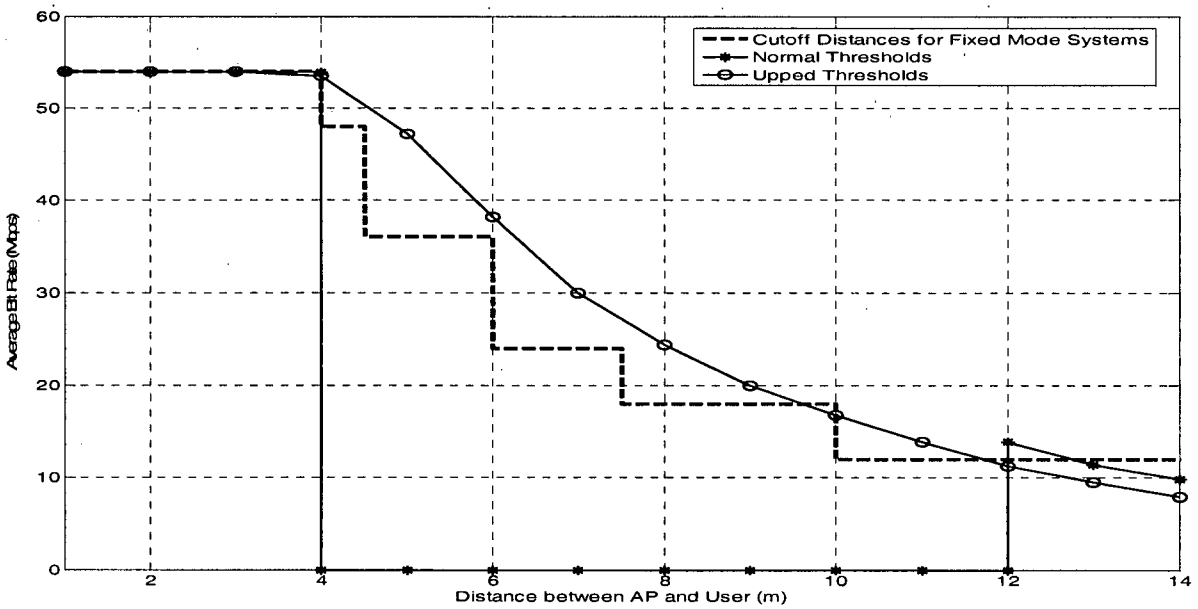

Figure 5.14: Bit rate vs. distance in the presence of NACI from an AP at $D_{separation}$ = 1m, Interfering AP using the Transmit filter for OOB spectrum reduction

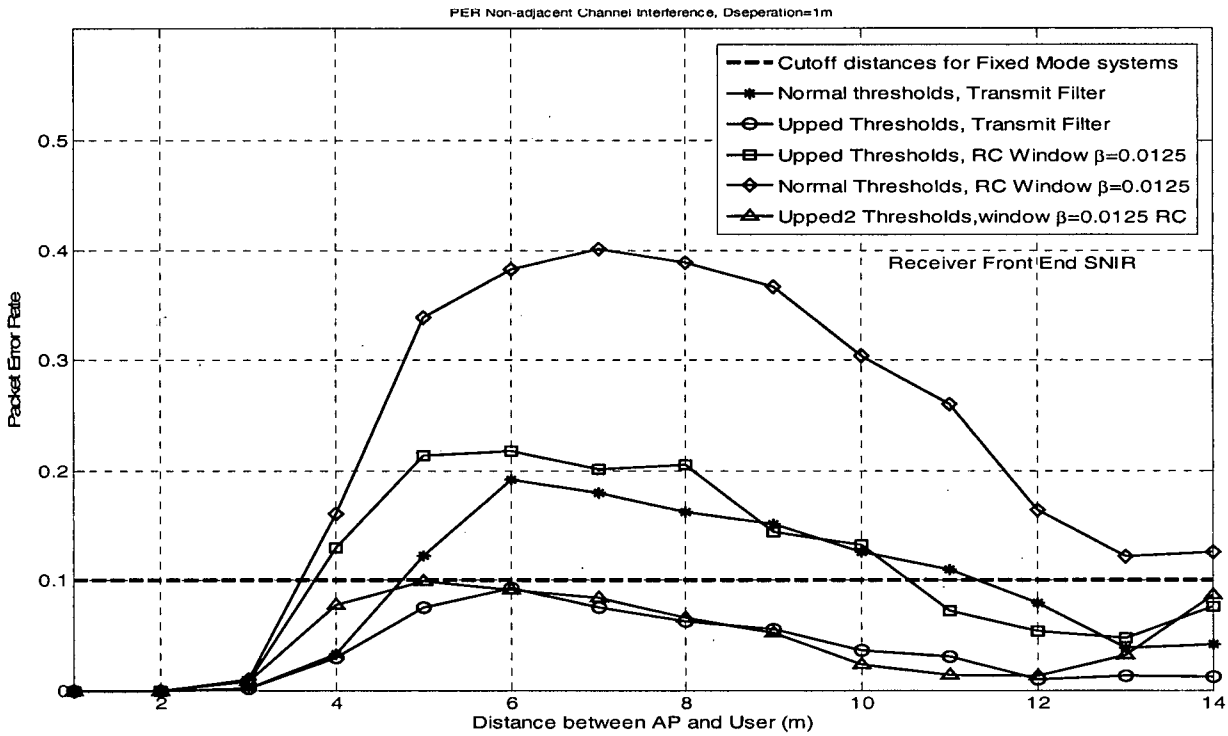

Figure 5.15: PER vs. distance in the presence of NACI from an AP at $D_{separation}$ = 1m

Results for part (b) (variable $D_{separation}$ distances), for the case of NACI from a co-located AP are shown in Figure 5.16 and Figure 5.17. In Figure 5.16 link adaptive system bit rates vs. distance results for varying $D_{separation}$ are shown for both OOB spectrum reduction techniques. Only points that conform to the 10% PER criterion are plotted. The corresponding curves for receiver front end SNIR as a function of distance are shown in Figure 5.17. At a $D_{separation}$ of 1m, if the interfering AP is using transmit filtering as opposed to RC windowing for OOB spectrum reduction, slightly better SNIRs are seen at the receiver. However, performance for any OOB spectrum reduction techniques for an AP at a separation distance of 1m are equally bad since, within the coverage area, the PER is above 10%. NACI interference from a co-located AP at $D_{separation}$ of 3 m and more for both spectrum reduction techniques show negligible performance degradation.

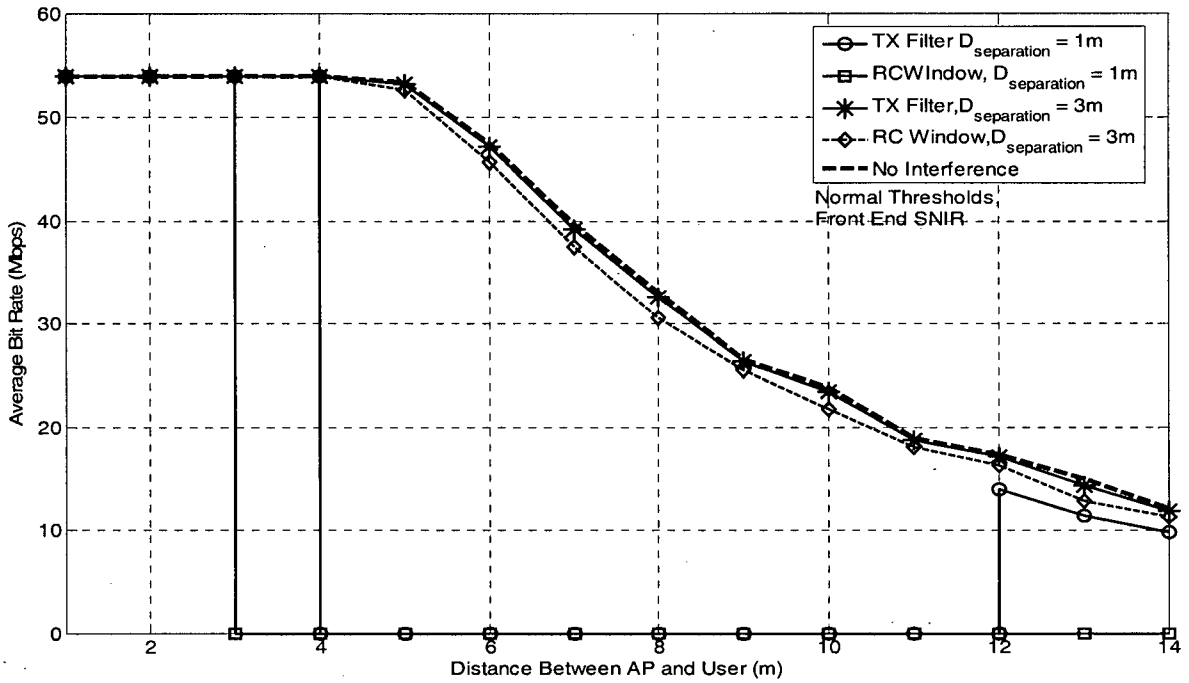

Figure 5.16: Bit rate vs. distance for various $D_{separation}$ for NACI from a co-located AP, link Adaptive System using Normal thresholds and Front End SNIR

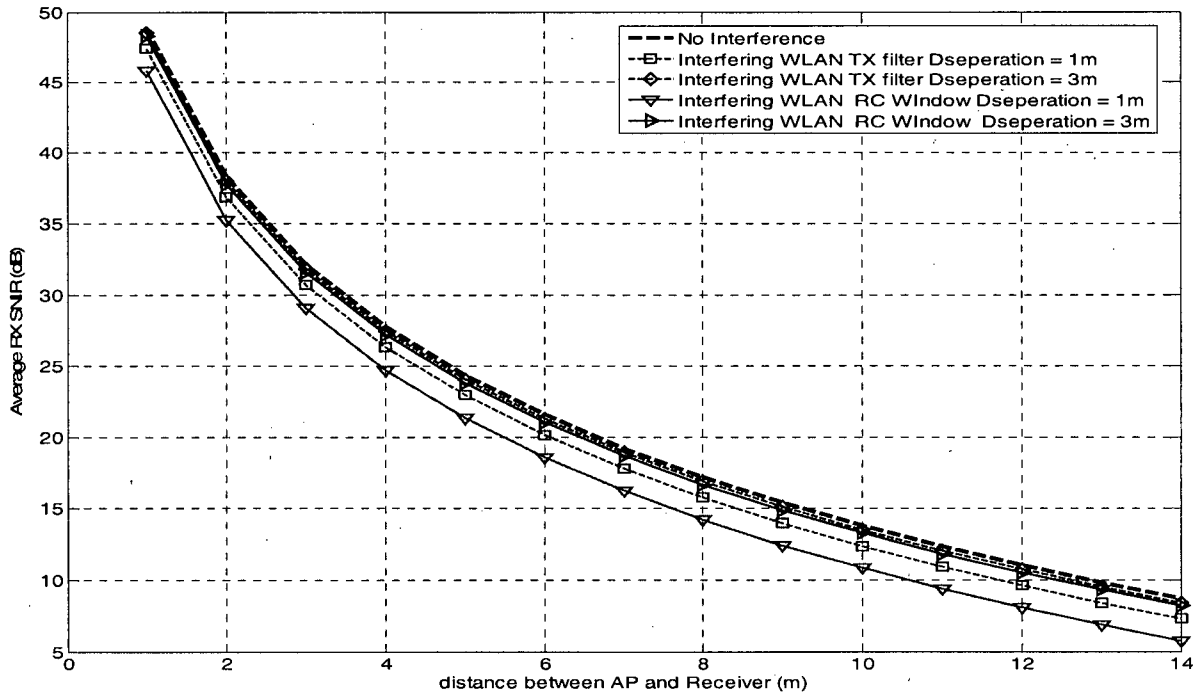

Figure 5.17: RX front end SNIR vs. distance for various $D_{separation}$ for ACI from a co-located AP

In Table 5.1 cut off distances for all fixed mode systems for a separation distance of 1m between APs are listed. Furthermore, the amount of constriction due to ACI and NACI compared to the no interference case are also listed. From the results it can clearly be seen that lesser degradation occurs if the interfering AP uses transmit filtering for OOB spectrum reduction as compared to the conventional RC windowing technique.

Table 5.2 states the minimum separation distances between APs for negligible ACI.

Table 5.1: Comparison of 10% PER cutoff distances for ACI, NACI from a co-located AP at $D_{separation}$ of 1m with no interference case. All distances given in meters

Mode	No Interference case	Adjacent Channel Interferer				Non-Adjacent Channel Interferer			
		RC Window with β = 0.0125		Transmit Shaping Filter		RC Window with β = 0.0125		Transmit Shaping Filter	
		Actual	Drop compared to no Interference case	Actual	Drop compared to no Interference case	Actual	Drop compared to no Interference case	Actual	Drop compared to no Interference case
8	6	2	4	3	3	3.5	2.5	4	2
7	7	2	5	3	4	4	3	4.5	2.5
6	9	2.5	6.5	4	5	5	4	6	3
5	11.5	3.5	8	5.5	6	6	5.5	7.5	4
4	13.5	4	9.5	7.5	6	8.5	5	8.5	5
3	17	5	12	11	6	13	4	15.5	1.5
2	17	5	12	11	6	13	4	15	2
1	20	6	14	11.5	8.5	14.5	5.5	16	4

Table 5.2: Minimum separation distances between AP for negligible ACI interference

Case	Minimum Separation Distance (m)
Co-located AP on Adjacent Channel Using Raised Cosine Windowing with β=0.0125	>10
Co-located AP on Adjacent Channel Using Transmit Filter with β=0.0125	5
Co-located AP on Non-Adjacent Channel Using Raised Cosine Windowing with β=0.0125	3
Co-located AP on Non-Adjacent Channel Using Transmit Filter	3

Chapter 6

Mitigation Techniques for Adjacent Channel Interference in Co-located WLANs

In the previous section, it was shown that a co-located AP operating on a standard defined non-overlapping channel causes significant performance degradation on nearby APs. Minimum separations distances between AP that reduce this interference to negligible levels were found. In this chapter we propose different mitigation techniques that can be used in place of the minimum separation distances. Three techniques are discussed: (1) mode switch over thresholds modification, (2) new definition of signal to noise plus interference ratio and (3) switching off severely distorted subcarriers. In each technique the 10% PER cutoff distances for a co-located AP at a separation distance 1m is analyzed and the effects of the mitigation techniques are observed both on the fixed mode scheme and the link adaptive system.

6.1 Modified Switch over Thresholds

In the link adaptive system simulations, it was observed that the defined mode switch over thresholds, Normal thresholds, do not conform to the 10% PER criteria in the presence of an interfering AP at small separation distances. This was due to the much lower SNIR on subcarriers closest to the interfering AP's channel compared to the average across all subcarriers SNIR on which feedback to the transmitter is based. The pragmatic approach to solving this problem is to increase each mode switch-over threshold by a factor, such that the link adaptive system switches to higher modes at higher SNIR values and not at the 10% PER cut-off boundaries. Although this approach lowers throughput, fewer packet errors occur at the receiver. However such an approach would allow reliable communication within the coverage area. We defined the *upped* thresholds array as the same *normal*

thresholds array with a cushioning factor cushioning factor of 1.5 dB and the *Upped2* threshold with a cushioning factor of 3 dB. The cut-off distances of individual modes do not change as no other changes are made to this system. The results of using the *Upped* thresholds in the link adaptive system for a $D_{separation}$ of 1m for the case of an adjacent channel interfering AP are shown in Figure 5.6 through Figure 5.10 and the results for a non adjacent channel interfering AP in Figure 5.13 Figure 5.15. Figure 6.1 and Figure 6.2 below show the bit rate vs. distance results for the link adaptive system with *Upped* thresholds for various $D_{separation}$ distances.

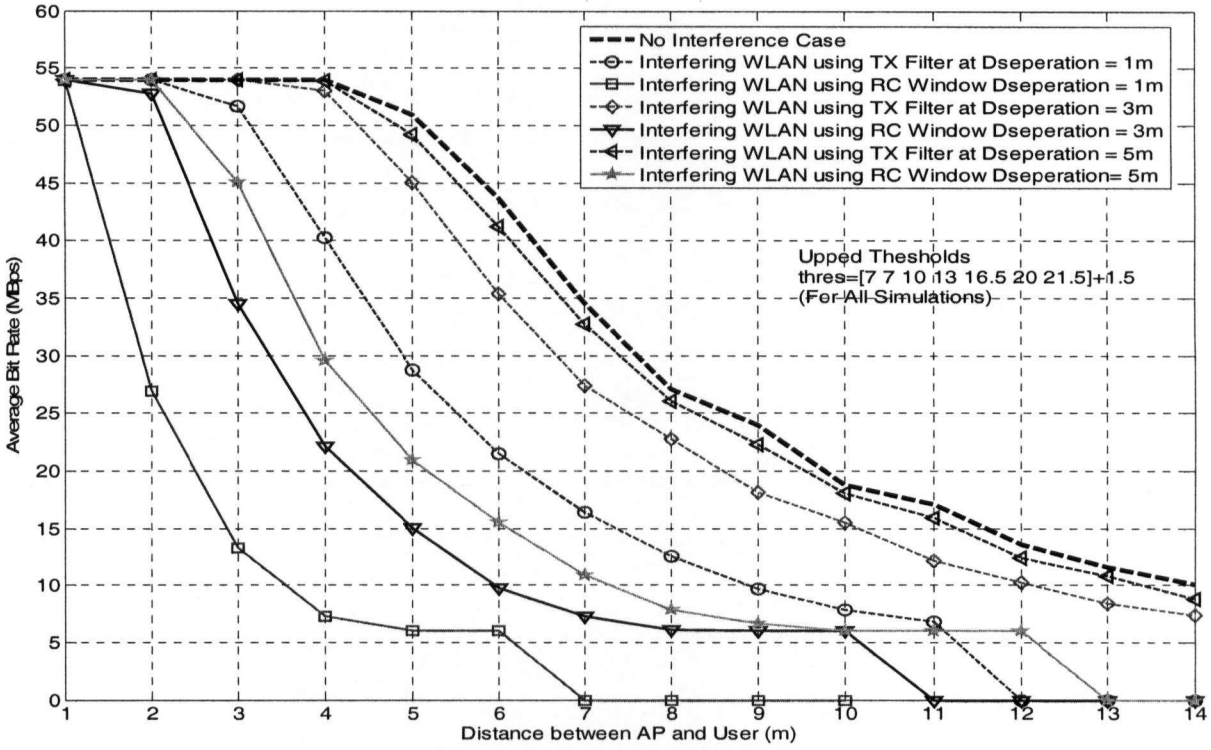

Figure 6.1 Bit rate vs. distance for various $D_{separation}$ for ACI from a co-located AP when link adaptive system is using the upped thresholds

From the PER curves in Figure 5.10 and Figure 5.15, using *Upped* thresholds lowers the PER to under 10% for an interfering AP at a $D_{separation}$ of 1m that is using the transmit filter whether it is on an adjacent or a non-adjacent channel. By doing so the system is able to provide reliable communication within its coverage area but at slightly reduced bit rates. If the interfering AP is using RC windowing for OOB spectrum reduction and is operating on an adjacent channel using these

thresholds has no effect on the PER. Using *Upped* thresholds cannot increase the cut-off distances of the fixed mode systems, which is the main reason for the poor performance for this case. If the interfering AP is using RC windowing for OOB spectrum reduction and is operating on a non-adjacent channel the *Upped* threshold lower the PER but do not limit it to under 10%. Higher threshold values are needed and more bit rate needs to be sacrificed to provide this. The *Upped2* is needed to limit the PER to within 10 % PER for this case. The PER results when using this threshold array for this case are plotted in Figure 5.15, while the bit rates vs. distance curve is plotted in Figure 5.16.

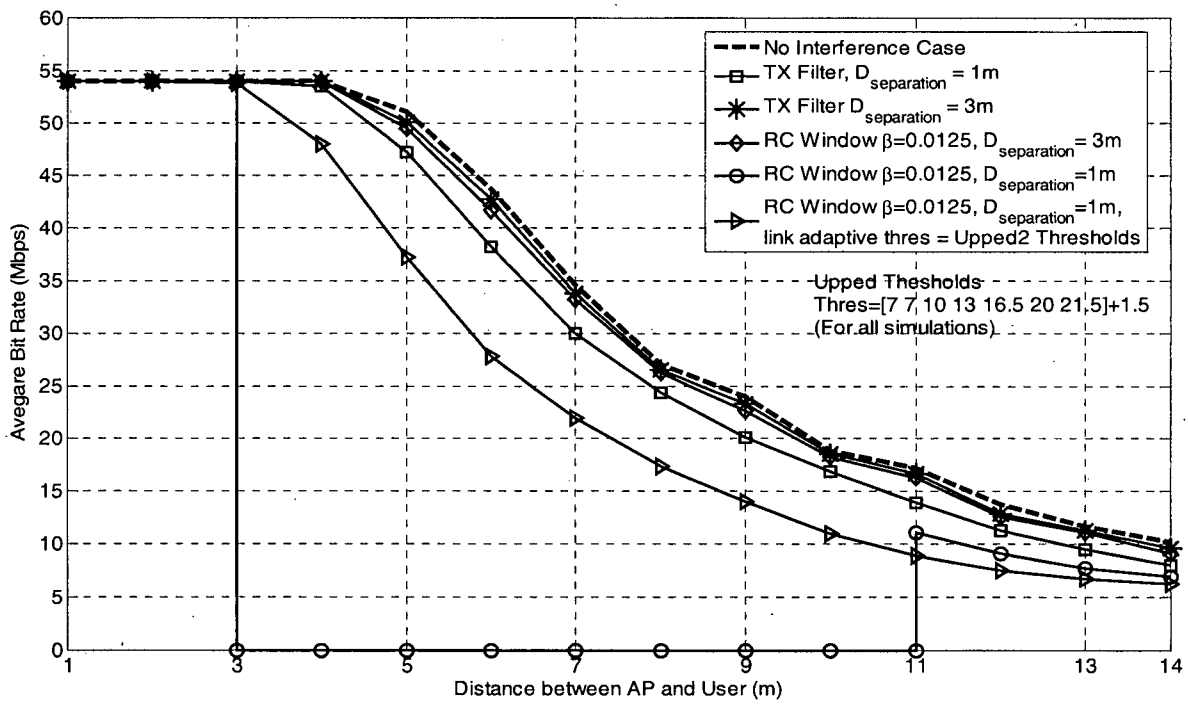

Figure 6.2: Bit rate vs. distance for various $D_{separation}$ for NACI from a co-located AP when link adaptive system is using the upped thresholds

Modifying the mode switch-over thresholds improves the performance of the link adaptive system only. However, link adaptive performance cannot be improved to better then the cutoff distances of the fixed modes. As can be seen from Table 5.1, these are still severely distorted. The mitigation techniques that follow try to improve cutoff distances to improve system performance. However, this is a simple technique which can be used to improve performance in the presence of the interfering

APs. Furthermore, as it does not require a change in the structure of the OFDM frame format or any other part of the system, it is a simple standard compliant technique. Routines to switch over to the modified thresholds in the presence of an interfering AP can easily be incorporated into the system.

6.2 New SNIR Ratio

A comparison of the link adaptive systems bit rate vs. distance plots, show that the link adaptive system does not strictly follow the cut-off boundaries defined by the fixed mode cut-off values. In some cases, for example when the interfering AP at a $D_{separation}$ of 1m and is using RC windowing the link adaptive system under performs, Figure 5.8. While this may be attributed to the unsuitability of the link adaptive systems mode switch-over thresholds in the presence of interference from a co-located AP, it is also possible that the SNIR defined at the front end of the receiver is not the best SNIR definition to use as input to the link adaptive system. We define a new SNIR using the demodulated data symbols. At the receiver, after FFT modulation and after all overhead symbols (pilot symbols, channel estimation symbols, zeros subcarriers) have been removed, a data vector containing all the data symbols in the OFDM frame is formed from the received OFDM frame. This data vector is equalized by multiplying with the appropriate channel transfer function and sent into a hard demodulator. These demodulated bits are re-modulated and the resultant vector of data symbols is compared to the data vector. The difference between these two vectors can be used to calculate the noise plus interference power.

$$r_n[k] = G_n x_n[k] + w_n[k] \tag{6.1}$$

where $r_n[k]$ is the received data symbol on subcarrier n on the k OFDM symbol, G_n is the channel frequency response on the *nth* subcarrier, $x_n[k]$ is the transmitted symbol on subcarrier n on OFDM symbol k. $w_n[k]$ is the associated AWGN power.

$$w_n[k] = r_n[k] - G_n \hat{x}_n[k] \tag{6.2}$$

where $\hat{x}_n[k]$ is the re-modulated data symbol obtained by hard demodulating $r_n[k]$

A comparison of the link adaptive system bit rates and receiver SNIRs using the two SNIR definitions is given in Figure 6.3 and Figure 6.4 for the case of an adjacent channel interferer at $D_{separation}$ =1m.

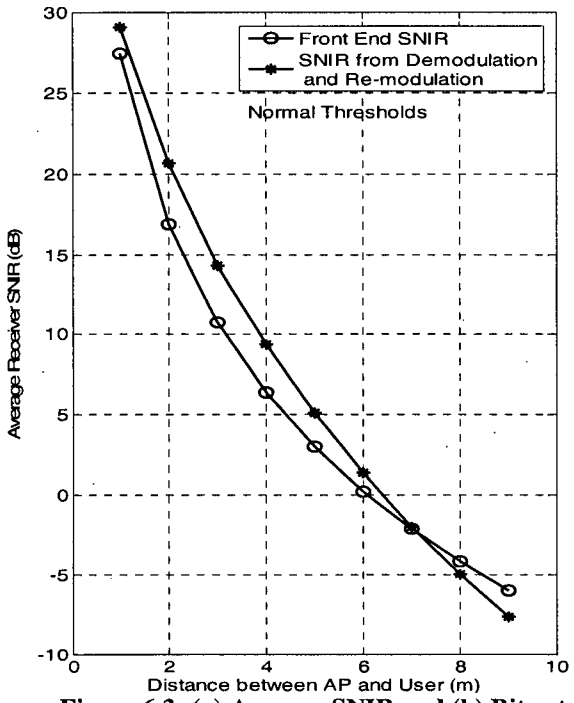

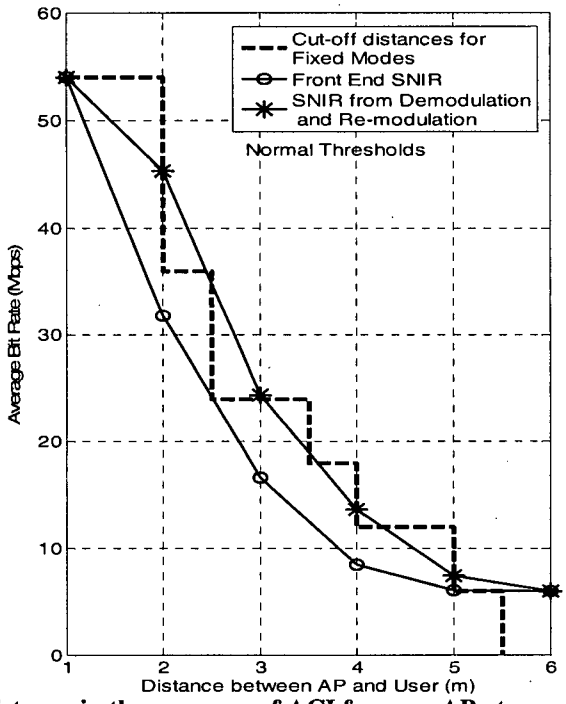

Figure 6.3: (a) Average SNIR and (b) Bit rate vs. distance in the presence of ACI from an AP at $D_{separation}$ = 1m, Interfering AP using RC windowing with β = 0.0125 for OOB spectrum reduction

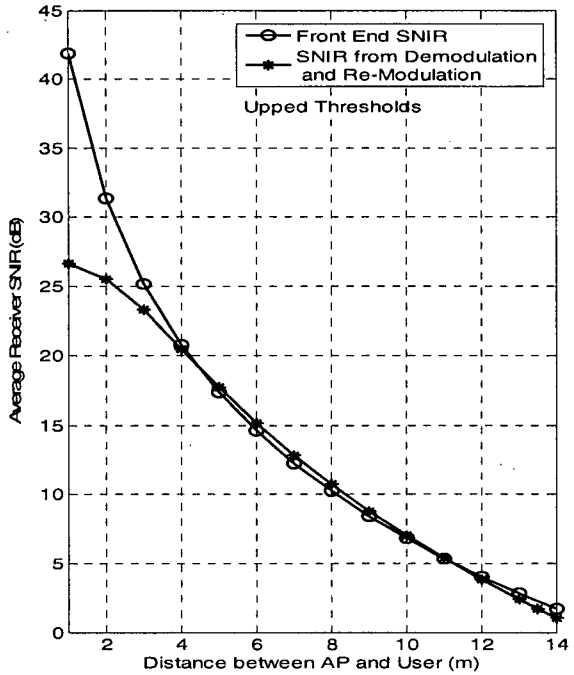

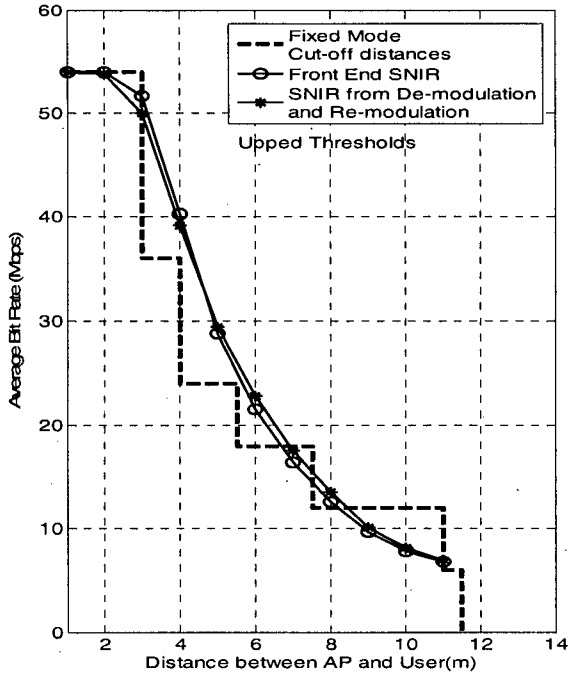

Figure 6.4: (a) Average SNIR and (b) Bit rate vs. distance in the presence of ACI from an AP at $D_{separation}$ = 1m, Interfering AP using the transmit filter for OOB spectrum reduction

System performance is significantly improved when the new SNIR ratio is used with the link adaptive system for the case of an interfering AP that is using RC windowing for OOB spectrum reduction, cf. Figure 6.3. If the interfering AP is using transmit windowing for OOB spectrum reduction, system performance is approximately the same Figure 6.4. The new SNIR definition is better at coping with the non-constant interference from the interfering AP, as the demodulated symbols are equalized and normalized prior to taking the SNIR ratio. Therefore, for the remaining simulations, the new SNIR ratio will be taken as input to the link adaptive system.

6.3 Switching off Severely Distorted Subcarriers

A more intuitive method to deal with this spectrally non-flat interference would be to switch off subcarriers most affected by it. However, standard compliant systems have a fixed frame format with a defined number of data carrying subcarriers per OFDM symbol. A change in the number of data subcarriers would require fundamental changes to the system. Although this would make the system standard non-compliant, it is still interesting to investigate how effective this technique would be in limiting ACI. In this section we investigate the effects on achievable bit rates, PER and cut-off distances when data subcarriers closest to the interfering AP's channel are turned off. We restrict our analysis to the case when the interfering AP is operating on an adjacent channel at a $D_{separation}$ of 1m as this particular scenario provides the greatest interference, Figure 5.8 and Figure 5.10. From Figure 5.7, it can be predicted that this technique should be more effective for the case when the interfering AP is using RC windowing for OOB spectrum reduction as compared to one using the transmit filter. In the former case, subcarriers closest to the interfering AP channel experience much high levels of distortion then the average over all subcarrier SNIR on which feedback to the transmitter is based. Therefore, if these subcarriers are not used to transmit data better performance can be achieved. For the latter case, there is lesser disparity between the SNIR on these subcarriers and the average over all subcarriers SNIR. Switching off subcarriers should not improve performance by much.

Four cases are considered, the number of data subcarriers turned off in each case are:

Case (1): 48 Data Subcarriers (Normal IEEE 802.11a Defined format)

Case (2): 47 Subcarriers (1 subcarrier cutoff)

Case (3): 43 Subcarriers (5 Subcarriers cutoff)

Case (4): 38 Subcarriers (10 Subcarriers cutoff)

For simplicity we do not employ any variable bit loading techniques on individual subcarriers and all subcarriers are loaded with data symbols from the same modulated and coded symbol set in one OFDM frame. As a consequence of this, switching off data subcarriers will directly affect the bit rate each mode provides. The new reduced bit rate is given by

$$BitRate = mRN_{SD}\left(\frac{1}{T_o}\right) \tag{6.3}$$

where m is the modulation order, R is the coding rate, N_{SD} is the number of data subcarriers in one OFDM symbol, T_o is the OFDM symbol duration including guard interval time.

In addition to changing the OFDM frame format, the standard defined interleaver\de-interleaver also need to be modified as these are specifically designed for a 48 data subcarriers per OFDM symbol format. We replace this with a random interleaver that interleaves\de-interleaves across all encoded bits used in an OFDM frame. As explained earlier, the standard defined interleaving\de-interleaving algorithms are not ideal [32] as bits are interleaved only across one OFDM symbol. Interleaving across an OFDM frame improves BER performance by increasing interleaver depth. This in turn should increase performance in terms of the parameters we are interested in.

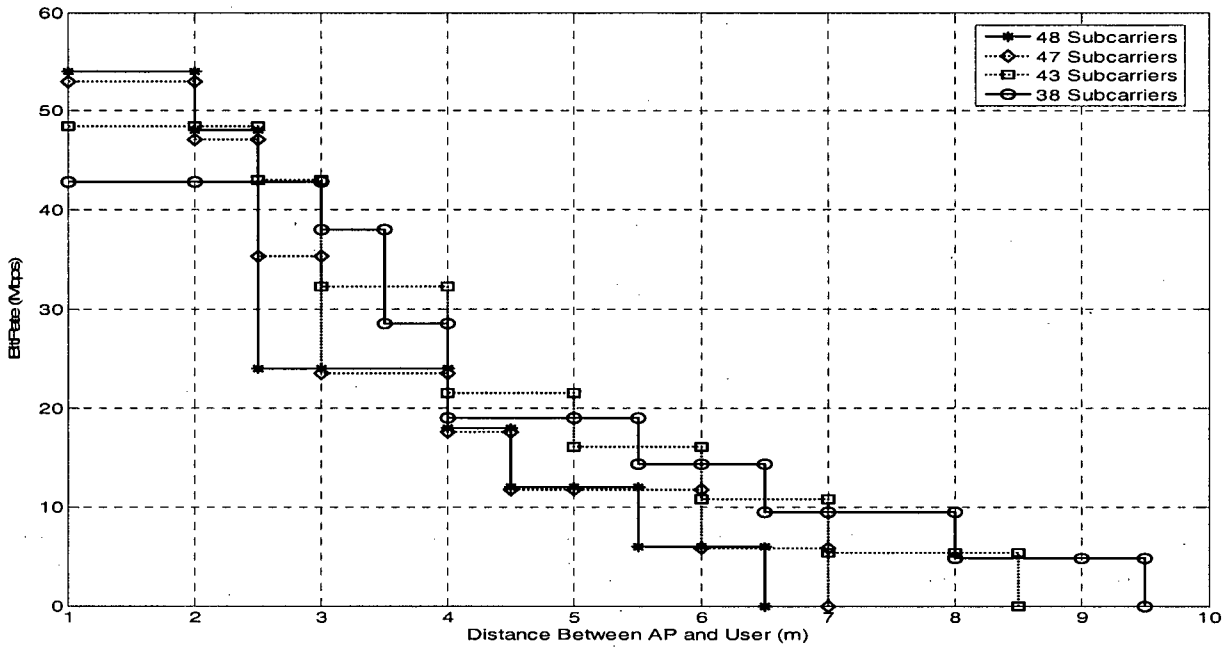

Figure 6.5: Cut-off distances for different modes number of subcarriers for the case of ACI from an AP at $D_{separation}$ = 1m using a RC windowing with β = 0.125. Random interleaver used for all cases.

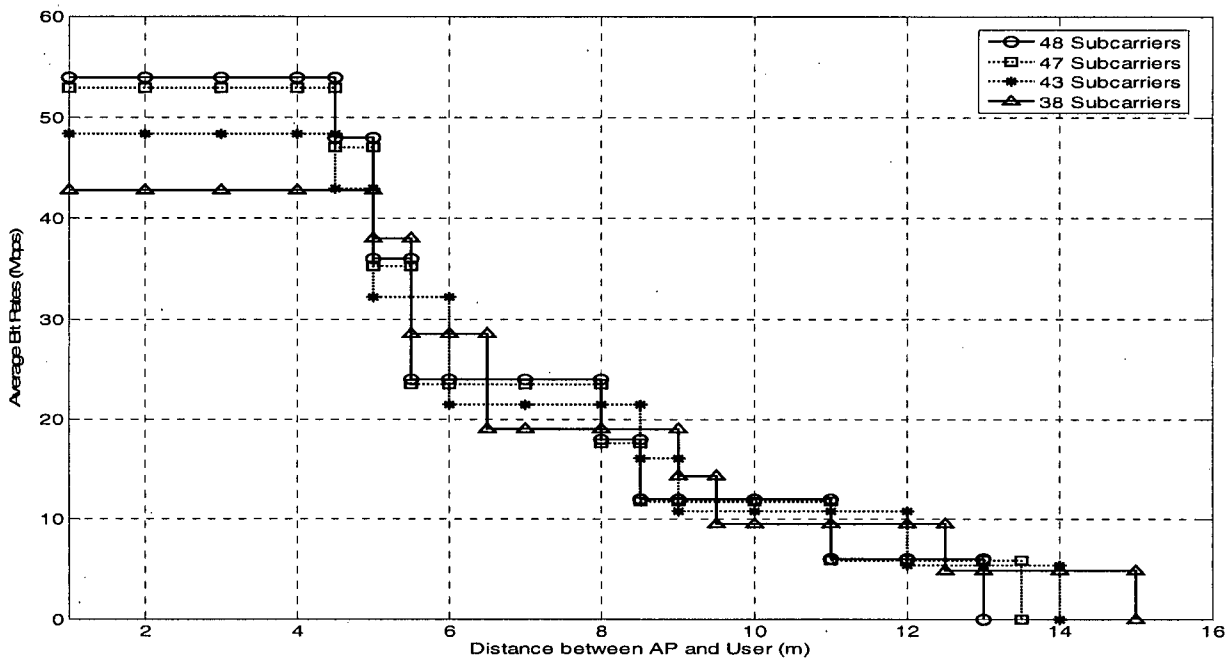

Figure 6.6: Cut-off distances for different modes number of subcarriers for the case of ACI from an AP at $D_{separation}$ = 1m using the transmit filter. Random interleaver used for all cases.

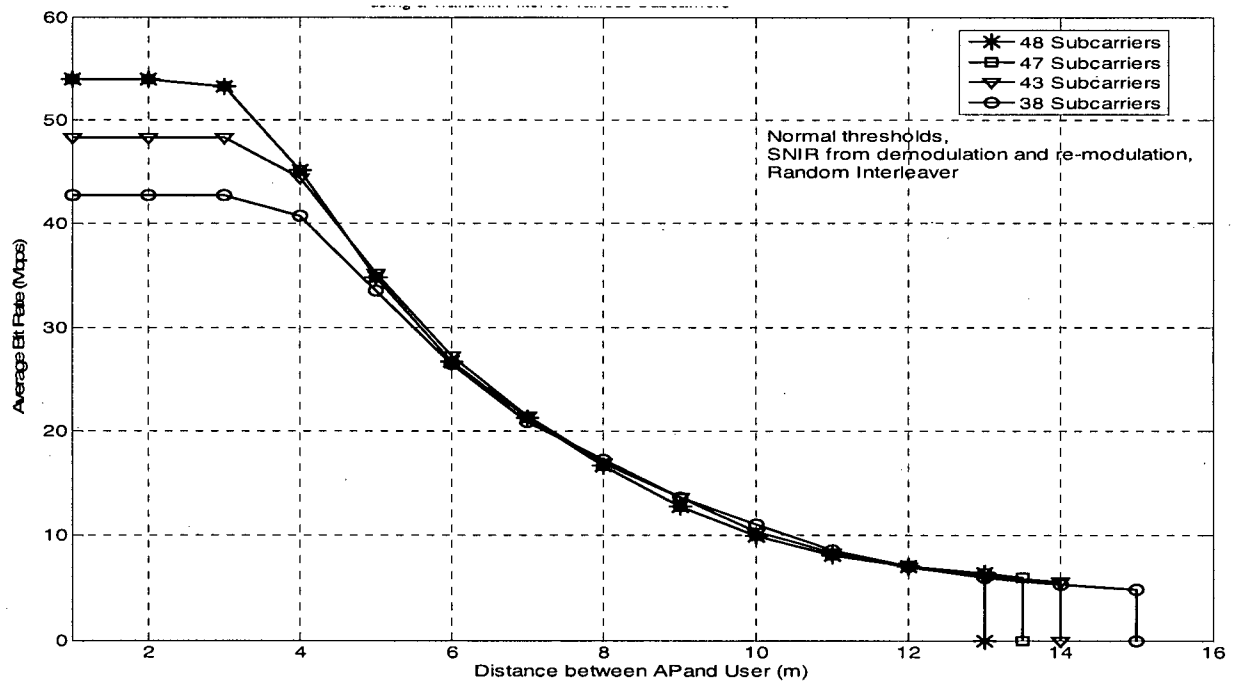

Figure 6.7: Bit Rate vs. distance for the case of ACI from an AP at $D_{separation}$ = 1m using the transmit filter for OOB spectrum reduction - for various number of data subcarriers

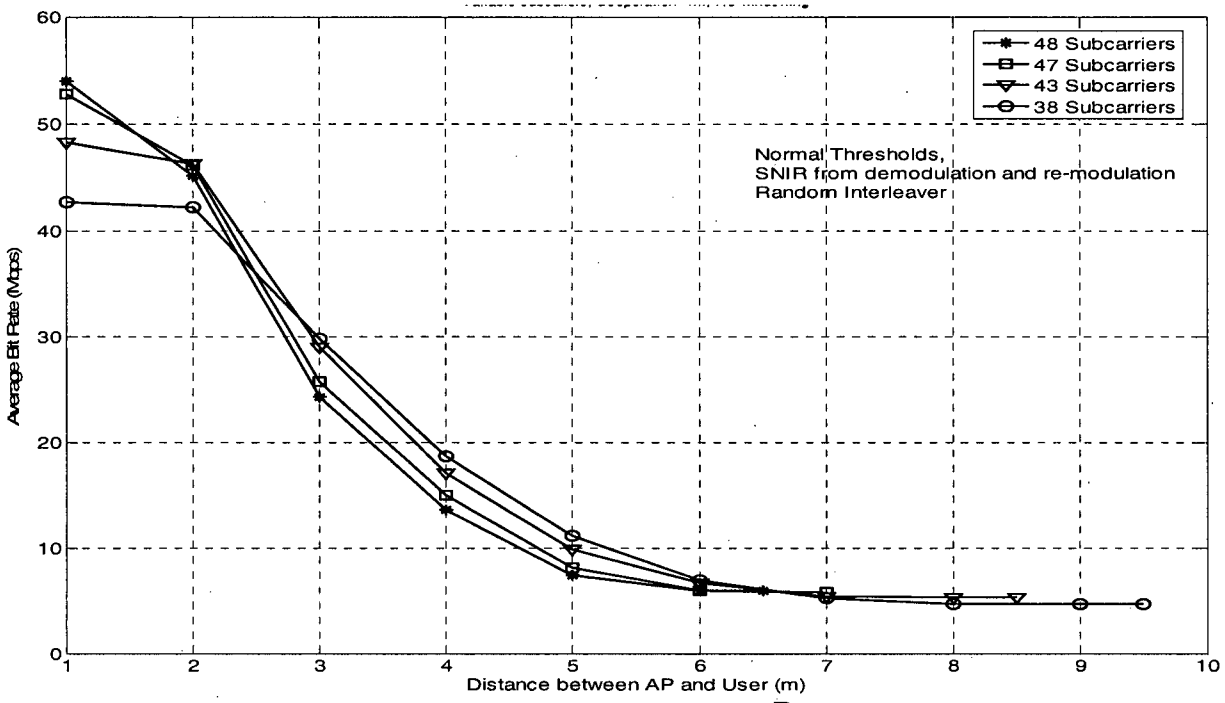

Figure 6.8: Bit Rate vs. distance for the case of ACI from an AP at $D_{separation}$ = 1m using the RC window with β = 0.0125 for OOB spectrum reduction - various number of data subcarriers

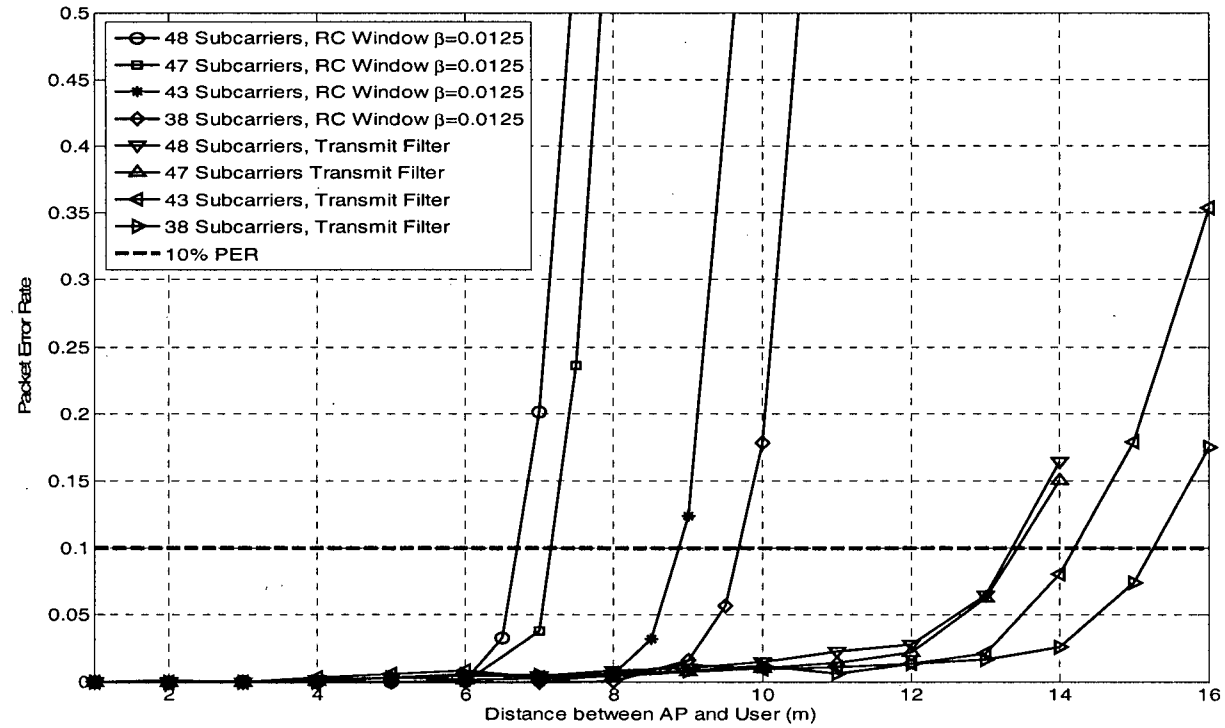

Figure 6.9: PER vs. distance for the case of ACI from an AP at $D_{separation}$ = 1m - various number of data subcarriers

The cutoff distances for individual modes for all cases of ACI from an AP at $D_{separation}$ of 1m are plotted in Figure 6.5 and Figure 6.6 and are listed in Table 6.1. As predicted, greater performance enhancement is achieved for the case of an AP using RC windowing for OOB spectrum reduction as compared to the transmit filter, when subcarriers closest to the interfering APs channel are switched off. A similar trend is observed in the results of the link adaptive system simulations as can be seen Figure 6.7 Figure 6.8. The small increase in cut-off distances as the number of data carrying subcarriers is decreased is due to OFDM frame power normalizing prior to transmission; since lesser data subcarriers are used, individual subcarriers have higher power.

The difference between the cut-off distances for the case of 48 subcarriers reported in this section and in previous sections can be attributed to the BER improvement achieved through the use of the random interleaver. In addition to increasing cut-off distances, the random interleaver also allows the 48 subcarrier system to function below 10% PER within the coverage area for an ACI from an AP using *Normal* thresholds for its link adaptive system, Figure 6.8 and Figure 6.9.

The PER curves also show a greater improvement when the interfering AP uses RC windowing compared to the transmit filter for OOB spectrum suppression. Moreover, for the RC windowing case, the amount of improvement achieved decreases as the number of subcarriers switched off increases. The interference signal distortion is highest on the subcarrier closest to the interfering signals channel and decreases for subcarriers further away. The PER curves for the transmit filter case, show a more linear trend, with each subcarrier shut off having almost a equal impact on PER performance.

Table 6.1: Cut-off distances for all modes for various number of data carrying subcarriers

				RC WINDOW with β=0.0125		FILTER	
Number of Data Subcarriers (NSD)	Mode	Bit Rate (Mbps)	Bit Rate Drop Compared to standard defined Format (Mbps)	10% PER Cut-off Distance (m)	Change in 10% Cut-off Distance compared to standard defined format (m)	10% PER Cut-off Distance (m)	Change in 10% Cut-off Distance compared to standard defined format (m)
48	1	6.0	0.0	6.5	0.0	13.0	0.0
	2	9.0	0.0	5.5	0.0	10.0	0.0
	3	12.0	0.0	5.5	0.0	11.0	0.0
	4	18.0	0.0	4.5	0.0	8.5	0.0
	5	24.0	0.0	4.0	0.0	8.0	0.0
	6	36.0	0.0	2.5	0.0	5.5	0.0
	7	48.0	0.0	2.5	0.0	5.0	0.0
	8	54.0	0.0	2.0	0.0	4.5	0.0
47	1	5.9	0.1	7.0	0.5	13.5	0.5
	2	8.8	0.2	5.5	0.0	10.5	0.5
	3	11.8	0.3	6.0	0.5	11.0	0.0
	4	17.6	0.4	4.5	0.0	8.5	0.0
	5	23.5	0.5	4.0	0.0	8.0	0.0
	6	35.3	0.8	3.0	0.5	5.5	0.0
	7	47.0	1.0	2.5	0.0	5.0	0.0
	8	52.9	1.1	2.0	0.0	4.5	0.0
43	1	5.4	0.6	8.5	2.0	14.0	1.0
	2	8.1	0.9	6.5	1.0	11.0	1.0
	3	10.8	1.3	7.0	1.5	12.0	1.0
	4	16.1	1.9	6.0	1.5	9.0	0.5
	5	21.5	2.5	5.0	1.0	8.5	0.5
	6	32.3	3.8	4.0	1.5	6.0	0.5
	7	43.0	5.0	3.0	0.5	5.0	0.0
	8	48.4	5.6	2.5	0.5	4.5	0.0
38	1	4.8	1.3	9.5	3.0	15.0	2.0
	2	7.1	1.9	7.5	2.0	11.5	1.5
	3	9.5	2.5	8.0	2.5	12.5	1.5
	4	14.3	3.8	6.5	2.0	9.5	1.0
	5	19.0	5.0	5.5	1.5	9.0	1.0
	6	28.5	7.5	4.0	1.5	6.5	1.0
	7	38.0	10.0	3.5	1.0	5.5	0.5
	8	42.8	11.3	3.0	1.0	5.0	0.5

Chapter 7

Conclusion and Future Work

In this work we presented a detailed analysis of Adjacent Channel Interference (ACI) that access points (APs) of OFDM WLANs deployed in overlying coverage areas may experience even when individual APs operate on standard defined non-overlapping channels. Because standard defined non-overlapping channels are not truly non-overlapping but are based on limits set on the transmit signal spectrum, situations may arise where this interference will significantly degrade performance. Through simulation of these scenarios we investigate how the spatial separation between APs, frequency separation between their operating channels and the out-of-band (OOB) spectrum reduction techniques that they employ contribute to the severity of ACI. We also show that co-located AP operating on non-adjacent standard defined non-overlapping channels can also generate interference into neighboring WLANS - non-adjacent channel interference (NACI). Although the effects of NACI will not be as severe as those of ACI, they can still be significant. Effects of ACI and NACI include a constriction of the coverage area, a drop in the achievable bit rates of users associated with the AP and a reduction in their signal-to-noise-plus-interference ratios. ACI also degrades the performance of the adaptive coding and modulation in WLANs.

We show that the raised cosine (RC) windowing for OOB spectrum reduction creates an interfering signal that is non-flat across the channel of neighboring WLANs. Because of this spectrally non-flat interfering signal, individual subcarriers of the OFDM signal will experience different levels of distortion; subcarriers closest to the channel of the interfering WLANs channel see significantly more distortion. Link adaptive feedback to the transmitter is based on a SNIR ratio averaged across all subcarriers. Therefore, 10% PER are observed even within the coverage area as fixed modulation and coding is used on all subcarriers. In fact for small separation distances between APs, PER may degrade to the point where reliable communication (a PER of less then 10% for a PSDU of length 1000 bytes) cannot be maintained within the coverage area.

We use the results of our investigation to design a transmit filter that causes a comparatively more spectrally flat interfering signal across channels of neighboring APs. Our transmit filter results in lesser PERs and link adaptive performance degradation. The results of our analysis are used to find minimum separation distances between APs for negligible ACI for the scenarios that we modeled. Furthermore, we develop several ACI mitigation techniques that can be used to limit ACI if the minimum separation distance criterion can not be fulfilled. To improve PER and link adaptive bit rate performances we suggest the use of a cushioning factor on mode switchover thresholds. Although this drops the achievable bit rates slightly, it increases the PER resilience of the system. Including this cushioning factor allows reliable communication to be maintained within the coverage area for very small AP separation distances as well. We also investigate the effects of turning off severely distorted subcarriers on system performance. Turning off severely distorted subcarriers is more effective for RC windowing than for transmit filtering as there is a greater disparity been individual subcarrier SNIRs and the mean subcarrier SNIR for the former OOB spectrum reduction technique.

The results of our analysis can be used to improve network deployment strategies and to develop routines that can be used to limit ACI in areas with a high number of overlapping WLANs with no network planning, such as residential flats. Our work suggests several interesting directions for future work on this topic. In our investigation we limited our analysis to a minimum separation of 1m between APs. This was done to ignore the effects of mutual coupling between AP antennas and non-uniform antenna patterns. However, in residential flats it is quite possible that smaller separation distances between APs are observed. It would be interesting to study interference effects at distances less then 1m - in particular, the case of no separation (vertically stacked APs). It would also be useful to study the effects of several other factors that affect the OOB spectrum of OFDM signals, such as peak-to-average-power of OFDM systems and transmitter induced non-linearities on ACI. Also interesting would be an investigation into the effects of other link adaptive techniques.

Bibliography

[1] IEEE Standard 802.11a: "Wireless LAN medium access control (MAC) and physical layer (PHY) specifications, amendment 1: High-speed physical layer in the 5 GHz band," December 1999 (Revised 2000).

[2] IEEE standard 802.11, "Part 11: wireless LAN medium access control (MAC) and physical (PHY) layer specifications," November 1997.

[3] R. Prasad, and R. Van Nee, *OFDM for Wireless Multimedia Communications*, Artech House, Artech House Universal Personal Communications Series, 2000

[4] Jui-Hung Yeh, Jyh-Cheng Chen and Chi-Chen Lee, "WLAN standards," *IEEE Potentials*, vol. 22, pp. 16-22, October - November 2003.

[5] U. Varshney, "The status and future of 802.11-based WLANs" *Computer*, vol.36, pp. 102-105, June 2003.

[6] J. Bellorado, S.S. Greenstein, T. Sveinsson, and V. Tarokh, "Coexistence of ultra-wideband systems with IEEE-802.11a wireless LANs," *IEEE GLOBECOM '03*, vol. 1, pp. 410-414, December 2003.

[7] ____ "The effects of adjacent channel rejection and adjacent channel interference on 802.11 WLAN performance," *Texas Instruments White Paper,* http://www.cwnp.com/learning_center/search_details.php? doc_id=NCGYJK0R, November 2003.

[8] A.K. Arumugam, A. Doufexi, A.R. Nix, and P.N. Fletcher, "An investigation of the coexistence of 802.11g WLAN and high data rate Bluetooth enabled consumer electronic devices in indoor home and office environments," *IEEE Transactions on Consumer Electronics*, vol. 49, pp. 587-596, August 2003.

[9] D. Leiss, "Co-interference between military radars and 802.11a WLAN networks," *Proceedings of the IEEE System Readiness Technology Conference*, pp. 290-293, September 2003.

[10] Jin-A Park, Seung-Keun Park, Dong-Ho Kim, Pyung-Dong Cho, and Kyoung-Rok Cho, "Experiments on radio interference between wireless LAN and other radio devices on a 2.4 GHz ISM band," *The 57th IEEE Semi-annual Vehicular Technology Conference*, vol. 3, pp 1798-1801, April 2003.

[11] M. Unbehaun, and M. Kamenetsky, "On the deployment of pico-cellular wireless infrastructure," *IEEE Wireless Communications*, vol. 10, pp. 70 – 80, December 2003.

[12] A. Hills, "Large-scale wireless LAN design," *IEEE Communications Magazine*, vol. 39, pp. 99-107, November 2001.

[13] E. Biglieri, John G. Proakis, and S. Shamai, "Fading channels: information-theoretic and communications aspects," *IEEE Transactions on Communications Theory*, vol. 44, pp. 2619-2691, October 1998.

[14] William C. Jakes, Microwave *Mobile Communications*, Wiley-Interscience, John Wiley and Sons Publication, 1994.

[15] John G. Proakis, *Digital Communications*. Fourth Edition, McGraw-Hill, 2001.

[16] S. Weinstein, and P. Ebert, "Data transmission by frequency-division multiplexing using the discrete Fourier transform," *IEEE Transactions on Communications Theory*, vol. 19, pp. 628-634 October, 1971.

[17] European Telecommunications standards Institute (ETSI), "Broadband radio access networks (BRAN) HIPERLAN Type 2 technical specification, physical (PHY) layer," August 1999.

[18] IEEE Standard 802.16, "Part16: Air interface for fixed broadband wireless access systems," *IEEE Standards for Local and Metropolitan Area Networks*, October, 2004.

[19] ECMA-368 standard, "High rate ultra wideband PHY and MAC standard," ECMA International, First Edition, December 2005.

[20] ETSI EN 300 401, "Radio broadcasting systems: digital audio broadcasting to mobile portable and fixed receivers," February 1995.

[21] ETSI EN 300 744 Standard, "Digital video broadcasting (DVB), framing structure, channel coding and modulation for digital terrestrial video," June 2004.

[22] J. Bingham, *ADSL, VDSL and Multicarrier Modulation,* October 2001.

[23] S. Weinfurtner, "OFDM for wireless communications: nyquist windowing, peak-power reduction, and synchronization," PhD dissertation, University of Erlangen-Nuernberg, Erlangen, Germany, April 2000.

[24] L. Lampe "Multicarrier Modulation," Course Notes for ECE 563, The University of British Columbia, Vancouver, Canada, 2005.

[25] A. J. Goldsmith, and Chua Soon-Ghee, "Variable-rate variable-power MQAM for fading channels," *IEEE Transactions on Communications*, vol. 45, pp. 1218-1230, October 1997.

[26] H. Hashemi, "The indoor radio propagation channel," *Proceedings of the IEEE*, vol. 81, Issue 7, pp.943 – 968, July 1993

[27] A. Saleh, and R. Valenzuela, "A statistical model for indoor multipath propagation," *IEEE Journal on Selected Areas in Communications*, vol. 5, pp. 128-137, February 1987.

[28] J. Melbo, and P. Schramm, "Channel models for HIPERLAN/2 in different indoor scenarios," 3ERI085B, *Hiperlan/2 ETSI BRAN Contribution*, 30 March 1998.

[29] A. Doufexi, S. Armour, M. Butler, A. Nix, D. Bull, J. McGeehan, and P. Karlsson, "A comparison of the HIPERLAN/2 and IEEE 802.11a wireless LAN standards," *IEEE Communications Magazine*, vol. 40, pp. 172-180, May 2002.

[30] G. Ungerboeck, "Channel coding with multilevel/phase signals," *IEEE Transactions on Information Theory*, vol. 28, pp. 55-67, January 1982.

[31] D. Divsalar, "The design of trellis coded MPSK for fading channels: performance criteria," *IEEE Transactions on Communications*, vol. 36, pp 1004 - 1012, September 1988.

[32] Kee-Bong Song, and S. A. Mujtaba, "On the code-diversity performance of bit-interleaved coded OFDM in frequency selective fading channels," *IEEE Vehicular Technology Conference*, 2003, vol.1, pp.572-576, October 2003.

[33] E. Zehavi," 8-PSK trellis Codes for a Rayleigh channel," *IEEE Transactions on Communications*, vol. 40, pp. 873 – 884, May 1992.

[34] G. Caire, G. Taricco, and E. Biglieri, "Bit-interleaved coded modulation," *IEEE Transactions on Information Theory*, vol. 44, pp. 927 - 946, May 1998.

[35] S. Goff and Y. Le, "Signal constellations for bit interleaved coded modulation," *IEEE Transactions on Information Theory*, vol. 49, pp. 307-313, January 2003.

[36] F. Tosato, and P. Bisaglia, "Simplified soft output demapper for binary interleaved COFDM with application to HIPERLAN/2," *IEEE International Conference on Communications*, 2002. vol. 2, pp. 664 – 668, May 2002.

[37] Li Yuan and Sumei Sun "Comparison of TCM and BICM in wireless LAN system over indoor wireless channels," *International Conference on Communications Systems*, vol.1, pp. 299 - 303, November 2002.

[38] Cai Xiaodong and G. B. Giannakis, "Error probability minimizing pilots for OFDM with M-PSK modulation over Rayleigh-fading channels," *IEEE Transactions on Vehicular Technology*, vol. 53, January 2004.

[39] M. R. D. Rodrigues, "modeling and performance assessment of OFDM communication systems in the presence of non-linearities," PhD dissertation, Department of Electronic and Electrical Engineering, University College London, October 2002.

[40] S. Khan, T. Khattab and H. Alnuweiri, "Analysis and modeling of physical layer alternatives in OFDM based WLANs," *Proceedings of IEEE WirelessCom*, June 2005.

[41] J. –C. Dunat, L. Elicegui and C. Bonnet, "Impact of inter-cell interference in an IEEE 802.11a Network with overlapping cells," *IEEE International Symposium Personal Indoor and Mobile Radio Communications 2004*, vol. 2, pp. 825 – 829, September, 2004.

[42] P. Jeongho, Kim Dongkyu, Kang Changeon, and Hong Daesik, "Effect of partial band jamming on OFDM-based WLAN in 802.11g," *IEEE International Conference on Acoustics, Speech and Signal Processing*, vol. 4, pp. 560-563, April 2003

[43] A. Grilo, and M. Nunes, "Link-adaptation and transmit power control for unicast and multicast in IEEE 802.11 a/h/e WLANs," *IEEE International Conference on Local Computer Networks*, pp. 334 - 345, October 2003.

[44] M. El-Tanany, Wu Yiyan and L. Hazy, "Impact of adjacent channel interference on the performance of OFDM Systems over frequency selective channels," *IEEE Vehicular Technology Conference*, vol. 3, pp. 2241 – 2245, May 1998.

[45] K. A. Mohamed, and L. Pap, "Inter-cell interference in spread-spectrum wireless LANs employing handshake protocols," *International Conference on Communications*, vol. 1, pp. 151-155, June 1998.

[46] David G. Michelson (private communication), Radio Science Lab, University of British Columbia, Vancouver, Canada., December 2005

[47] Li Xiaodong and L. J. Jr. Cimini, "Effects of clipping and filtering on the performance of OFDM," *IEEE Vehicular Technology Conference*, vol. 3, pp. 1634 – 1638, May 1997.

[48] F. Donald, "Interpolation by the FFT revisited-an experimental Investigation," *IEEE Transactions on Acoustics, Speech & Signal Processing*, vol. 48, May 1989.

[49] Theodore S. Rappaport, *Wireless Communications Principles and Practice*, Second Edition, Prentice Hall, 2002

[50] Clark, Martin, "IEEE 802.11a WLAN model," http://www.mathworks.com/matlabcentral/fileexchange/loadFile.do?objectId=3540&objectType=file, August, 2003